CONVERSION OF LIGNOCELLULOSIC FEEDSTOCKS TO RENEWABLE FUELS

SONIL NANDA

A DISSERTATION SUBMITTED TO
THE FACULTY OF GRADUATE STUDIES
IN PARTIAL FULFILLMENT OF THE REQUIREMENTS
FOR THE DEGREE OF
DOCTOR OF PHILOSOPHY

GRADUATE PROGRAM IN BIOLOGY
YORK UNIVERSITY
TORONTO, ONTARIO

November 2013

ABSTRACT

The increased worldwide demand for energy has led to the search for a long-term solution of a reliable source of clean energy. The major possible additions to the current energy portfolio include ethanol, butanol and bio-oils produced from lignocellulosic biomass. A great deal of research is being made in the fields of biomass conversion through biochemical and thermochemical pathways to biofuels. Much attention is focused on identifying a suitable biomass species that can provide high energy outputs to replace the fossil fuels. The current study focuses on some commonly available waste biomasses in Canada originating from forests (pinewood), energy crop systems (timothy grass) and agriculture (wheat straw) for their usage towards next generation biofuel production. The biomasses were examined physico-chemically to understand their chemistry through various analytical, structural and spectroscopic approaches. Pinewood, timothy grass and wheat straw contained 34-39 wt.% cellulose, 24-30 wt.% hemicellulose and 16-20 wt.% lignin. In order to have a comparative evaluation of bio-oil, biochar and gas yields, the feedstocks were pyrolyzed at 450°C with slow (2°C/min) and high (450°C/min) heating rates. The slow heating rate pyrolysis generated 41-44 wt.% biochars, 18-24 wt.% bio-oils and 24-27 wt.% gases, whereas high heating rate pyrolysis produced 21-24 wt.% biochars, 40-48 wt.% bio-oils and 17-24 wt.% gases from the three feedstocks. Lignin acts as a barrier for biomass conversion to alcohols. Moreover, its chemistry and distribution in the plant cell wall is least understood. With this objective, the in-situ characterization of lignin arrangement in untreated, hydrothermally pretreated and delignified biomasses was performed through chemical maps generated from Raman spectroscopy. Furthermore, the biomass conversion to ethanol and butanol was evaluated using *Saccharomyces cerevisiae* and *Clostridium beijerinckii*, respectively. The highest ethanol and butanol concentrations reached in the range of 22.6-24.1 and 10.8-11.6 g/L from biomass hydrolysates, respectively. As a result of biomass pretreatment, significant amount of hydrolysis residues were generated. The pyrolysis of these hydrolysis residues at 600°C produced bio-oils (18.6-22.3 wt.%), biochars (38.9-41.7 wt.%) and gases (24.9-28.8 wt.%) that demonstrated remarkable energy and environmental benefits.

ACKNOWLEDGEMENTS

I deeply thank my supervisors Dr. Janusz A. Kozinski and Dr. Ajay K. Dalai for their continuous support and encouragement throughout my PhD session. Their guidance and motivation played a very integral part in completing my PhD research. I would like to express my appreciation to my supervisory committee members Dr. John C. McDermott and Dr. Dasantila Golemi-Kotra for their helpful comments and suggestions towards the progress of my dissertation.

I extend my appreciation towards the Saskatchewan Structural Sciences Centre at University of Saskatchewan where most of the structural characterization studies, involved in this dissertation, were performed. My acknowledgement also goes to Lassonde School of Engineering at York University and the Department of Chemical and Biological Engineering at University of Saskatchewan for providing the state-of-art facilities in performing this PhD research.

I am also thankful to Natural Sciences and Engineering Research Council of Canada (NSERC), Canada Research Chair (CRC) program and BioFuelNet Canada for the financial support in this biomass conversion research.

TABLE OF CONTENTS

List of Tables

List of figures

List of abbreviations

Atomic force microscopy (AFM)

Brunauer-Emmett-Teller (BET)

Carbon-hydrogen-nitrogen-sulfur (CHNS)

Charge-couple device (CCD)

Combined heat and power (CHP)

Crystallinity index (CrI)

Delignified pinewood (PWDL)

Delignified timothy grass (TGDL)

Delignified wheat straw (WSDL)

Fourier transform infrared (FT-IR) spectroscopy

Gas-to-liquid (GTL)

Gas chromatography-mass spectrometry (GC-MS)

Greenhouse gas (GHG)

High heating rate (HHR)

High heating rate pinewood bio-oil (HPWBL)

High heating rate pinewood biochar (HPWB)

High heating rate timothy grass bio-oil (HTGBL)

High heating rate timothy grass biochar (HTGB)

High heating rate wheat straw bio-oil (HWSBL)

High heating rate wheat straw biochar (HWSB)

High pressure liquid chromatography (HPLC)

Higher heating value (HHV)

Hydrothermally treated (HT)

Hydrothermally treated pinewood (PWHT)

Hydrothermally treated timothy grass (TGHT)

Hydrothermally treated wheat straw (WSHT)

Hydroxymethylfurfural (HMF)

Inductively coupled plasma-mass spectrometry (ICP-MS)

Kilojoule per cubic meter (KJ/m^3)

Lower heating value (LHV)

Megajoules per kilogram (MJ/kg)

Megajoules per liter (MJ/L)

Million dry tons (MDT)

Motor octane number, MON

Nuclear magnetic resonance (NMR)

Pinewood (PW)

Pinewood bio-oil (PWBL)

Pinewood biochar (PWB)

Pinewood hydrolysis residue (PWR)

Research octane number (RON)

Scanning electron microscopy (SEM)

Slow heating rate (SHR)

Slow heating rate pinewood bio-oil (SPWBL)

Slow heating rate pinewood biochar (SPWB)

Slow heating rate timothy grass bio-oil (STGBL)

Slow heating rate timothy grass biochar (STGB)

Slow heating rate wheat straw bio-oil (SWSBL)

Slow heating rate wheat straw biochar (SWSB)

Timothy grass (TG)

Timothy grass bio-oil (TGBL)

Timothy grass biochar (TGB)

Timothy grass hydrolysis residue (TGR)

Thermogravimetric analysis (TGA)

Wheat straw (WS)

Wheat straw bio-oil (WSBL)

Wheat straw biochar (WSB)

Wheat straw hydrolysis residue (WSR)

X-ray diffractometry (XRD)

Chapter One: The bio-based society and the importance of biomass for fuels

1.1. Introduction

The present energy crisis is considered as one of the serious threats to the world in terms of sustainability of human development and civilization. With the rapid industrialization worldwide, there is an increasing demand for energy, especially in the developing countries. For instance, in the global transportation sector, about 806 million vehicles were on roads in 2007 (Balat, 2011). However, this estimation is projected to increase to 1.3 billion by 2030 and to over 2 billion by 2050. Although, about 27% of primary energy from fossil fuels is used for transportation, yet it is the fastest growing sector and currently contributes to nearly 80% of anthropogenic greenhouse gas (GHG) emissions (IEO, 2011). Over 97% of transportation fuels (e.g., petroleum, gasoline, diesel etc.) are derived from fossil fuels whose demands are ever-increasing, although the knowledge of their exhausting resources is well-known. The consumption of petroleum and other liquid transportation fuels was 85.7 million barrels per day in 2008, which is expected to increase to 112.2 million barrels per day by 2035 (IEO, 2011). Figure 1.1 shows the trend of some significant consumer countries of petroleum over the years (1980-2011).

This amplifying demand for fossil fuels has led to the search for alternative supplies of energy from renewable resources that can fulfill future energy requirements. Low molecular weight alcohols such as methanol (CH_3OH), ethanol (C_2H_5OH), propanol (C_3H_7OH) and butanol (C_4H_9OH) have great potentials to replace fossil fuels in the transportation sector. Biofuels from renewable resources have the tendency to reduce GHG emissions and mitigate global warming, enhance overall energy efficiency of the fuel and improve employment in agricultural sector. In the recent times, biomass-derived oils and alcohols (e.g, ethanol and butanol)

have emerged as attractive biofuels, generating a great deal of interest in their production pathways.

During the last decades, bioethanol was produced from fermentation of a variety of food-based materials including grains such as corn, potato mashes, fruit juices, beet and sugarcane. The ethanol production from corn became commercially viable in USA during 1980s. With an annual yield of 13 billion gallons of ethanol from corn, USA utilized 23% of its corn harvest in 2009 for ethanol production which resulted in the rise in corn prices for food consumption (Demain, 2009). The use of such starch-based feedstocks for ethanol production is mostly surrounded by "food versus fuel" paradigm linked with the risk of diverting farmlands for fuel production, thereby affecting the food supply on a global scale. On the other hand, lignocellulosic biomasses are considered as prospective resources for biofuels not only because they are available on a surplus and renewable basis but also they have no net release of CO_2 into the atmosphere.

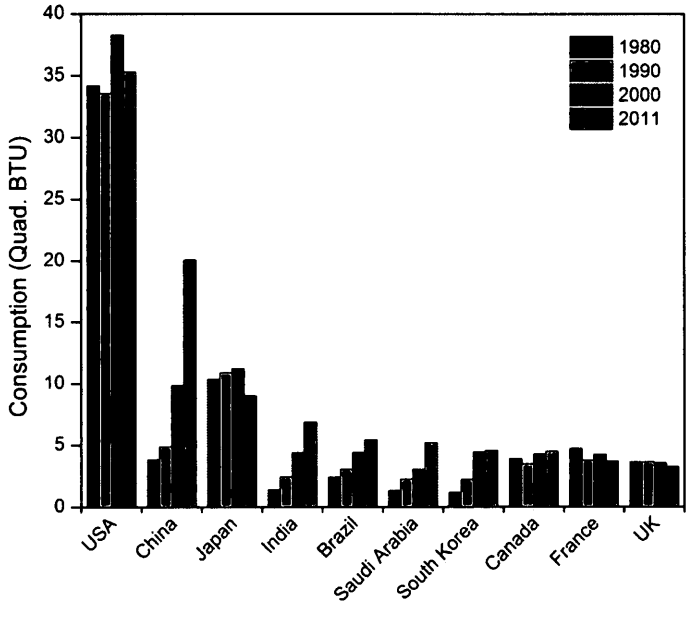

Fig. 1.1 Worldwide consumption of petroleum, 1980-2011 (Data: USEIA, 2013)

Lignocellulose comprises about half of the plant matter produced by photosynthesis and is the most abundant renewable organic resource (Sanchez, 2009). The utilization of waste biomass in the production of sustainable energy signifies bioenergy. Bioenergy or biomass energy refers to any source of renewable energy produced from non-fossil biological materials. In fact, bioenergy is a potential solution to the challenges faced by the world economy for energy security due to dependency on depleting fossil fuel resources. Bioenergy has the ability to decrease net emissions of carbon into the atmosphere per unit of energy delivered, making its use as environmental friendly. Although CO_2 is released during combustion of biofuels, it is also reutilized to grow new biomass which leads to no net CO_2 accumulation in the atmosphere.

1.2. Utilization of lignocellulosic feedstocks for bioenergy

Waste biomasses from agriculture, forestry, municipal, industrial and urban residues are potential raw materials for biofuel production. The global production of biomass from terrestrial plants is $170\text{-}200\times10^9$ tons, with an estimated 70% made of plant cell walls (Pauly and Keegstra, 2008). Exploring the potential of these plant residues for biofuel production is essential to minimize the need for other energy sources and to promote their ecofriendly utilization. Substrates for ethanol production contain raw materials that can be transformed into sugars. These raw materials are classified as directly fermentable sugars, starch-based and lignocellulosic materials. Among these substrates, starch and sugar-containing materials do not require extreme and costly pretreatments. There is an ease of hydrolysis and the sugars in these feedstocks are relatively easy to extract, transform into glucose and ferment to produce ethanol. In addition to the bioconversion of biomass, ethanol can only be produced through thermochemical pathways. Synthesis gas or syngas (H_2 + CO) is a product of thermochemical conversion of biomass. The syngas can be directly used as a fuel or can be converted into liquid fuels such as ethanol and other alcohols and hydrocarbons via gas-to-liquid (GTL) routes.

Ethanol or ethyl alcohol is an oxygenated fuel containing 35% O_2 which reduces the emission of particulate matters and GHG emissions from combustion. As a fuel, it can be used directly (95% ethanol and 5% water) or as a gasoline blend. Ethanol, when blended with gasoline can oxygenate, thus reducing the formation of CO and ozone. Bioethanol has a potential to replace 32% of global gasoline consumption when used in E85 (85% ethanol and 15% gasoline) for a midsize passenger vehicle (Kim and Dale, 2004). The countries that have implemented ethanol-gasoline blending programs include USA (E10 and E85 for flexible-fuel vehicles: FFV), Canada (E10 and E85 for FFV), Sweden (E5 and E85 for FFV), Brazil (E20 and E25 for FFV), China (E10), Australia (E10), Thailand (E10), Columbia (E10), Peru (E10), Paraguay (E7) and India (E5) (Balat, 2011).

The current five major bioethanol producing countries are USA, Brazil, China, Canada and France. Figure 1.2 highlights these major bioethanol producers along with their production trend since 2007. At present, USA and Brazil produce over 90% of world's bioethanol. In 2008, Canada produced about 800 million liters of bioethanol representing a 400% increase over its production in 2005 (Mabee and Saddler, 2010). Canada has a potential to meet about 50% of its gasoline demand from the lignocellulosic biomass accessibility, out of which 12-28.5% is from the energy crop systems. It could be predicted that by 2020 the total international utilization of bioethanol as fuel will reach 10 million metric tons.

Very recently, butanol or butyl alcohol has emerged as a superior biogenic fuel over ethanol in its energy content and applications (Durre, 2007). Unlike ethanol, butanol can be used in pure form or blended in any concentration with gasoline. In contrast to ethanol, butanol can be used in the existing vehicular fuel engines without any mechanical modification. In addition, butanol's low vapor pressure and less corrosiveness make it safer to handle. While, ethanol requires blending with gasoline shortly before use, butanol's non-hygroscopic nature allows its blending with gasoline at the refinery well ahead of storage and distribution. Furthermore, the energy content of butanol is higher (29.2 MJ/L) than ethanol (21.2

MJ/L), increasing the mileage/gasoline blend ratio. Similar to ethanol, butanol can also be produced via biomass bioconversion pathways and GTL routes. However, bioconversion seems to be economically the method of choice.

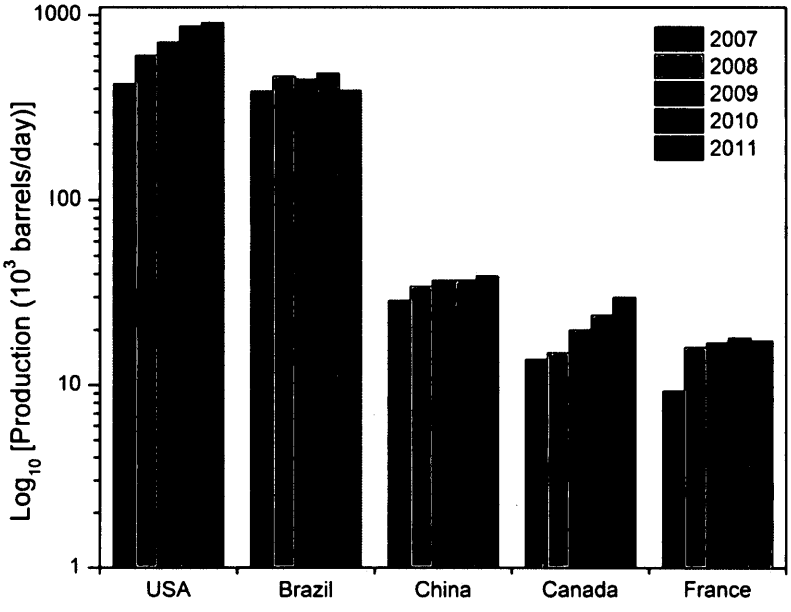

Fig. 1.2 Top five bioethanol producing countries, 2007-2011 (Data: USEIA, 2013)

Bio-oil is a synthetic fuel obtained from the thermochemical conversion i.e., pyrolysis of biomass. Bio-oils are complex mixture of oxygenated compounds namely alcohols, acids, aldehydes, esters, ketones and many other aromatic compounds. Bio-oils have found wide range of applications in industrial boilers for power generation and in synthesis of chemicals. Upon upgrading, these bio-oils can be used as transportation fuels. Bio-oil from lignocellulosic biomass is a heterogenous mixture of thermochemical derivatives from cellulose, hemicellulose and lignin. The typical degradation products from cellulose and hemicellulose in bio-oil include acids, esters, alcohols, ketones, aldehydes, sugars, furans and miscellaneous oxygenates, whereas lignin derivatives include phenols, guaiacols and syringols (Joshi and Lawal, 2012).

1.3. Scope, objectives and outline of the research

1.3.1. Scope

The environmental concerns associated with the use of fossil fuels demand a transition to renewable sources (e.g., sun, wind, water, geothermal, biomass) for energy. However among all, biomass provides the only renewable source for transportation fuels and chemicals. Biomass is converted via different technologies to produce fuels (e.g., bio-oils, alcohol-based fuels), heat and various bio-products (e.g., biochar, carbon fibers). Bioconversion of biomass can lead to the production of alcohol-based fuels such as ethanol and butanol (Nanda et al., 2012). However, prior to bioconversion, the biomass is required to be hydrolyzed through a series of acid and enzymatic pretreatments to recover fermentable sugars that could be microbially or enzymatically converted to alcohols.

On the other hand, thermochemical degradation of lignocellulosic biomass through pyrolysis could be essential in generating bio-oils along with an array of useful products such as combustible gas, biochar and valuable chemicals. Nevertheless, it is the interplay between the biomass components such as cellulose, hemicellulose and lignin to deliver various fuel products through biochemical or thermochemical pathways. Since the three major biomass polymers i.e., cellulose, hemicellulose and lignin possess dissimilar chemical and thermal reactivities, the type and amount of degradation products are tunable by proper selection of the conversion process. Moreover, this makes it very important to study the physico-chemical characteristics of biomass prior to its conversion. The diverse chemical properties of biomass with respect to source and origin (e.g., agricultural, forestry, prairies, municipal, etc.), climate and even species level, vastly influence the theoretical yield of various fuels and bio-products.

1.3.2. Objectives

The major objective of the work presented in this thesis is to define optimal pathways for bioconversion and thermochemical conversion of

lignocellulosic biomass for the production of ethanol, butanol and bio-oils as listed below. This thesis focuses on commercially available biomass (e.g., pinewood, timothy grass and wheat straw) and assesses their potential for biofuel (e.g., bio-oil, ethanol and butanol) production. The emphasis has been placed onto the five following elements:

(i) Physico-chemical and biochemical characterization of the above biomass.
(ii) Pyrolysis of the above biomass for evaluation of their bio-oil, biochar and gas yields.
(iii) In-situ study of lignin distribution and its removal during delignification and pretreatment of lignocellulosic biomass.
(iv) Dilute acid pretreatment and enzymatic hydrolysis of biomass followed by ethanol and butanol production by *Saccharomyces cerevisiae* and *Clostridium beijerinckii*, respectively.
(v) Pyrolysis of hydrolysis residues obtained from biomass pretreatment for the production of biochar, bio-oils and gases.

1.3.3. Outline

The logistics of the research progress have been illustrated in Fig. 1.3 and linked to individual chapters. Within the framework of the past and current technological development, Chapter 1 highlights an overview of the thesis with the general background knowledge and research outline.

Chapter 2 gives a comprehensive review of the literature pertaining to the current research. The chapter throws light on lignocellulosic biomass with their classification, composition and characteristics. The biomass classification in terms of forestry residues, energy crops and agricultural residues is discussed. The compositional discussion is based on cellulose, hemicellulose, lignin, extractives and inorganic components in biomass. The chapter also focuses on various

biomass pretreatment technologies for bioconversion. Conversion pathways such as biochemical and thermochemical are summarized in this chapter.

Chapter 3 is based on the physico-chemical characterization of three lignocellulosic feedstocks from forestry (pinewood), energy crop systems (timothy grass), and agriculture (wheat straw) to determine their candidacy for biofuel production. The chapter mentions various analytical tools for studying proximate and ultimate composition as well as thermogravimetric, structural and spectroscopic properties of the biomasses.

The thermochemical conversion of the three biomasses is given in Chapter 4. Both slow and fast pyrolysis of the feedstocks is highlighted for a comparative analysis of their biochar, bio-oil and gas yields. The bio-oils from both pyrolysis processes are analyzed along with biochars to determine their energy and fuel values.

Chapter 5 gives a comprehensive structural analysis of the three feedstocks during delignification and hydrothermal pretreatment. Delignification is a very essential step for effective biomass conversion to fuel alcohols. Hence, this chapter focuses on the illustrative study of lignin distribution in untreated, delignified and hydrothermally pretreated biomasses. A novel approach of chemical mapping technique is developed through Raman spectroscopy of the feedstocks as discussed in this chapter.

Chapter 6 is focused on the dilute acid and enzymatic pretreatment of the biomasses to recover fermentable sugars. Various concentrations of dilute sulfuric acid are employed on the biomasses to evaluate their sugar recovery. Furthermore, a mixture of cellulolytic enzymes is used to degrade the biomass cellulose and hemicelluloses to monomeric sugars of glucose and xylose. The biomass hydrolysates containing monomeric sugars are fermented using *S. cerevisiae* for ethanol production and *C. beijerinckii* for butanol production, respectively.

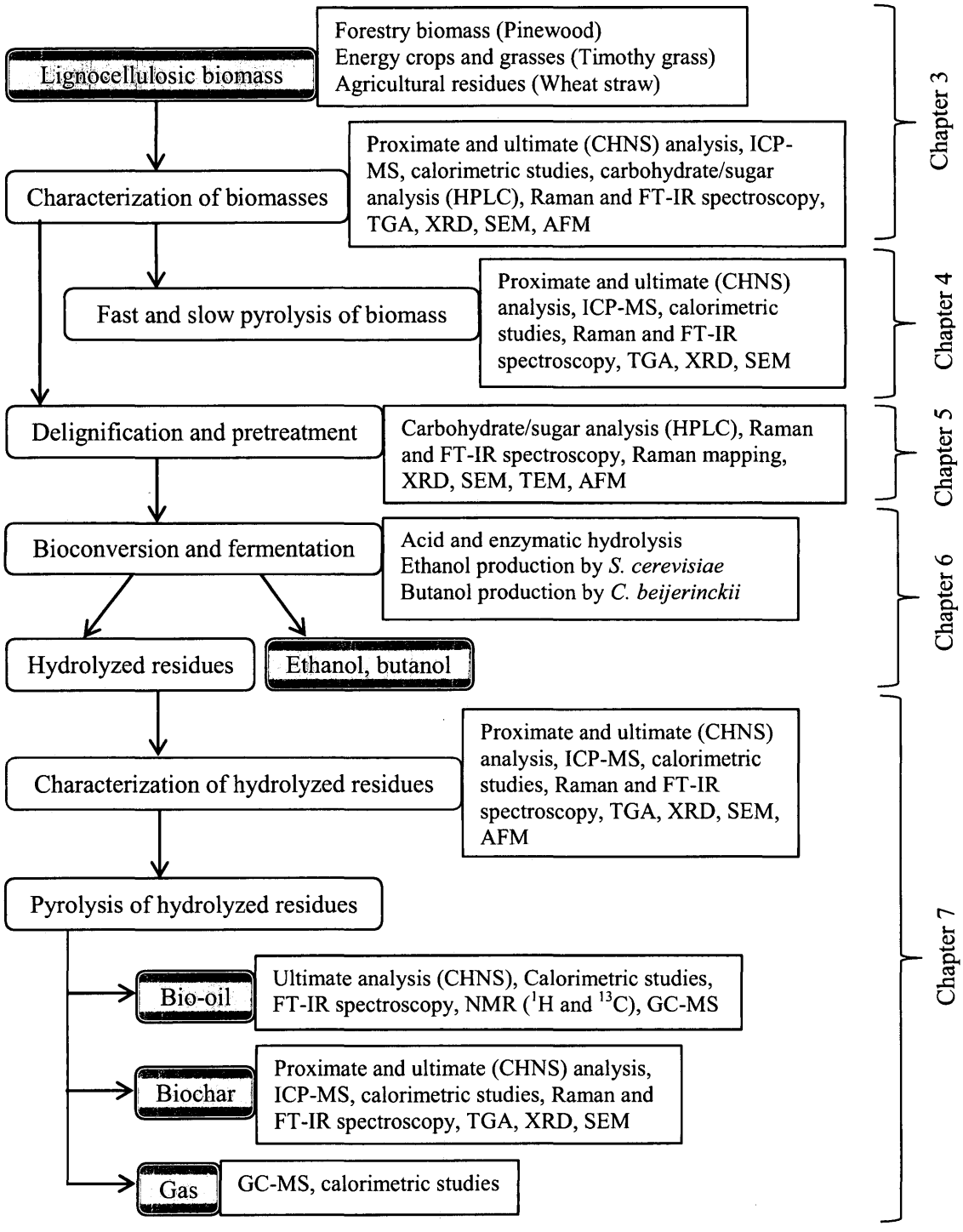

Fig. 1.3 Schematic representation of the research outline

Chapter 7 is focused on the waste valorization. As a result of pretreatment and bioconversion, a considerable amount of hydrolysis residues are generated. These residues are rich in recalcitrant carbon, although the majority of cellulose and hemicelluloses are extracted during biomass hydrolysis. In contrast to distillers grains, lignocellulosic hydrolysis residues cannot be used as livestock feed due to its relatively low nutrition value. With the rationale of their effective utilization, Chapter 7 describes the pyrolysis of hydrolysis residues to produce essential biochars, bio-oils and gases along with value-added chemicals.

Chapter 8 summarizes the major findings in the study along with addressing the developments and limitations encountered during individual phases of research. Based on these, some recommendations have been put forward that would help scale-up the processes and find solutions to some unknowns.

Finally, the contributions made in this dissertation to the existing knowledge are discussed in Chapter 9. This chapter aims to bridge the knowledge gaps and mentions several novelties brought by this study.

Chapter Two: Review of the literature

2.1. Lignocellulosic biomass assessment

Lignocellulosic feedstocks are economical resource that are abundantly available and have the capability to support the sustainable production of renewable fuels. Lignocellulosic biomass is usually classified into agricultural and forage crops (e.g., corn stover, wheat straw, sugarcane bagasse, alfalfa etc.), dedicated energy crops (e.g., timothy grass, switchgrass, hybrid poplar etc.), wood residues from soft- and hardwood (e.g., saw mill residues, paper mill discards etc.) and municipal paper waste.

The annual availability of lignocellulosic materials in USA and Canada is in the range of 6-256 and 64-561 million dry tons (MDT), respectively (Gronowska et al., 2009). The agricultural residues and energy crops comprise a larger category of biomass in USA, while the bulk category is reserved to energy crops and wood residues in Canada. The estimate for annual agricultural residue harvest in USA and Canada ranges up to 1147 MDT (Jones et al., 2007) and 2.7-18 MDT (Gronowska et al., 2009), respectively. The potential bioethanol production in Canada from agricultural residues generated by cereal crops is estimated to be between 0.3 and 4.9 billion liters per annum (Mabee and Saddler, 2010). The agricultural residue supply from USA is consistently higher than that of Canada. This is due to large areas of agricultural lands in USA which is around two and a half times more than those of Canada. This results in the production of more cereal and corn than Canada, indicating a greater residual biomass from agricultural residues and energy crops. Across Canada, the initial lignocellulosic feedstocks are cereal residues in agricultural areas and wood residues in forested regions.

Energy crops, principally switchgrass and hybrid poplar are not yet produced on a commercial scale in USA and Canada but they are an attractive next generation feedstock as they are fast growing and tolerant to a broad range of soil and climatic conditions. Moreover, there is an ease in their bulk handling and storage unlike the

first generation feedstocks (e.g., corn). This is due to presence of plant waxes on their aerial parts that significantly prevents them from decay. The annual availability of energy crops in USA and Canada ranges up to 3383 MDT (Jones et al., 2007) and 433 MDT (Yemshanov and McKenney, 2008), respectively.

The forest residue harvest in USA ranges from 60-100 MDT (Gronowska et al., 2009), whereas in Canada it is 9.8-46 MDT (Mabee and Saddler, 2010). The saw mill residues are reported to be available up to 135 MDT per annum in USA, while in Canada the range is between 3 and 17 MDT per annum (Gronowska et al., 2009). The saw mill residues include wood chips and particles that are utilized in the manufacture of commercial value-added materials and in pulp and paper industries. A kind of non-renewable lignocellulosic feedstocks is also accessible which is referred as "disturbance wood and crops" that are typically the forest and crop resources damaged by insects, pests and disease. For instance, the mountain pine beetle outbreak in the forests of British Columbia, Canada generates about 9.3-12.3 MDT of beetle-damaged wood every year (Mabee and Saddler, 2010). This has a potential to generate 2.8-3.6 billion liters ethanol per annum. Despite many benefits, most lignocellulosic biomasses are accessible seasonally by biorefineries based on their region or country of origin, which increases their cost. The cost includes those related to biomass shredding, packaging, transportation and storage.

The United States is likely to produce nearly 229 billion liters of ethanol from lignocellulosic feedstocks annually by the year 2030 (De La Torre Ugarte et al., 2007). Currently, USA and Brazil produce over 90% of world's bioethanol (Oosterveer and Mol, 2010). Today, 44% of the Brazilian energy supply is renewable and 13.5% is derived from sugarcane (Soccol et al., 2010). From the total land area available for agriculture (340 million hectares) only 0.9% is in use for sugarcane cultivation. From such a small proportion of land available for sugarcane farming, Brazil has emerged as the largest producer of sugarcane with its yearly harvest of 495 billion tons. The Brazilian production of sugarcane bagasse is currently estimated at 186 million tons per year. The sugarcane bagasse is

considered as a model feedstock for Brazilian ethanol industries as the country's bioprocessing facilities are usually annexed with the existing sugar-ethanol infrastructures. As a result of this, the bioproduction of ethanol requires lower investments, transport logistics and energy supply. Furthermore, the bagasse is generated at the industrial units that restrict the transportation costs. This has made Brazil a successful nation in utilizing 10 MDT of biomass to generate 2.3 billion liters of ethanol (Soccol et al., 2010).

2.2. Lignocellulosic biomass – composition and chemistry

Lignocellulose is a major component of plants that provides them structure and is usually present in roots, stalks and leaves. Plant cell walls are primarily made of cellulose $(C_6H_{10}O_5)_n$, hemicellulose $(C_5H_8O_4)_m$, lignin $[C_9H_{10}O_3(OCH_3)_{0.9\text{-}1.7}]_x$, pectin and glycosylated proteins (Nanda et al., 2013b). Pectins are cross-linked polysaccharides forming a hydrated gel that holds the cell wall components together. The primary functions of glycosylated proteins are in plant growth and development, physical strength, metabolite conduction and defence against pathogens. Lignocellulose forms a complex crystalline structure held together by covalent bonding, intermolecular bridges and van der Waals forces that makes it hydrophobic and robust to attack by enzymes.

A typical lignocellulosic biomass has 35-55% cellulose, 20-40% hemicellulose and 15-25% lignin (Sukumaran et al., 2010). About 90% of dry matter in lignocellulosic biomass comprises of cellulose, hemicelluloses and lignin, whereas the rest consists of extractives and ash. Extractives are regarded as non-structural biomass components that are soluble in neutral organic solvents or water. They comprise of structural biopolymers such as terpenoids, steroids, resins, fats, lipids, waxes and phenolic constituents in the form of stilbenes, flavanoids, lignans and tannins (Nanda et al., 2013b). The composition of cellulose, hemicellulose and lignin vary in different lignocellulosic feedstocks as shown in Table 2.1.

Table 2.1 Distribution of cellulose, hemicellulose and lignin in some lignocellulosic feedstocks and organic wastes

Feedstock	Cellulose	Hemicellulose	Lignin	Reference
Bagasse	41	23	18	Pauly and Keegstra (2008)
Bamboo	26-43	15-26	21-31	Sanchez (2009)
Banana waste	13	15	14	Sanchez (2009)
Barley straw	32	26	23	Naik et al. (2010)
Bast fiber jute	45-53	18-21	21-26	Sanchez (2009)
Bast fiber kenaf	31-39	22-23	15-19	Sanchez (2009)
Bast fiber seed flax	47	25	23	Sanchez (2009)
Blue gum	36	12	31	Ballesteros et al. (2004)
Coastal Bermuda grass	25	36	6	Prasad et al. (2007)
Coconut coir	48	26	18	Raveendran et al. (1995)
Coconut shell	36	25	29	Raveendran et al. (1995)
Coffee pulp	35	46	19	Sanchez (2009)
Coir pith	29	15	31	Raveendran et al. (1995)
Corn cobs	45	35	15	Prasad et al. (2007)
Corn stalks	43	24	17	Raveendran et al. (1995)
Corn stover	40	22	18	Kim et al. (2003)
Cotton gin waste	78	16	-	Raveendran et al. (1995)

Cotton seed hair	80-90	5-20	-	Prasad et al. (2007)
Elephant grass	22	24	24	Sanchez (2009)
Esparto grass	33-38	27-32	17-19	Sanchez (2009)
Ethiopian mustard	33	14	19	Ballesteros et al. (2004)
Flax straw	29	27	22	Naik et al. (2010)
Grasses	25-40	25-50	10-30	Malherbe and Cloete (2002)
Groundnut shell	36	19	30	Raveendran et al. (1995)
Hardwood bark	22-40	20-38	30-55	Malherbe and Cloete (2002)
Hardwood stem	40-50	24-40	18-25	Prasad et al. (2007)
Leaves	15-20	80-85	-	Prasad et al. (2007)
Millet husk	33	27	14	Raveendran et al. (1995)
Newspaper	40-55	25-40	18-30	Prasad et al. (2007)
Nut shells	25-30	25-30	30-40	Prasad et al. (2007)
Oat straw	31-37	27-38	16-19	Sanchez (2009)
Orchard grass	32	40	5	Sanchez (2009)
Pinewood	39	24	20	Nanda et al. (2013c)
Poplar wood	35	17	26	Ballesteros et al. (2004)
Rice husk	31	24	14	Raveendran et al. (1995)
Rice straw	37	23	14	Raveendran et al. (1995)
Rye grass (early leaf)	21	16	3	Sanchez (2009)

Rye grass (seed setting)	27	26	7	Sanchez (2009)
Rye straw	33-35	27-30	16-19	Sanchez (2009)
Sabai grass	-	24	22	Sanchez (2009)
Softwood stem	45-50	25-35	25-35	Malherbe and Cloete (2002)
Subabul wood	40	24	25	Raveendran et al. (1995)
Sorted plant refuse	60	20	20	Prasad et al. (2007)
Sweet sorghum bagasse	45	25	18	Ballesteros et al. (2004)
Switchgrass	45	31	12	Sanchez (2009)
Timothy grass	34	30	18	Nanda et al. (2013c)
Wheat straw	39	24	16	Nanda et al. (2013c)

The biomass is a heterogeneous mixture of both organic and mineral composites (Vassilev et al., 2010). The mineral matter in biomass includes both major elements (e.g., Na, Mg, K, Ca and Si) and minor elements (e.g., Al, Fe, Mn, P and S). Furthermore, the chemical composition of biomass is influenced by the plant's genetic and environmental factors that vary considerably (Nanda et al., 2013c; Malherbe and Cloete, 2002).

Cellulose is a glucose polymer consisting of β-1,4 linked D-glucose subunits with an average molecular weight of around 100,000 that are synthesized at the plant cell membrane and aggregate by H-bonding and van der Waals forces. These H-bonding and van der Waals forces contribute to the stability of cell wall. Cellulose is a straight chain polymer derived from the dehydration of glucose ($C_6H_{12}O_6$) molecules. Cellobiose is the repeat unit of cellulose and its molecular weight is approximately 30,000. The linear nature of cellulose molecules makes them able to form both intra and inter molecular hydrogen bonding. Cellulose contains both amorphous and crystalline regions alternating with each other in the form of microfibrils. Because of the fibrous nature and strong hydrogen bonding cellulose is found to be insoluble in majority of the solvents (Sjostrom, 1993).

Hemicellulose is a mixture of polysaccharides composed of pentose and hexose sugars such as glucose, mannose, xylose and arabinose as well as sugar acids such as methylglucuronic and galaturonic acids. The individual pentose and hexose sugar molecules polymerize to form hemicellulose. The degree of polymerization for hemicelluloses is predicted to be nearly 200. Consequently, the molecular weight of a hemicellulose molecule is much lower than a cellulose molecule, precisely < 30,000. The main components of hemicellulose are glucose, galactose, manose, xylose, arabinose and glucuronic acid (e.g., carboxylic acid). Unlike cellulose that requires severe hydrolysis conditions for denaturation to simple glucose units due to its crystalline structure, hemicellulose is relatively easy in denaturation using acids, bases or enzymes.

Lignin is a phenyl propane polymer linked with ester bonds that acts as glue and tightly binds with cellulose and hemicellulose. The lignin fraction of biomass consists of macromolecules that contain phenolic substances those are highly branched. The phenyl propane units in lignin are joined by ether (C–O–C) and C–C linkages. The C–O–C linkages are higher than the C–C linkages in lignin. Lignin is also known to contain methoxyl, phenolic, hydroxyl and terminal aldehyde groups in the side chain with limited solubility in most solvents. The average molecular weight of lignin is in the order of 20,000.

The presence of lignin in biomass makes it difficult to obtain cellulose and hemicellulose to produce fermentable sugars. During the degradation process, lignin can form furan compounds that could inhibit fermentation. Generally, softwoods are reported to have higher lignin content than hardwoods. In contrast, hardwoods have a greater amount of holocellulose (i.e., sum of cellulose and hemicellulose) and extractives than softwoods (Demirbas, 2006).

2.3. Pretreatment technologies for lignocellulosic biomass

The production of biofuels from lignocellulosic feedstocks can be achieved through two major processing pathways, namely biochemical and thermochemical. In the biochemical pathway, the enzymes and microorganisms are used to convert the cellulosic and hemicellulosic sugars to alcohols. The thermochemical pathway involves thermal degradation of lignocellulosic materials through pyrolysis, gasification, liquefaction, torrefaction and supercritical water conversion. Although, the chief product in most thermochemical conversions is bio-oil, certain amount of biochar and gases are also obtained depending on the operating conditions. The major focus in this thesis is on the ethanol and butanol production through biochemical conversion and bio-oil and biochar production through pyrolysis. Figure 2.1 illustrates the pathways and sub-pathways for lignocellulosic biomass conversion to biofuels.

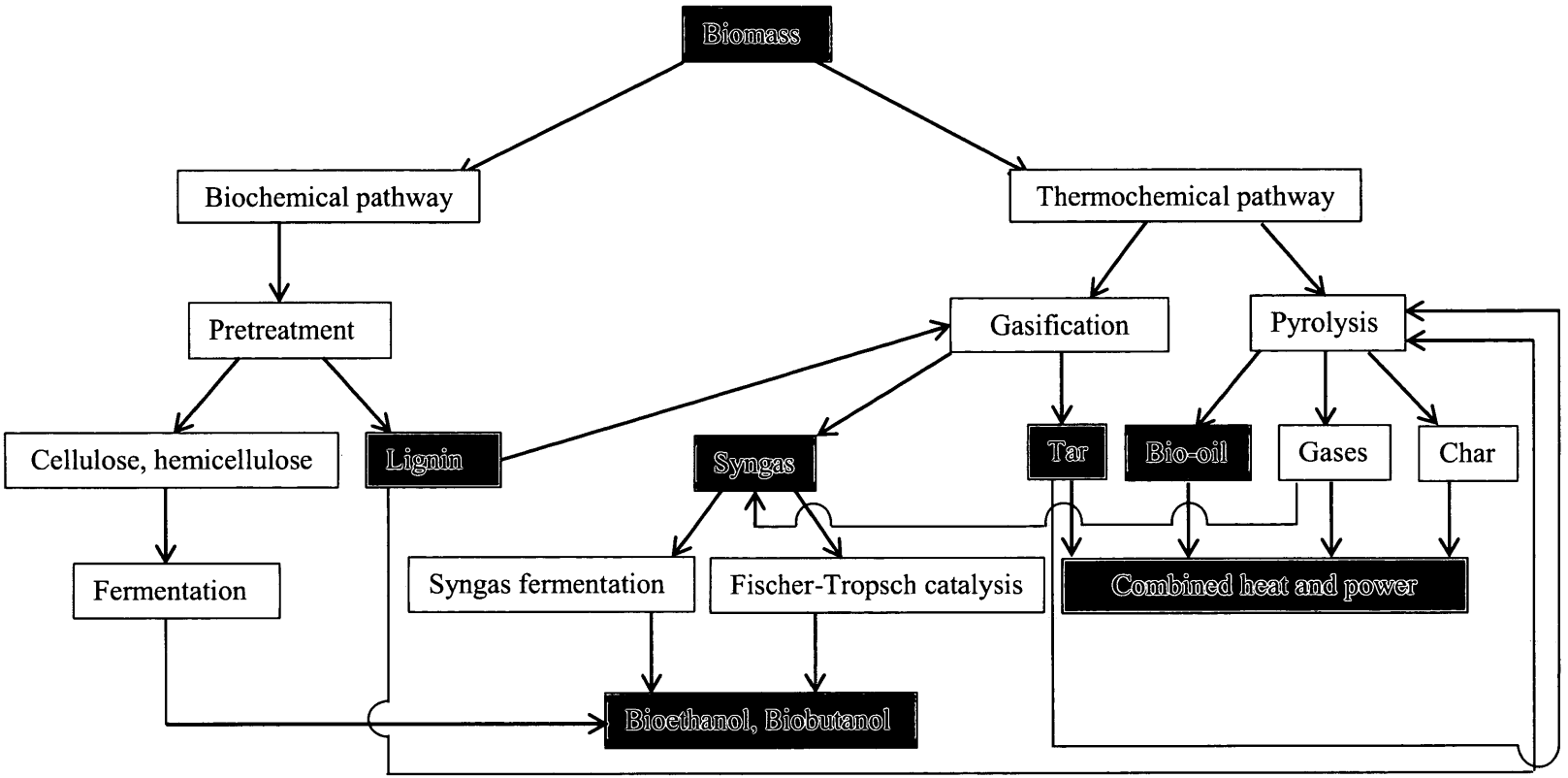

Fig. 2.1 Lignocellulosic biomass conversion to alcohols and bio-oils by biochemical and thermochemical pathways

The bioconversion of lignocellulosic requires: (i) delignification to liberate cellulose and hemicellulose from the complex with lignin, (ii) depolymerization of the carbohydrate polymers to produce free sugars, and (iii) fermentation of mixed hexose and pentose sugars to ethanol. The initial step is separation of cellulose and hemicellulose from lignin followed by hydrolysis. The presence of five sugars (e.g., glucose, galactose, mannose, xylose and arabinose) found within cellulosic materials makes it relatively difficult for hydrolysis compared to starch, which is associated with the single sugar (glucose). A suitable pretreatment of biomass is necessary to ensure good yields of sugars from the polysaccharides. Pretreatment disrupts the plant cell wall and improves enzymatic access to the polysaccharides as raw and untreated biomass is usually resistant to enzymatic degradation (Kumar et al., 2009).

2.3.1. Physico-chemical pretreatment

It is very important for any pretreatment technology to be effective on biomass particles with increased surface area. This is mostly achieved by chipping, grinding and milling the biomass to reduce their particle size. This not only increases the surface area of the biomass but also reduces the crystallinity of cellulose for better hydrolysis. There are a number of pretreatments available today and are mostly categorized into physico-chemical, thermochemical and biological pretreatments (Kumar et al., 2009). Some of the physico-chemical pretreatments include ammonia fibre explosion (AFEX), ozonolysis and organosolv process. In AFEX, lignocellulosic biomass is exposed to liquid NH_3 at high temperature (60-200°C) and pressure (1.4-4.8 MPa) for certain time intervals (10-60 min) that causes biomass breakdown and removal of lignin. Although, AFEX can significantly improve the saccharification rates, yet it is not efficient for biomass with high lignin content. On the other hand, ozonolysis uses ozone to degrade lignin and hemicellulose in biomasses. The process is carried out at room temperature and requires considerable amount of ozone.

In the organosolv process, water and dissolved organic solvents such as ethanol, methanol and acetone in combination with an acid at 180-200°C solubilize the lignin and hydrolyze the hemicellulose (Zhao et al., 2009; Pan et al., 2006). The major drawback of this pretreatment is the production of furfurals that may inhibit subsequent processes and result in lower recovery of pentose sugars. Furfural is a significant inhibitor of ethanol production from hemicellulose hydrolysate and even its low concentrations of 3-15 mM can adversely affect the ethanol production rates (Zaldivar et al., 1999).

Chemical pretreatments deal with the use of acids and bases. Acid hydrolysis employs concentrated and diluted sulphuric acid or hydrochloric acid to treat the lignocellulosic biomass. Dilute acids have replaced the concentrated acids in biomass hydrolysis due to the fact that concentrated acids are: (i) hazardous to handle and need reactors resistant to corrosion, (ii) required to be recovered after biomass digestion to make the process economically feasible and (iii) less efficient in achieving high reaction rates than dilute acids. Moreover, certain undesirable components are found in biomass hydrolysates produced from concentrated acids that are inhibitory to fermentation. These components include sugar degradation products (e.g., furfural, hydroxymethylfurfural or HMF, levulinic acid), hemicellulose degradation products (e.g., acetic acid, ferulic acid, glucuronic acid, *p*-coumaric acid) and lignin breakdown products (e.g., syringaldehyde, syringic acid).

Alkaline hydrolysis uses bases such as NH_4OH or NaOH. However, this pretreatment is expensive and the recovery and recycling of bases from the system is often difficult (Mosier et al., 2005; Wyman et al., 2005). Among all bases, NaOH is widely used because it improves cellulose digestion (Correa et al., 2010). Alkaline hydrolysis of lignocellulosic biomass depends on its lignin content and overrules acid hydrolysis in degrading lesser sugars with easy recovery of caustic salts.

2.3.2. Thermochemical pretreatment

Boiling of lignocellulosic biomass in liquid hot water is a traditional thermochemical pretreatment, commonly known as cooking of biomass. During this process, a phase of high pressure with hot water (200-230°C) enhances elevated recovery rates for pentose sugars (Tomas-Pejo et al., 2008). About 40-60% of the total biomass gets dissolved during boiling with a recovery rate of 4-22% cellulose, 35-60% lignin and 100% hemicellulose (Garrote et al., 1999).

Steam explosion is a type of thermochemical pretreatment in which chipped biomass is treated with high-pressure saturated steam (160-260°C) with a swift reduction in pressure. The reduction in pressure causes the organic material to undergo an explosive decomposition including hemicellulose degradation and lignin transformation, thus enhancing the cellulose hydrolysis. During the operation there is a disruption of the lignin-carbohydrate matrix that generates compounds inhibitory to microorganisms in downstream processing (McMillan, 1994).

Supercritical fluids are a novel advancement in thermochemical pretreatment of biomass. A compound above its critical temperature and critical pressure but below the pressure required to condense it into a solid is called supercritical fluid. Some commonly investigated supercritical fluids are CO_2 and water. Water at a pressure and temperature higher than its critical point (i.e., 22.1 MPa and 374°C) is known as supercritical water (SCW). SCW has gas-like viscosity and liquid-like density, providing better mass transfer and solvation properties for biomass (Girio et al., 2010). Near the critical point, the ionic product of water increases considerably which makes it behave as a weak polar solvent to hydrolyze many compounds catalyzed by its ions (H^+ and OH^-) and dissolve organic substances (Ehara and Saka, 2005). Such conditions facilitate complete separation of hemicellulose from the lignocellulosic network and significantly enhance their enzymatic digestibility.

In most thermochemical pretreatments, there is a generation of inhibitory byproducts such as furfural, hydroxymethylfurfural and acetic acid that have adverse effects on enzymatic hydrolysis and fermentation. Hence, it is essential to employ enzymes and microorganisms that are resistant to such inhibitory compounds or to minimize their production levels and implement additional steps to eliminate them. Most of the physico-chemical and themochemical pretreatments result in a reduced yield of fermentable sugars due to their extreme treatment conditions (Shi et al., 2009).

Additionally, these pretreatments necessitate high energy, high pressure and corrosion resistant reactors and generate acidic or alkaline waste residues that require certain pre-disposal procedures to ensure environmental safety which increases their overall operational costs. In contrast, biological pretreatment is a benign substitute that is accomplished by microorganisms for degrading hemicelluloses, followed by the production of cellulases and other fermentative enzymes. The most widely used lignocellulosic biomass pretreatments are dilute acid and enzymatic hydrolysis. The benefits and limitations of these pretreatments are summarized in Table 2.2.

2.3.3. Biological pretreatment

Saccharification is the process of breaking down of a complex carbohydrate (e.g., starch or cellulose) into its monosaccharide components. During hydrolysis, cellulose is degraded by cellulase enzyme to produce monomeric sugars that are fermented to ethanol by microorganisms. Compared to other pretreatments, the operational cost of enzymatic hydrolysis is low but the process is time intensive. In addition, the process involves mild reaction conditions (e.g., pH 4.8 and temperature of 45-50°C) and does not have a corrosion problem with reactors (Duff and Murray, 1996).

Table 2.2 Advantages and disadvantages of acidic and enzymatic pretreatments

Pretreatment	Advantages	Disadvantages
Dilute acid	(i) Lower consumption of acids (ii) Short reaction time (iii) Acid recovery usually not required (iv) Lesser amount of inhibitory products	(i) High temperature required (ii) Ineffective for cellulose hydrolysis (iii) Might need neutralization of hydrolysate
Concentrated acid	(i) Low temperature required (ii) Higher yield of sugars	(i) Corrosion of reactor (ii) Higher consumption of acids (iii) Higher amount of inhibitory products (iv) Longer reaction time (v) Acid recovery required (vi) Extra energy and cost involved
Enzymatic	(i) Mild reaction conditions (40-50°C, pH 4.5-5.0) (ii) Higher yield of sugars (iii) No formation of inhibitors	(i) Longer reaction time (several days) (ii) Costly process due to involvement of enzymes (iii) Feedstock pretreatment required

References: Garcia et al. (2011); Taherzadeh and Karimi (2007a, b)

The pretreatment of biomass removes the lignin, hydrolyzes the hemicellulose and de-crystallizes the cellulose. As a result of the de-crystallization of cellulose, cellulase enzymes gain increased access to the cellulose fibres (Hu and Ragauskas, 2012). Microorganisms involved in ethanol production from lignocellulosic feedstocks include delignifiers (e.g., fungi) and cellulase producers (e.g., fungi, yeast and bacteria). Plant cell wall degrading enzymes occur in cellulosomes that are found in anaerobic bacteria and fungi. In contrast, the aerobic microorganisms produce discrete enzymes secreted into their growth media as secondary metabolites (Gray et al., 2006). The production and regulation of cellulases and hemicellulases in microorganisms has been extensively investigated. The widely used industrial cellulases are obtained from *Trichoderma reesei* and *Saccharomyces* spp. with optimal catalytic conditions at pH 4.5 and temperature 55°C and 37°C, respectively.

Cellulases comprise three types of hydrolytic enzymes: (i) endoglucanases which attack regions in cellulose fibre with low crystallinity creating free chain ends, (ii) exoglucanases (i.e., cellobiohydrolases) which further degrade the molecule by removing cellobiose units from the free chain ends, and (iii) β-glucosidases which hydrolyze soluble cellobiose to produce glucose. Hemicellulases include glucuronidase, acetylesterase, xylanase, β-xylosidase, galactomannanase and glucomannanase. Hemicellulases aid in cellulose hydrolysis by exposing the cellulose fibres making them more accessible for saccharification. The application of hemicellulase depends on the pretreatment method. In the case of dilute acid pretreatment, most of the hemicelluloses are removed before saccharification (Gray et al., 2006). However, with non-acid pretreatment methods the hemicellulose fraction remains intact requiring hemicellulases for hydrolysis (Mosier et al., 2005). In enzymatic hydrolysis, substrate inhibition may be a factor affecting saccharification. Unlike conditions of low substrate levels, where an increase in substrate concentration results in an

increased yield and hydrolysis, high substrate concentration often cause substrate inhibition which substantially lowers the hydrolysis rate.

White rot fungi are the most effective basidiomycetes used for bioconversion of lignocellulogic biomass. *Phanerochaete chrysosporium*, a white rot fungus, produces lignin-modifying enzymes, such as lignin peroxidases and manganese-dependent peroxidises as a response to carbon or nitrogen limitation during their secondary metabolism (Boominathan and Reddy, 1992). The peroxidase enzyme can catalyze lignin biodegradation in presence of H_2O_2 (Azzam, 1989). The lignin-modifying enzymes have found many applications in the degradation of wood cell walls.

2.4. Bioconversion of lignocellulosic biomass

2.4.1. Bioethanol production

Microorganisms for ethanol bioproduction can be assessed in terms of the process parameters, nutritional requirements, compatibility with existing products, type of fermentation and equipment. Diverse groups of microorganisms have been employed in the fermentation of lignocellulosic biomass to ethanol. An ideal microorganism for ethanol production should have: (i) ethanol yield of more than 90% of theoretical estimation, (ii) ethanol productivity of more than 1 g/L/h, (iii) ethanol tolerance of more than 40 g/L, (iv) robust metabolic characteristics with simple growth requirements preferably through inexpensive media formulation, (v) ability to grow in undiluted hydrolysates, (vi) growth conditions to retard contaminants, and (vii) resistance to inhibitors, acidic pH and higher temperatures (Dien et al., 2003).

Fungi, principally many yeast species, are well-known for ethanol production. For bacterial strains to be more efficient than yeast in ethanol production, the former should: (i) be able to produce ethanol reliably in larger bioreactors, (ii) greatly reduce needs for saccharification enzymes, and (iii) be able to ferment the media in bulk even though not fully aseptic. Some notable fungi belonging to genera

Neurospora, *Monilia*, *Paecilomyces*, *Fusarium*, *Sclerotium*, *Phanerochaete*, *Trichoderma*, *Aspergillus*, *Schizophyllum* and *Penicillium* are reported to have the ability to ferment cellulose directly to ethanol (Duff and Murray, 1996). The yeast *Schizosachharomyces pombe* has a characteristic feature of resisting a high osmotic pressure within the fermenter (Fukuda et al., 2009).

Saccharomyces cerevisiae is one of the model organisms in industrial ethanol production with a relatively high ethanol tolerance and growth in limiting oxygenation conditions. A major drawback in using *S. cerevisiae* is that it is unable to ferment hemicellulose sugars, mostly xylose. However, it can ferment xylulose and in the presence of xylose isomerase, xylose is converted to xylulose which is then fermented to ethanol. Over the last five decades, aerobic fungus *Trichoderma reesei* has gained attention in research yielding cellulases for ethanol production. *T. reesei* secretes three types of extracellular cellulolytic enzymes that include five endoglucanases, two cellobiohydrolases and two β-glucosidases. Cellobiohydrolases are of special interest as they tend to constitute 60-80% of natural cellulase systems. *T. reesei* is also known for its xylanolytic activities to degrade hemicellulose by secreting two endo-β-xylanases- xylanase I and xylanase II. Besides *T. reesei*, *Aspergillus oryzae* is an efficient xylan degrading fungi with its β-xylosidase production.

A few bacteria and actinomycetes that have been explored for production of cellulase enzymes include *Clostridium*, *Cellulomonas*, *Bacillus*, *Ruminococcus*, *Bacteriodes*, *Erwinia*, *Acetovibrio*, *Microbispora* and *Streptomyces* (Bisaria, 1991). *Thermomonospora fusca* is an aerobic filamentous bacteria having the ability to produce β-1,4-endoglucanases, endo- and exo-cellulase, and xylanases. *Ruminococcus albus* is an anaerobic cellulolytic rumen bacterium that produces highly active cellulolytic enzymes and in which β-glucosidase catalyzes the hydrolysis of cellobiose and cello-oligosaccharides during the final degradation of cellulosic materials (Prasad et al., 2007). Thermophilic anaerobic bacteria are advantageous over the conventional yeasts in ethanol production for their capability

to withstand extreme temperatures and utilizing a variety of inexpensive feedstock but their low ethanol tolerance (< 2%, v/v) is a major impediment in fermentation (Georgieva et al., 2007).

Biofuel yields from lignocellulosics vary significantly among feedstocks. Some studies have shown that bioconversion is dependent upon the chemical nature of the feedstock and that the easiest bioconversions are achieved with herbaceous residues. Compared to woody biomass, agricultural residues have a higher surface area and small pore size which reduces their susceptibility to enzymatic hydrolysis (Houghton et al., 2004). In contrast to softwood residues, hardwood biomass has more cellulose and less hemicellulose which produce more glucose and xylose for easier bioconversion (Biely and Kremnicky, 1998). In addition, the hemicellulose of hardwood contains more xylose which is difficult to hydrolyse than other pentose sugars by naturally occurring yeast species.

2.4.2. Biobutanol production

Butanol, especially *n*-butanol is a four carbon primary alcohol that is recently gaining attention as a gasoline substitute to be used in pure or blended form. Butanol is considered to have superior fuel properties than ethanol that makes it a better replacement for gasoline (Table 2.3). The energy content of butanol (29.2 MJ/L) is 30% higher than that of ethanol (21.2 MJ/L) and 10% less than gasoline (32.5 MJ/L). On the other hand, the octane ratings (research octane number, RON and motor octane number, MON) of butanol are much closer to gasoline indicating similar fuel properties. Octane rating is a standard measure of the performance of a fuel. The higher the octane number, more compression the fuel can withstand before detonating and vice versa. RON and MON are determined by running the fuel in a test engine with variable compression ratios at 600 and 900 rpm engine speeds, respectively (Dabelstein et al., 2007). With the current vehicle engines, fuel specifications require minimum values both for RON and MON. In addition, air-fuel ratio is the mass ratio of air to fuel inside an

internal combustion engine. It is an important measure for anti-pollution and fuel performances.

With the fuel properties of butanol and gasoline being closer to each other, the former has a tendency to be used in the existing vehicle engines in pure form without any modification. In addition, the high crude oil prices and increasing concerns over global warming have renewed interest in the biotechnological production of butanol as an alternative fuel. For instance, a number of companies such as British Petroleum and DuPont have reflected this interest in their facilities. Recently, both the companies have announced a joint effort to develop a commercial fermentative butanol process (Durre, 2008). Many other companies such as Green Biologics, UK are also aiming to commercialize of biobutanol production (Green Biologics, 2013).

Table 2.3 Fuel properties of ethanol, butanol and gasoline

Property	Gasoline	Ethanol	Butanol	Reference
Calorific value (MJ/L)	32.5	21.2	29.2	Durre (2007)
Air-fuel ratio	14.6	3.0	11.2	Durre (2007)
Research octane number	91-99	129	96	Lee et al. (2008)
Motor octane number	81-89	102	78	Lee et al. (2008)
Heat of vaporization (MJ/kg)	0.4	0.9	0.4	Lee et al. (2008)

The biotechnological production of butanol for fuel and/or chemical is achieved through the ABE (acetone-butanol-ethanol) fermentation. Butanol production through ABE fermentation is carried out using *Clostridium* spp., particularly *C. acetobutylicum* and *C. beijerinckii*. The process is biphasic involving acidogenesis, i.e. production of acids (acetic and butyric acid) followed by solventogenesis, i.e. production of solvents (ABE). The typical production ratio of ABE is 3:6:1 (Jones and Woods, 1986). Clostridia are able to metabolize both pentose and hexose sugars in the biomass hydrolysates which makes them

advantageous over ethanol-producing *S. cerevisiae* that lag behind in pentose utilization (Qureshi et al., 2007).

C. acetobutylicum is the most widely studied of all butanol-producing clostridia. The bacterium typically results in butanol production with acetate, butyrate, acetone, butanol and ethanol as the liquid products, along with CO_2 and H_2 as the gaseous products (Fig. 2.2). The two phases of product formation, i.e. acidogenic phase and solventogenic phase are shown in the figure. The acidogenic phase mostly occurs during the lag phase of bacterial growth. However, the clostridia undergo a major shift in their metabolism during the end of lag phase (Gottwald and Gottschalk, 1985). Due to the formation of acetic acid and butyric acid, the pH of the fermentation medium lowers which inhibits the bacterial growth (Huang et al., 1985). As a result, the organism slows down acid production and utilizes the excreted acetic and butyric acids for converting them to acetone and butanol.

Considerable amounts of acetic and butyric acids remain undissociated to acetone and butanol, which start diffusing into the cytoplasm (Durre, 2008). This causes the proton gradient between inside and outside the cell to collapse causing cell death. Under normal conditions for cell survival, the proton gradient is higher outside the cell than inside. On the other hand, prior to the cell death through collapsing of the proton gradient, the produced butanol has adverse effect on the clostridia (Moreira et al., 1981). The accumulated butanol damages the cell membranes and some membrane proteins (Bowles and Ellefson, 1985). Hence, it is the normal metabolism of the bacteria that prevents it from utilizing all of the produced acids and remaining substrates to ABE. However, as a response to higher butanol concentrations, the bacteria synthesises endospores for survival (Durre, 2008), although that does not retrieve its ability to produce acetone and butanol from acetate and butyrate, respectively. This is a major disadvantage of biological butanol production process which results in very low final product yields and high residual substrate levels.

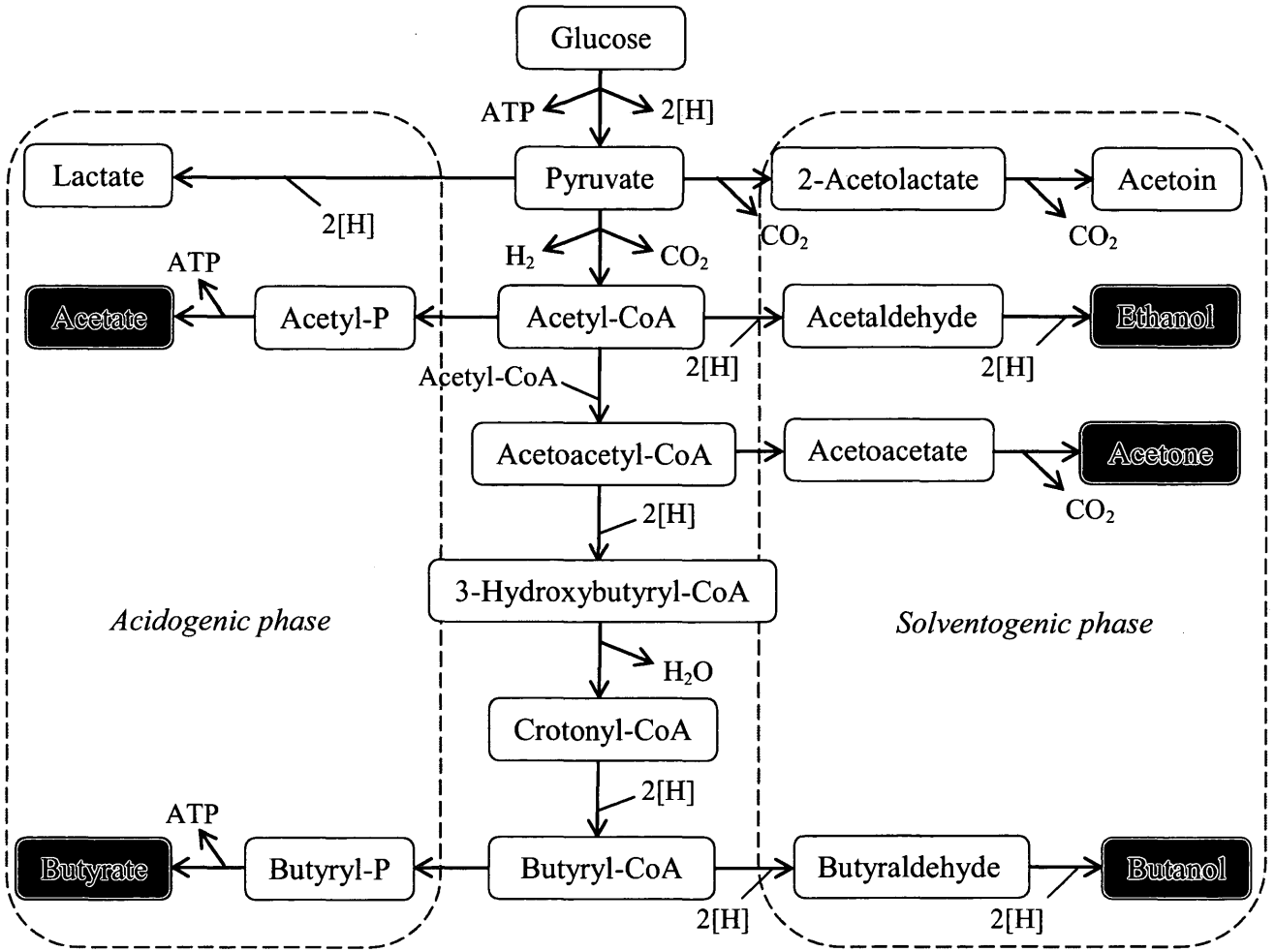

Fig. 2.2 ABE fermentation pathway followed by *Clostridium acetobutylicum*

The butanol toxicity is one of the major barriers for commercial production of butanol. Butanol-producing *Clostridium* spp. rarely tolerate more than 2% butanol (Lin and Blaschek, 1983). However, process engineering such as simultaneous removal of produced butanol from the fermentation medium through separation techniques such as membrane separation and gas stripping technologies could prevent product inhibition (Liu and Qureshi, 2009). Furthermore, the amendment of such technologies adds a major proportion of cost to the overall process economics (Qureshi and Blaschek, 2001).

2.4.3. Thermochemical conversion of lignocellulosic biomass

Thermochemical conversion has been defined as the chemical reforming process that converts long-chain organic compounds from the biomass into short-chain oxygenated hydrocarbons (Briens et al., 2008). The thermochemical conversion of lignocellulosic feedstocks is achieved mostly through pyrolysis and gasification. These are considered as the major thermochemical technologies for bio-oil and syngas production. Pyrolysis is defined as the degradation of macromolecular organic materials at elevated temperatures in the absence of oxygen. Pyrolysis can be divided into three basic types, namely slow (or conventional), fast and flash pyrolysis. These types of pyrolysis are performed by selectively varying the reactor conditions, especially operating temperature, heating rate, feedstock particle size and residence time (Mohanty et al., 2013).

Slow pyrolysis is usually performed at 300-700°C with a slow heating rate of 0.1-1°C/s and a solid residence time of 10-100 min, resulting in considerable amount of biochars (Bridgwater and Peacocke, 2000). Fast pyrolysis which operates at 400-600°C at a high heating rate of 10-200°C/s and residence time of 0.5-5s mostly yields bio-oils. Similarly, flash pyrolysis which results in significant amounts of bio-oils with reduced biochar and gas yields, operates at temperatures of 800-1000°C with heating rates above 1000°C/s and residence time less than 0.5 s. Fast and flash pyrolysis mostly result in about 50 and 75

wt.% bio-oils, 20 and 12 wt.% biochars and 30 and 13 wt.% gas products, respectively (Bridgwater and Peacocke, 2000). In contrast, bio-oil, biochar and gas yields from slow pyrolysis are around 30, 35 and 35 wt.%, respectively.

The organic vapor resulting from pyrolysis is a complex mixture of aerosols, mist, particulate matter and non-condensable gases. Pyrolysis of biomass leads to both primary and secondary reactions during the vapor release process. Primary reactions result in gas evolution from the biomass, which is quickly quenched during the condensation process. High vapor condensation efficiency at a fast rate is essential for enhanced quality and quantity of bio-oil. A low rate of vapor condensation results in secondary reactions that cause lower yields of bio-oil due to the release of non-condensable gases and water vapor. Secondary reactions usually lead to the formation of higher molecular weight compounds such as tar. Tars tend to plug the condenser lines and hence increase the shutdown frequency of the reactor which is a major issue in the refineries. The tar and other heavy compounds produced could be further recycled through pyrolysis for cracking into useful chemical compounds or used for combined heat and power (CHP) (see Fig. 2.1).

In general, slow pyrolysis with low to medium heating rates has been used for production of biochar targeted for adsorbent and solid fuel applications. Biochar also acts as a soil fertilizer as it contains alkali (e.g., Li, Na and K) and alkaline (e.g., Ca, Mg and Ba) earth metals. Unlike slow pyrolysis biochar, ash content of the fast pyrolysis biochar tends to be high because of its higher reactor temperatures and smaller biomass particle size requirements. This makes fast pyrolysis less valuable for biochar production. Currently, fast pyrolysis is the major pyrolysis process geared towards producing bio-oils as an alternative to the exhausting fossil fuel reserves. Flash pyrolysis is performed at high heating rates (10-100°C/s) with shortest residence times (< 1 s).

Bio-oil is a complex mixture of oxygenated aliphatic and aromatic compounds. It is an oxygenated hydrocarbon fuel that is known to recover 80% of

the energy content (maximum yield) from the feedstocks on a dry matter basis assuming that the biochars and gases are utilized in the pyrolysis process for heat generation. Moreover, bio-oil has almost half the high heating value of hydrocarbon fuels (petroleum: 42-44 MJ/kg) because of its high oxygen and water content. Removal of moisture and oxygen from bio-oils through upgradation techniques such as catalytic hydrodeoxygenation is found to enhance its heating value and other fuel properties (Boucher et al., 2000).

During pyrolysis, the polymeric components of biomass such as cellulose, hemicellulose and lignin undergo a series of complex thermal degradation reactions. Cellulose and hemicellulose undergo cycloreversion and dehydration reactions followed by transglycosylation. Both low molecular and high molecular weight compounds are formed during this holocellulosic decomposition. Bio-oil from lignocellulosic biomass is a heterogenous mixture of thermochemical derivatives from cellulose, hemicellulose and lignin (Joshi and Lawal, 2012). The pyrolysis liquid consists of organic and aqueous-rich fractions. These fractions are usually produced from the condensation process during biomass pyrolysis. Aqueous-rich fraction is termed as an acid phase, whereas the organic-rich fraction is termed as an oil phase. Oil phase consists mostly of phenolic and carbonyl compounds. Aqueous phase of the pyrolysis liquid consists mostly of water, acids and a small concentration of low molecular weight compounds such as aldehydes, ketones, alcohols and ethers (Boucher et al., 2000).

A significant fraction of non-condensable gases (e.g., H_2, CO, CO_2, CH_4, C_2H_4 and C_2H_6) are obtained from all pyrolysis processes. This is due to the secondary reactions that occur during the mass transfer process catalyzed by char fines and other forms of particulate matter. The non-condensable gases could be recycled for heat recovery during the pyrolysis process. The pyro-gases produced from pyrolysis could be used for CHP or recycled for process heat. These gases can also be converted to ethanol through gas-to-liquid technologies such as syngas fermentation and Fischer-Tropsch catalysis.

Recently, syngas fermentation has been found to be a bridge between the thermochemical and biochemical conversions. Fermentation of syngas to facilitate ethanol production requires acetogens which are capable of producing ethanol (solventogenic phase) over acetic acid (acidogenic phase). Acetogenic bacteria are able to generate acetate as a product of anaerobic respiration through acetogenesis. Acetogens are anaerobic in nature and mostly use CO_2 as carbon source and H_2 as energy source. A few mesophillic bacteria such as *Acetobacterium woodii*, *Clostridium carboxidivorans*, *Peptostreptococcus* spp., *Clostridium aceticum*, *Clostridium ljungdahlii*, *Clostridium carboxydivorans*, *Clostridium ragsdalei* and *Clostridium autoethanogenum* have been found to be useful in fermenting syngas to liquid fuels more effectively than the conventional catalytic process (Mohammadi et al., 2011; Heiskanen et al., 2007; Henstra et al., 2007).

Conversion of gaseous products (mostly CO and H_2) to alcohol-based fuels by using catalysts is known as Fischer-Tropsch catalysis. The biomass gasification products after purification are required to be adjusted for their H_2/CO ratio (~1-4) which is usually done via water-gas shift reaction. The syngas with specified ratio in the presence of suitable catalysts undergo various reactions to produce ethanol, butanol, higher alcohols and hydrocarbons (Dry, 2004).

2.5. Conclusions

A variety of biochemical and thermochemical conversion pathways of lignocellulosic biomass to alcohols (ethanol and butanol) and bio-oils have been discussed. Prior to the bioconversion of lignocellulosic biomass, an appropriate pretreatment procedure is critical to disrupt the plant cell wall and improve the enzymatic access to polysaccharides. This ensures an efficient release of fermentable sugars from the degradation of cellulose and hemicelluloses. This chapter gives an overview to choose the best combination of the viable pretreatment and fermentation methods for ethanol and butanol production from lignocellulosic biomass. In

addition, different pyrolytic routes involving slow and fast heating rates have been presented offering flexibility in the selection based on the desired product. For instance, the conversion of lignocelluoses to bio-oils requires a fast heating rate, whereas their conversion to biochars requires a slow heating rate pyrolysis. Furthermore, the flexible feed ratio of pyro-gases makes the potential syngas fermentation attractive to use the industrial off-gases as the feed gas for bioethanol production. Regardless of the conversion pathways, the future of biofuels as an alternative renewable fuel appears very bright because of the exhausting supplies of fossil fuels and booming demand for sustainable energy sources.

Chapter Three: Chemical characterization of lignocellulosic biomass: Determination of candidacy for biofuel production

3.1. Introduction

The climate change and depleting fossil fuel supplies are issues of acute concern for most countries in the world today. This projection throws light on waste plant biomass to view it as a means of achieving energy security and reducing GHG emissions. On the other hand, the use of lignocellulosic biomass is also a replacement for the debatable first generation feedstocks (e.g., corn) that are the dominant sources for today's bioethanol. The waste plant biomass is generally non-edible and lignocellulosic in nature. Lignocellulosic materials incorporate agricultural residues, energy crops (temperate grasses), wood residues and municipal paper waste.

Chemically, lignocellulosic biomass is composed of 35-55% cellulose, 20-40% hemicellulose and 10-25% lignin (Sukumaran et al., 2010). Furthermore, the intrinsic properties of biomass determine both the type of conversion process and any subsequent processing complexities that may arise (McKendry, 2002). The type of biomass (woody or herbaceous) equally explains the amount of energy stored in it. In addition, the sugar (pentose and hexose) composition in the biomass decides the theoretical yield of fuel alcohols and can thereby have a considerable impact on the process economics. Hence, it is the interaction between all these parameters that enables flexibility in utilization of biomass as an economic and efficient energy resource.

The primary aspect in utilizing biomass for fuel is to understand its basic composition and properties. Biomass is a complex heterogeneous mixture of key structural organic components such as cellulose, hemicellulose and lignin along with accessory organic and inorganic composites. The qualitative and quantitative characterization of such components in the biomass is essential for its application

perspectives. Hence, an overall characterization of biomass is necessary to expand the bioenergy and bioproduct sectors worldwide. With this objective, this chapter aims to characterize lignocellulosic biomass of different origin such as forestry (pinewood), agricultural (wheat straw) and perennial grass systems (timothy grass). The purpose of selecting wheat straw, pinewood and timothy grass in this study is because of their commercial availability in Canada. The annual availability of lignocellulosic biomass in USA and Canada is in the range of 6-256 and 64-561 MDT, respectively (Gronowska et al., 2009). It is noteworthy that biomass characteristics depend on local climate and environmental conditions. However, in this study only Canadian climatic conditions are considered.

3.2. Materials and methods

3.2.1. Lignocellulosic biomass

In this study, *Pinus banksiana* (pinewood, PW) as forest residue, *Phleum pratense* (timothy grass, TG) as energy crop and *Triticum aestivum* (wheat straw, WS) as agriculture residue were used as biomass sources. The biomasses were obtained from Saskatchewan, Canada. Wheat straw and timothy grass were procured from a local farm immediately after harvest, while pinewood was collected from a neighboring forest. The pinewood used in the study was without bark.

The feedstocks were collected between 3-5 kg in weight and the visible contaminants such as sand, soil or shell particles were removed. The feedstocks were then air-dried and crushed using a Wiley mill with a sieve screen of 1.18 mm. The pulverized biomass samples were stocked in glass jars at room temperature and used as necessary. The air-dried and pulverized biomasses are shown in Fig. 3.1.

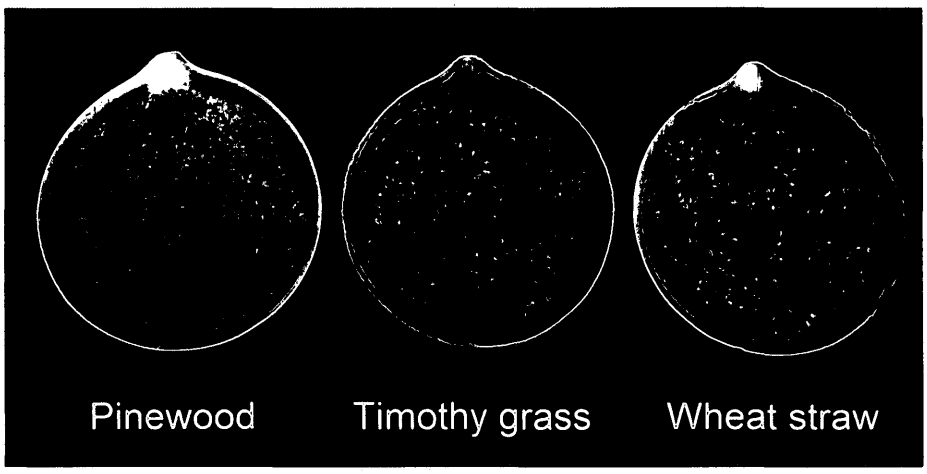

Fig. 3.1 Pulverized biomass samples (particle diameter < 1.18 mm)

3.2.2. Proximate and ultimate analysis

The moisture, ash and volatile matter content of the biomass samples were determined using the standard procedures described in ASTM E871-82 (ASTM E871-82, 2006), ASTM E1755-01 (ASTM E1755-01, 2007) and ASTM D3175-11 (ASTM D3175-11, 2011), respectively. For moisture determination, 1.0 g sample was taken in a crucible and placed in a muffle furnace at 105°C for 2 h. The loss in weigh after drying was determined as the moisture. Similarly, the conditions for ash and volatile matter determination were 575±10°C for 4 h and 950±10°C for 7 min, respectively. After each analysis the crucible was removed from furnace and placed in the desiccator until room temperature and weighed. Fixed carbon was calculated from the difference of moisture, ash and volatile matter.

For ultimate analysis, the presence of common elements such as C, H, N and S in biomass samples was determined through an Elementar Vario EL III (Hanau, Germany) elemental analyzer following the standard ASTM methods (ASTM D3176-09, 2009; ASTM D5373-08, 2008). Oxygen was calculated from the difference of C, H, N, S and ash. Major inorganic elements in biomasses and their ash were resolved through inductively coupled plasma-mass spectrometry

(ICP-MS) analysis using a microwave-assisted di-acid digestion method (HNO_3 and H_2O_2, 5:1 v/v) in a PerkinElmer NexION 300D ICP-MS (PerkinElmer, USA).

3.2.3. Calorific value

The calorific values for biomass were determined experimentally in a static bomb calorimeter using the procedures described by Anon et al. (1995), and theoretically as higher heating value (HHV). For experimental determination in a static bomb calorimeter (Parr instruments, USA), sample pellet of 1.0 g was prepared for each analysis. A cotton thread was attached to the platinum ignition wire and placed in contact with the pellet. The bomb was filled with oxygen at 441 psi with 1 mL of water added to it. The bomb was submerged in the calorimeter chamber filled with distilled water. The calorimeter jacket was maintained at constant temperature by circulating water at 25°C.

The calorific value for biomass was theoretically determined as HHV using the modified Dulong's formula (Theegala and Midgett, 2012) as mentioned below. The C, H and O in equation 1 represent the weight percent of their individual content as determined from the ultimate analysis (section 3.2.2).

$$\text{HHV (MJ/kg)} = \frac{33.5 \times \text{wt.\% C}}{100} + \frac{142.3 \times \text{wt.\% H}}{100} - \frac{15.4 \times \text{wt.\% O}}{100} \quad \text{(Equation 1)}$$

3.2.4. Fourier transform infrared (FT-IR) spectroscopy

The FT-IR spectra of biomass, biomass extractives and raffinate biomass were obtained to characterize the organic functional groups present in the samples. The FT-IR spectra were obtained by KBr pellet method in a PerkinElmer FT-IR spectrum 100GX model (PerkinElmer, USA). About 10 mg of the sample was mixed with 200 mg of KBr for preparation of pellets. Spectra were collected in the range of 400-4000 cm^{-1} at a spectral resolution of 2 cm^{-1} with an average of 128 scans (Himmelsbach et al., 2002).

3.2.5. Raman spectroscopy

A Renishaw inVia Raman microscope (Renishaw Inc., USA) equipped with 785 nm laser diode was used for biomass analysis with back scattering configuration. Biomass was analyzed under the laser to acquire Raman spectra in the range of 800-1800 cm^{-1}. The spectral resolution was 4 cm^{-1} with 10% laser power and 10 s of exposure time along with a total of 15 acquisitions.

3.2.6. Thermogravimetric analysis (TGA)

TGA analysis was performed to determine the weight loss of biomass during heat treatment in a PerkinElmer Pyris Diamond TG/DTA instrument (PerkinElmer, USA). To prevent heat and mass transfer limitations, 5-7 mg of biomass was heated up to 800°C under N_2 flow (100 mL/min) at 10°C/min (Carrier et al., 2011). The rate of weight loss was continuously recorded.

3.2.7. X-ray diffractometry (XRD)

XRD analysis was carried out to identify any crystallographic structures in the biomass and ash samples using a Bruker D8 Advance X-ray diffractometer (Bruker AXS, Germany). CuKα radiation at 40 kV, 130 mA and $\lambda = 0.154$ nm was used with 2θ scanning angle of 10-70° at a scanning speed of 0.2°/min.

3.2.8. Determination of biomass extractives

The biomass samples were subjected to a three-step extraction process using water, ethanol and hexane in a Soxhlet extraction apparatus (Sluiter et al., 2008b). In the first step, Milli-Q water was used to extract any inorganic materials and non-structural sugars from the biomass. In the second step, water-extracted biomass was subjected to ethanol extraction for separation of any polar compounds such as chlorophyll, waxes and sterols. Finally, hexane was used to extract the non-polar lipids, hydrocarbons and terpenoids from the biomass residues. The residual solvent after every extraction was removed through rotary

evaporation under reduced pressure. The raffinate biomass after hexane extraction was collected, air-dried and analyzed for XRD and FT-IR. The water, ethanol and hexane extractives were analyzed for FT-IR as well.

Small fractions of sugars, organic acids and sugar alcohols (e.g. xylitol) were expected in water, ethanol and hexane extracts for which the chromatographic analysis was done in an Agilent Series 1100 HPLC (Agilent Technologies Ltd., USA) equipped with refractive-index detector. The analysis was performed using an Aminex HPX 87H ion-exclusion column (BioRad, USA) with a Cation H micro-guard cartridge (BioRad). A 5mM H_2SO_4 solution was used as the mobile phase with a flow rate of 0.6 mL/min and column temperature of 55°C. Mixed standards of sugars (i.e., arabinose, cellobiose, glucose and xylose), organic acids (i.e, acetic acid and succinic acid) and sugar alcohol (i.e, xylitol) were used for the quantitative analysis.

3.2.9. Determination of sugars in biomass

The biomass was acid hydrolyzed for conversion of cellulose and hemicellulose to water soluble sugars using the NREL method (Sluiter et al., 2008a). The biomass samples were hydrolyzed with 72% H_2SO_4 at 30°C for 1 h followed by 4% H_2SO_4 at 121°C for 1 h. The hydrolyzed sugars were quantified through HPLC using an Aminex HPX 87H ion-exclusion column with similar operating conditions as mentioned in section 3.2.8.

3.3. Results and discussion

3.3.1. Proximate and ultimate analysis

During sample analysis, care was taken for reproducibility in duplicates with standard deviation less than ± 5%. The proximate and ultimate analyses together with calorific values of the biomass samples are presented in Table 3.1. Compared to TG (5.6 wt.%) and WS (5.2 wt.%), PW exhibited a high moisture content (6.8 wt.%). The biomass moisture is a mineralized fluid that contains many key cations

(Al, Ca, Fe, K, Mg, Mn, Na, Ti) and anions (Br, Cl, CO_3, F, HCO_3, H_2PO_4, I, NO_3, OH, PO_4, SO_4) that are significant in plant physiology (Werkelin et al., 2005). In addition, thermochemical conversion requires biomass with low moisture (< 15%), whereas high moisture containing biomass are favorable for biochemical conversion.

Table 3.1 Proximate and ultimate analysis of biomass samples

Analyses	Pinewood	Timothy grass	Wheat straw
Proximate analysis (wt.%)			
Moisture	6.8 ± 0.2	5.6 ± 0.3	5.2 ± 0.3
Ash	2.3 ± 0.1	3.6 ± 0.3	4.4 ± 0.2
Volatile matter	71.7 ± 1.5	78.2 ± 2.1	70.1 ± 0.9
Fixed carbon	19.2	12.6	20.3
Ultimate analysis (wt.%)			
C	48.9	43.4	44.1
H	6.2	6.1	6.0
N	0.1	1.3	0.4
S	0.1	0.1	0.01
O	42.5	45.4	45.0
Atomic ratio			
H/C	1.5	1.7	1.6
O/C	0.7	0.8	0.8
N/C	0.001	0.03	0.01
Calorific value (MJ/kg)			
Experimental	18.1 ± 1.2	15.9 ± 1.5	15.6 ± 1.3
Theoretical, HHV	18.6	16.3	16.4
Chemical formula	$CH_{1.5}O_{0.7}N_{0.001}$	$CH_{1.7}O_{0.8}N_{0.03}$	$CH_{1.6}O_{0.8}N_{0.01}$

Note: All the data are average of replicate measurements with standard deviation < 5%.

The ash content among the three feedstocks increased in the order: PW (2.3 wt.%) < TG (3.6 wt.%) < WS (4.4 wt.%). The ash content helps in approximating the concentration of elements in the inorganic or organic matter of biomass. The chemical composition of ash is an important parameter to be considered during the thermochemical conversion which can lead to significant operational issues such as formation of slag at higher temperatures, thus reducing the process efficiency and increasing the overall economics.

The carbon (48.9 wt.%) and hydrogen (6.2 wt.%) content in PW was higher compared to TG and WS which was because of its woody nature. The analogous variation of carbon and hydrogen indicates their association and occurrence in biomass as carbohydrates and in their bio-oils and biochars as hydrocarbons. TG (1.3 wt.%) showed noticeable levels of nitrogen among the biomasses which was in agreement with the findings of Obernberger et al. (2006).

The chemical formulae for PW, TG and WS in this study were established from the atomic ratios (H/C, O/C and N/C) as $CH_{1.5}O_{0.7}N_{0.001}$, $CH_{1.7}O_{0.8}N_{0.03}$ and $CH_{1.6}O_{0.8}N_{0.01}$, respectively. The calorific values of the biomass samples were estimated both experimentally through bomb calorimeter and theoretically (HHV) from their respective C, H and O contents. Values from both the determinations matched with an error percent within ± 5. Both experimental and theoretical HHV of PW was high compared to TG and WS due to its relatively higher C and H contents (Table 3.1). The calorific value of a feedstock is equivalent to its maximum value of the energy produced or available (McKendry, 2002).

Table 3.2 gives the inorganic metal composition of biomasses and their ash samples. Significant amount of elements such as Li, Na, K, Ca and Zn were detected in WS compared to TG and PW. In the same way, Mg, P, Ni and Cu were detected in higher amounts in TG. Calcium content was found to be high in TG (3056 ppm) and WS (3586 ppm) compared to PW (1459 ppm). In plants, Ca is found in parenchyma cells of leaves through precipitation of calcium oxalate crystals as raphides (Werkelin et al., 2005). The concentrations of heavy metals such as Cr, Fe,

Co, Cd and Pb were high in PW and PW ash. In a biofuel industry, volatile toxic heavy metals such as Pb and Cd are enriched in fly ash fractions (Saarela et al., 2005).

Table 3.2 ICP-MS analysis for determination of inorganic elements (in ppm) in biomass and ash samples

Element	Biomass			Ash		
	PW	TG	WS	PW ash	TG ash	WS ash
Li	0.1	0.3	0.3	1	13	11
Na	17	54	2720	24634	4481	36443
Mg	256	1973	1021	26275	19253	12841
Al	113	57	113	4242	429	891
P	94	1819	1195	17675	27887	13586
K	591	18254	25747	78499	219701	208550
Ca	1459	3056	3586	312633	59816	141891
Cr	2	1	2	106	11	9
Mn	78	54	15	4874	640	176
Fe	654	123	125	21592	3137	1681
Co	0.2	0.1	0.1	10	1	1
Ni	1	3	1	294	37	16
Cu	2	3	1	1302	511	615
Zn	24	23	32	1610	257	106
Rb	1	4	5	44	11	13
Sr	7	13	14	221	35	39
Cd	0.1	0.1	0.1	6	1	1
Pb	59	2	1	6	62	56

Note: All the data are average of replicate measurements.

Abbrev. Pinewood (PW), timothy grass (TG) and wheat straw (WS)

The high levels of alkaline metals such as Na, Mg, K and Ca were noticed in herbaceous biomass (TG and WS) than in PW. This is because the feedstocks with high annual growth rates are rich in alkaline elements as they are readily taken up from the soil (Vassilev et al., 2010). The presence of alkali metals is a factor for consideration in the thermochemical conversions as their reaction with silica present in ash can form slag-like liquid that blocks the pipelines in the furnace and boiler plants as discussed earlier. This significantly adds to the processing cost.

3.3.2. Spectroscopic analysis

The FT-IR spectra of biomass samples, their extractives (water, ethanol and hexane), and raffinate materials were analysed to determine the functional groups. The major peaks in the spectra are tabulated in Table 3.3 with their component assignments. Peaks with intensities of strong, medium, broad and weak were due to different C–H, C–O, C–O, O–H, N–H, C–N and NO_2 bonds available in these compounds.

The FT-IR spectra of biomass (Fig. 3.2A) showed the most prominent peaks originating from –OH stretching vibration (3300-3400 cm^{-1}) and CH_2 and CH_3 stretching vibrations (2915-2935 cm^{-1}) (Silverstein and Webster, 1998). Many intense peaks for biomass in the region 1620-1745 cm^{-1} originated from the carbonyls mainly ketones and esters. These bands were predicted from waxes, fatty acids, fatty esters, aldehydes and ketones (Himmelsbach et al., 2002). The 1000-1280 cm^{-1} stretch in the biomass spectra can be assigned broadly to alcohols, ethers, carboxylic acids and esters.

The bands due to C–O–C aliphatic (1097 cm^{-1}) and C–O alcohol (1175 cm^{-1}) represented oxygenated functional groups of cellulose, whereas the peaks at 1516 and 1616 cm^{-1} were assigned to C–C and C–O aromatic rings signifying lignin (Chen et al., 2008). The C–O–C stretching at 1097 cm^{-1} in the biomasses is characteristic to cellulose and hemicellulose (pyranose rings and guaiacyl

monomers). The most characteristic bands of lignin were at 870, 1263, 1506 and 1601 cm^{-1} (Moore and Owen, 2002).

Table 3.3 Functional group assignments for different FT-IR bands in biomass

Wave number (cm^{-1})	Assignment
450-554, 1630	C–C aromatic rings
625-903, 1410, 1442, 2860- 2970	C–H alkynes, aliphatics, alkanes, phenyl rings
1097	C–O–C symmetric stretching
1051, 1070, 1175	C–O alcohol, ethers, carboxylic acids
1220	C–O phenols
1254	C–N amines, C–O alcohol, ethers, carboxylic acids, esters
1280	C–O aromatics
1380	CH_3 aliphatic, NO_2 nitro compounds
1516, 1616	C–C aromatics, N–H amines
1668	C=C alkene, C–H phenyl rings
1745	C=O aldehydes, esters, ketones, carboxylic acids
2095	C≡C alkynes
3450-3670	–OH stretching, alcohols, phenols

The biomass peaks at 2860 and 2928 cm^{-1} were assigned to CH_2 stretching bands from plant waxes. However, due to the series of solvent (hexane and ethanol) washing during Soxhlet extraction, most of the waxy components were removed in the raffinate biomass (Fig. 3.2B). Furthermore, these waxes were noticed again in the hexane extracts of the three biomasses (Fig. 3.2C) confirming the washing out effect. Similar washing-out effect was noticed in the case of biomass peak for C–H alkynes and phenyl rings at 782 cm^{-1}.

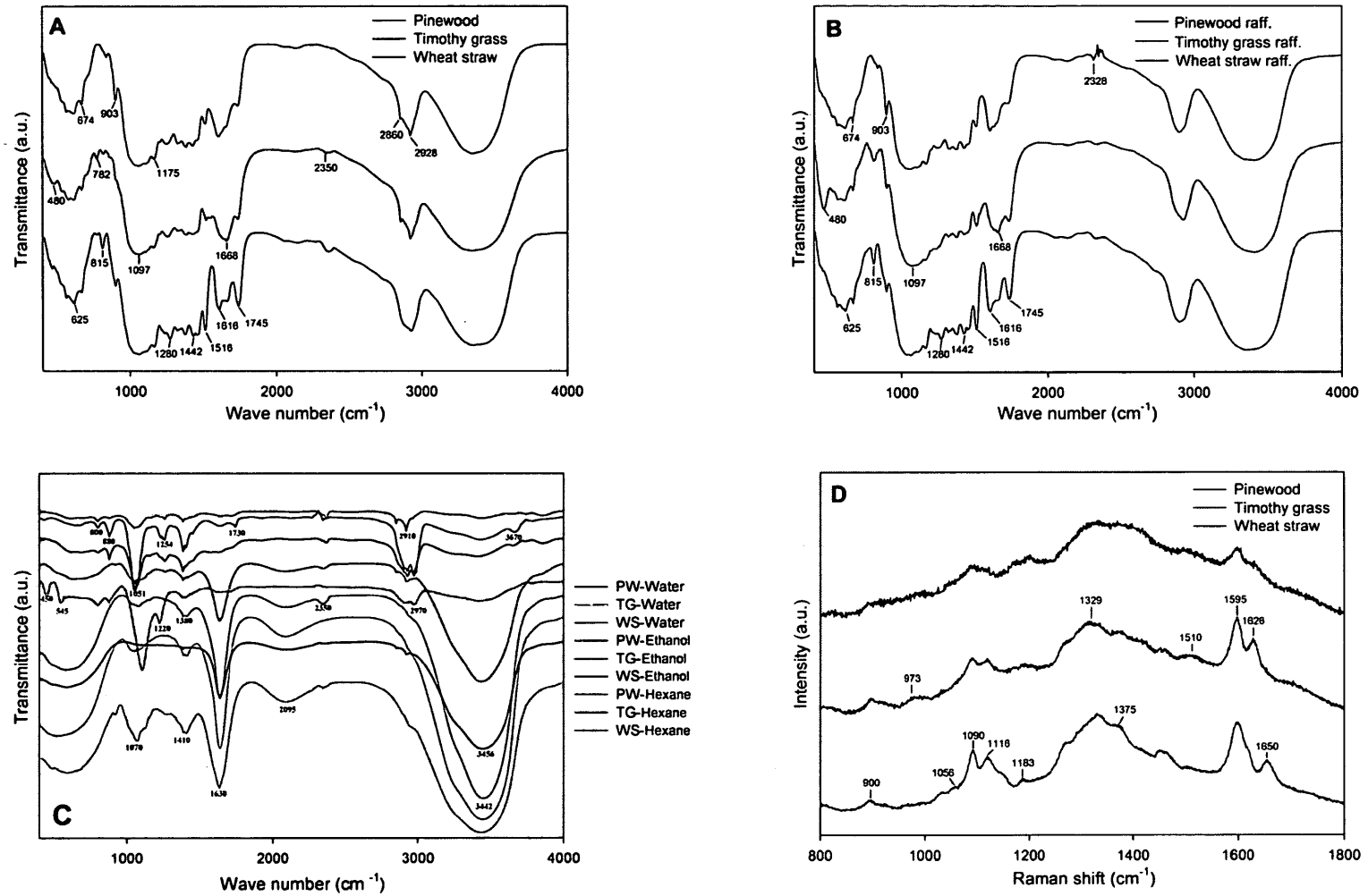

Fig. 3.2 FT-IR spectroscopy of (A) biomass, (B) raffinate biomass and (C) biomass extractives. (D) Raman spectroscopy of biomass

In Fig. 3.2C, broad peaks centered at 3200-3600 cm^{-1} originated from H-bonds of alcohols or phenols. In the case of hexane extract, the CH_2 and CH_3 vibrations occurred in biomass spectra at 2910-2973 cm^{-1}. These vibrations were due to the extraction of some hemicellulosic and cellulosic materials. Some peaks at 1620-1760 cm^{-1} in water and ethanol extracts were due to the aldehydes, ketones, carboxylic acids and esters (Ozcimen and Ersoy-Mericboyu, 2010).

Extractives with hexane and ethanol exhibited less intense –OH peaks (3450-3670 cm^{-1}) indicating the partial loss of waxy materials from –OH groups into the organic solvents. In the spectra of extractives, peaks between 1056 and 1603 cm^{-1} represented C–H and O–H bending frequencies which were due to lignin. Peaks at 1516-1616 cm^{-1} in biomasses and 1254 cm^{-1} in extractives were from aliphatic and aromatic N-heterocyclics as amine groups that are available in the form of N–H and C–N functional groups.

FT-IR precisely identifies the O-containing functional groups in carbonaceous materials but it has restricted application in exploring less-polar aromatics. In contrast, Raman spectrometry is widely used to study the structural features of such materials as it is sensitive to crystalline and amorphous structures. In the Raman spectrum of biomasses (Fig. 3.2D), major vibrations in the region 1595-1650 cm^{-1} were due to lignin (Agarwal and Ralph, 1997), whereas cellulosic and hemicellulosic components occurred in the spectral range of 973-1183 cm^{-1}. Li et al. (2010) reported the presence of aromatic skeletal lignin at 1510 cm^{-1}, and syringyl and guaiacyl condensed lignin at 1329 cm^{-1} in switchgrass. Moreover, the bands at 1056 cm^{-1} represented C–O stretch in cellulose and hemicelluloses, while the 1375 cm^{-1} band represented C–H deformation in cellulose and hemicellulose, respectively.

3.3.3. Thermal and structural analysis

Thermogravimetric analysis was carried out to evaluate the pyrolytic degradation and decomposition behaviour of the three lignocellulosic biomasses

(Fig. 3.3A). The devolatilization process started between 200-250°C with the maximum weight loss occurring in the range of 300-350°C. A characteristic change in weight loss of the biomass samples was found at 370-400°C following a slower weight loss indicating char formation. The initial weight loss of the feedstocks was due to their moisture and volatile components, whereas the later weight loss was attributed by the degradation of fibrous material from cellulosic and hemicellulosic contents (Fisher et al., 2002).

TGA analysis is essential in predicting the pyrolytic behaviour of a feedstock as pyrolysis can be divided into four phases such as moisture evolution, hemicellulose decomposition, cellulose decomposition and lignin decomposition. After the release of water and light volatiles, there is a sharp drop in weight of the samples up to 350°C. This stage is termed as active pyrolysis zone (Fig. 3.3A). Subsequently, a change in the weight loss can be observed, indicating the passive pyrolysis. This zone is characterized by a slower loss of weight until 750°C with negligible weight loss thereafter. Figure 3.3B shows the differential thermogravimetric spectra of the feedstocks. The spectra revealed the major peak along with some shoulder peaks. Carrier et al. (2011) have assigned the major peak as per the degradation of hemicellulose (200-300°C) and the shoulders with the degradation of cellulose (250-350°C) and lignin (200-500°C).

The XRD patterns of biomass, raffinate biomass and ash samples are presented in Fig. 3.4. The XRD pattern of biomass is often characterized by an intensive amorphous halo with a major maximum at 20-23° and a minor maximum at 13-17° which signifies the occurrence of cellulose (Vassilev et al., 2012). In the XRD pattern of biomass, the peaks at 15.5° (d-space ~5.51 Å), 21.7° (d-space ~3.96 Å) and 34.5° (d-space ~2.59 Å) are assigned to Cellulose I, Cellulose II and hemicellulose, respectively (Fig. 3.4A). The degree of crystallinity of biomass materials at 13-17° and 20-23° is reported to be due to these cellulosic polymorphs (Correa et al., 2010), while some reports suggest the crystallinity to be due to occurrence of lignin at 15° (Sarkar and Adhikari, 2001).

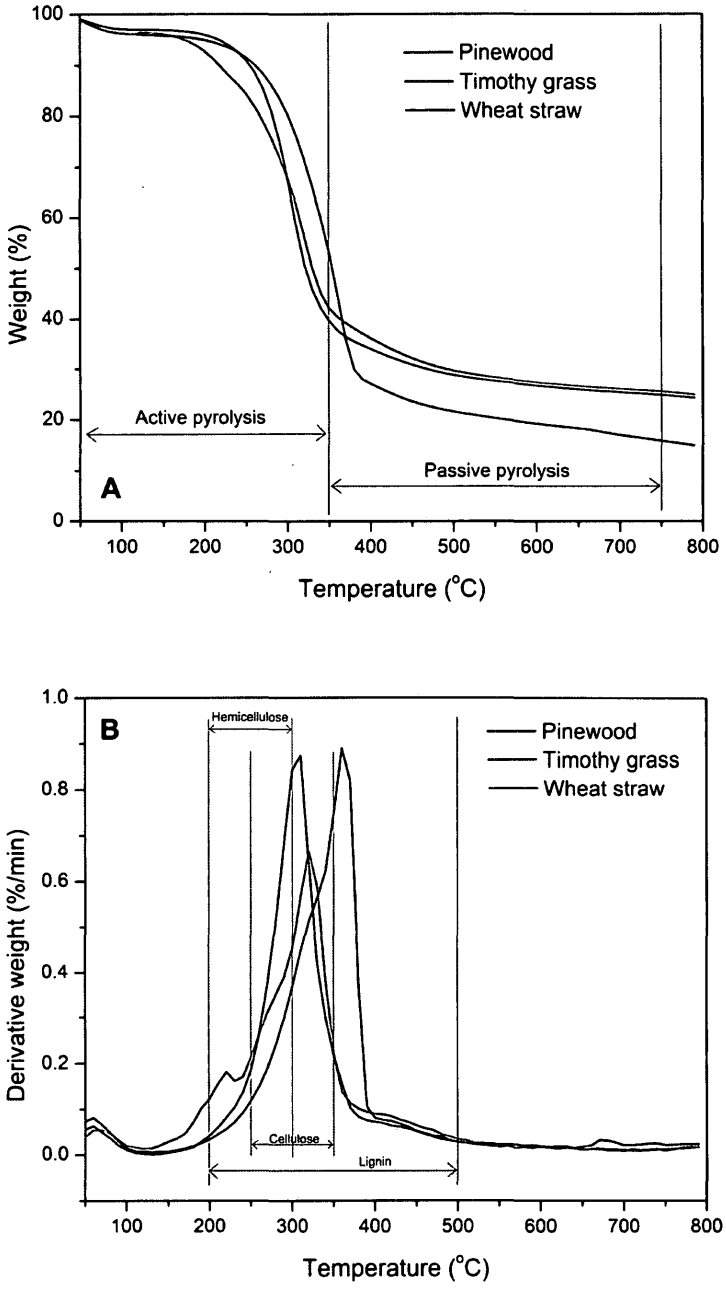

Fig. 3.3 (A) Thermogravimetric and (B) differential thermogravimetric analysis of biomass

Some crystalline phases originally present in biomass samples (57.4° and 67.7°) were not found in their raffinate portions (Fig. 3.4B) but surprisingly appeared in the ashes (Fig. 3.4C). The diffraction peaks of biomass at 57.4° (d-space ~1.61 Å) was due to the presence of halite (Lopez-Buendia et al., 2007), whereas 67.7° (d-space ~1.38 Å) represented sylvite (Jensen et al., 2000).

The absence of halite and sylvite in raffinate biomasses was due to their washing out during the Soxhlet extraction. However, these chloride peaks were found in the biomass ashes at 36.6° (d-space ~2.45 Å) and 66.3° (d-space ~1.41 Å) for halite and 48.3° (d-space ~1.87 Å) for sylvite, respectively (Vassilev et al., 1999). With the removal of these minerals in the raffinate portions, the relative intensities of the organic components at 15.5°, 21.7° and 34.5° increased than the untreated biomass.

A few crystalline and semi-crystalline, mostly poorly crystallized or cryptocrystalline phases which were close to the XRD detection limit belonging to some minerals commonly Na, Mg, Al, Ca, Fe and Mn were identified in the ash samples. These elements were detected in considerably higher amounts in ash samples through the ICP-MS analysis as well (Table 3.2).

Peaks at 20.9° (d-space ~4.25 Å), 23.2° (d-space ~3.78 Å) and 28.4° (d-space ~3.15 Å) were due to silicates such as plagioclase, quartz and feldspar, respectively (Vassilev et al., 1999). Considerable amount of silicates are found in straws and grasses (Jensen et al., 2000). Peaks at 23.2° (gypsum) and 29.5° (anhydrite) in feedstock ashes are characteristic to sulphate group of minerals. Vassilev et al. (1999) reported various carbonate peaks in biomass ashes e.g., calcite at 26.7°, 43.2°, 50.2°, 57.4°, 67.9°, fairchildite at 32.3°, 39.5° and natrofairchildite at 36.6°.

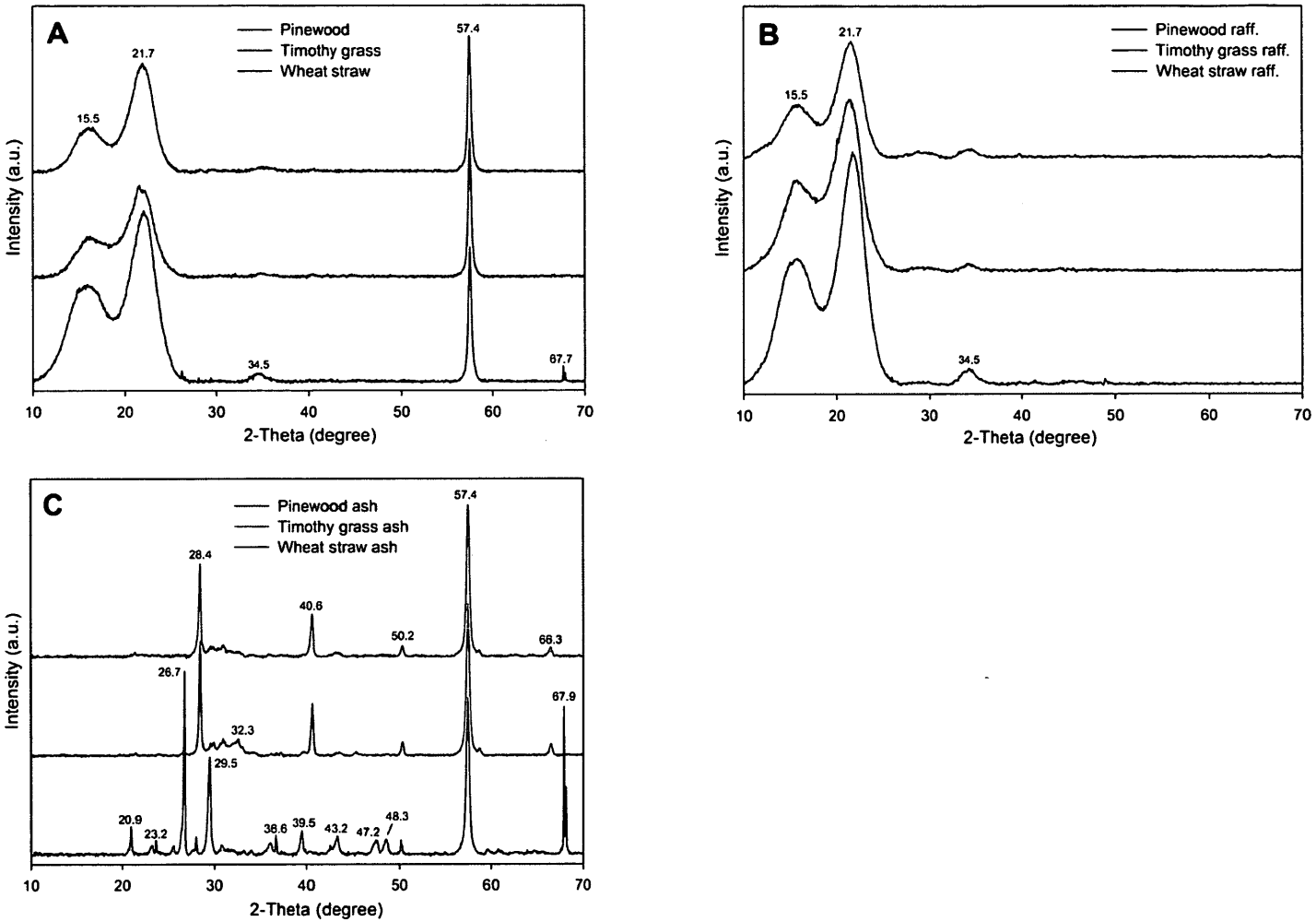

Fig. 3.4 X-ray diffractometry analysis of (A) biomass, (B) raffinate biomass and (C) ash samples

3.3.4. Compositional analysis

The biomass materials were analyzed biochemically to determine their lignocellulosic and extractive compositions. The yield of water, ethanol and hexane extracts for the biomass samples are given in Table 3.4. The yield of total extractives in PW, TG and WS were 15.7, 16.5 and 19.2 wt.%, respectively. PW revealed low amount of water soluble extracts (6.7 wt.%), whereas WS presented a higher amount of water extracts (13.2 wt.%). As a result of hexane extraction, PW produced appreciable amount of hexane soluble materials (4.3 wt.%), which might be due to higher amount of terpenoids that are soluble in non-polar solvent such as hexane. The high amount of extractives in WS is a strong indication for possible recovery of some minor components such as terpenes, tannins, resins, fats, oils, lipids, proteins and organic acids (Tamaki and Mazza, 2010).

Table 3.4 Extractives and lignocellulosic composition in biomass

Component (wt.%)	Pinewood	Timothy grass	Wheat straw
Extractives			
Water	6.7 ± 0.8	9.3 ± 1.1	13.2 ± 1.3
Ethanol	4.7 ± 0.7	4.8 ± 0.7	3.9 ± 0.8
Hexane	4.3 ± 0.3	2.4 ± 0.4	2.1 ± 0.2
Lignocellulose			
Cellulose	38.8 ± 1.4	34.2 ± 1.2	39.1 ± 0.8
Hemicellulose	23.6 ± 0.8	30.1 ± 1.0	24.1 ± 0.6
Lignin	20.4 ± 1.0	18.1 ± 0.7	16.3 ± 1.2
Ash	1.5 ± 0.2	1.1 ± 0.4	1.3 ± 0.1

Note: All the data are average of replicate measurements

Small amount of sugars and other degradation products were detected in the water and solvent extracts which were analysed in HPLC. Table 3.5 gives the composition of sugars in the hydrolysates and other organic components in the

extracts. Fair amounts of glucose (7 and 4.4 mg/mL) were obtained in WS and TG extractives, respectively. Some of the degradation products detected in the biomass extracts were xylitol, succinic acid and acetic acid. The presence of xylitol, a reduced product of xylose, in the extracts was in the range of 0.8-1.1 mg/mL. The incidence of xylitol which is a sugar alcohol suggests that along with potentials for biofuels, the feedstocks have tendencies for generation of industrially-significant bioproducts. The level of succinic and acetic acid in the extracts were in the range of 0.1-1.1 and 1.4-2.3 mg/mL, respectively.

Table 3.5 Composition of sugars and extractives in biomass

Compound	Pinewood	Timothy grass	Wheat straw
Components (mg/mL) in the extractives			
Cellobiose	0.01	1.1	2
Glucose	0.2	4.4	7
Xylose	0.1	7	9.5
Arabinose	0.04	0.1	0.5
Xylitol	0.8	0.6	1.1
Succinic acid	0.1	0.6	1.1
Acetic acid	2	2.3	1.4
Sugars (%) in the hydrolysates			
Cellobiose	2.6 ± 0.1	1.5 ± 0.1	2.1 ± 0.2
Glucose	49.8 ± 1.2	53.2 ± 1.4	53.8 ± 1.1
Xylose	26.4 ± 0.7	40.7 ± 1.1	28.8 ± 1.0
Arabinose	21.2 ± 0.6	4.6 ± 0.2	15.3 ± 0.8

Note: All the data are average of replicate measurements.

The amount of glucose in the biomass hydrolysates ranged between 49.8-53.8 wt.% (Table 3.5), however the amount of xylose was high in TG (40.7 wt.%). Assuming a complete conversion, the composition of glucose and

cellobiose is recognized as cellulose and that of xylose and arabinose as hemicellulose (Lenihan et al., 2010). WS and PW resulted in equivalent cellulose levels of 39.1 and 38.8 wt.%, respectively. Compared to PW (23.6 wt.%), hemicellulose content was high in TG (30.1 wt.%) and WS (24.1 wt.%). PW demonstrated a relatively high lignin fraction of 20.4 wt.%. Lignin has about 30% higher energy content than cellulose and hemicellulose. Hence, a high lignin containing biomass would exhibit a comparatively high calorific value (Novaes et al., 2010), which was reflective of the high calorific value of PW (Table 3.1). Presence of lignin makes cellulose and hemicelluloses hydrolysis difficult, hence delignification is one of the chief goals of biomass pretreatment, as removal of lignin would expose the cellulosic fibers for enzymatic saccharification to fermentable sugars.

3.4. Conclusions

The physico-chemical characteristics of woody and herbaceous biomasses were discussed in this chapter. From the TGA analysis, pinewood was found to be thermally stable due to its devolatilization at 380°C instead of 350°C as in the case of timothy grass and wheat straw. The biomass ash demonstrated various mineral components such as carbonates, silicates, sulphates and chlorides. The higher amount of hemicelluloses in timothy grass and wheat straw was because of their herbaceous and fast-growing nature. The similar reason also applies for higher amount of alkaline metals in timothy grass and wheat straw than in pinewood. In addition, high lignin in pinewood was due to its characteristic tightly bound fibrous texture in contrast to the loosely bound fibers in herbaceous plants. FT-IR and Raman spectroscopy revealed the presence of waxes, fatty acids, aldehydes, alcohols, ethers, carboxylic acids and esters with cellulose, hemicellulose and lignin in biomasses. The physico-chemical resemblance of timothy grass with wheat straw suggests that perennial grasses (short-rotation crops) could supplement the anticipated demand of agro-residues in future as next generation feedstocks.

Chapter Four: Pyrolysis of lignocellulosic feedstocks: Production of bio-oil, biochar and gases

4.1. Introduction

There are a number of evidences to explain global warming due to anthropogenic GHG emissions with extreme climatic consequences such as rise in ocean levels, melting of arctic ice, desertification, increased strength of hurricanes, heat waves and tropical storms. The renewable energy strategies are capable in offsetting GHG emissions but they cannot reverse climate change. A hopeful approach in lowering atmospheric CO_2, while producing energy is biochar, which is a major byproduct of biomass pyrolysis. Biochar is recognized to have both bioenergy and remarkable environmental advantages. With stably sequestering atmospheric carbon, biochar has tremendous agronomic benefits to revitalize rural and agricultural communities. Biochar is rich in carbon and resistant to chemical and microbial breakdown, thus allowing the carbon to be sequestered for periods of time approaching hundreds to thousands of years (Lehmann et al., 2003). The use of biochar could not only curb GHG emissions but also capture CO_2 from the atmosphere, thereby reducing global warming.

While fast pyrolysis of biomass mostly yields bio-oil for subsequent upgrading to transportation fuels, slow pyrolysis produces significant amount of biochars (Brown et al., 2011). During slow heating rate pyrolysis (typically between 400-500°C), biomass undergoes endothermic degradation and produces large amount of biochar, gas and heat which could be captured to produce electricity, bio-oil or H_2. On the other hand, high heating rate pyrolysis (typically between 400-600°C) has a heating rate more than 300°C/s and a residence time as low as 5s. High heating rate (HHR) pyrolysis is mostly operated in fluidized-beds having short vapor residence time of 1-2 s but there are a few studies to demonstrate HHR pyrolysis in fixed-bed reactors having residence time of about 38-88 s (Siengchum et al., 2013;

Putun, 2010; Tsai et al., 2007). In addition, these studies have reported the operation of HHR pyrolysis in fixed-bed reactors in batch mode unlike the most usual continuous mode operations in fluidized-beds. Based on these studies, a fixed-bed reactor was used for high and slow heating pyrolysis runs.

The role of biochar in increasing soil fertility is many fold, including increased cation exchange capacity and water holding capacity, reduced soil compaction, enhanced bacterial and fungal population in soil for promoting symbiotic exchange of water, nutrients and organic compounds between plant roots and soil environment (Liang et al., 2006). All these features make biochar a valuable material in retaining essential nutrients in the soil, thus improving crop yields and decreasing environmental pollution by addition of inorganic nutrients. In this chapter, a comparative evaluation of bio-oil, biochar and gas yields from pinewood, timothy grass and wheat straw is made using two pyrolysis scenarios, namely HHR and SHR pyrolysis. In addition, the energy and agronomic values of biochars produced from both pyrolysis processes are estimated.

4.2. Materials and methods

4.2.1. Biomass pyrolysis

HHR and SHR pyrolysis of pinewood (PW), timothy grass (TG) and wheat straw (WS) were performed in a wire-mesh fixed-bed reactor (Fig. 4.1). The details of collection and physico-chemical characterization of the above biomasses are discussed in Chapter 3. HHR and SHR pyrolysis were carried out under N_2 atmosphere (80 mL/min) in fixed-bed inconel tubular reactor (length 55 cm, internal diameter 1.1 cm) which was placed in an ATS furnace.

The pyrolysis temperature was selected as 450°C based on thermogravimetric analysis of biomasses that showed a slower weight loss beyond 400°C, indicating biochar production (see Fig. 3.2A). For HHR pyrolysis, 10 g of biomass was heated to 450°C at a high heating rate of 450°C/min with a residence time of 30 s. For SHR pyrolysis, 10 g of biomass was heated to 450°C at a slow

heating rate of 2°C/min with a residence time of 30 min. All the experiments were performed with three time reproducibility.

The volatile components from reactor were flushed by N_2 gas into an ice-cooled condenser for condensation to liquid products. The yields of pyrolysis liquids and biochars were determined by weighing. The bio-oils after pyrolysis were separated into organic and aqueous phases using diethyl ether extraction process (Azargohar et al., 2013). Subsequently, the solvent was removed from organic phase using a rotary evaporator at 25°C. The extracted bio-oil was used for further chemical analysis.

The pyrolysis temperature (450°C) was attained in most of the experiments without being affected by N_2 flow rate (80 mL/min). The furnace temperature and mass flow controller were calibrated before performing all experiments. To calibrate the temperature, a thermocouple was inserted into the reactor from top with its tip being in the middle of biomass bed. The same height of silica sand was also used for calibration with same gas flow rate.

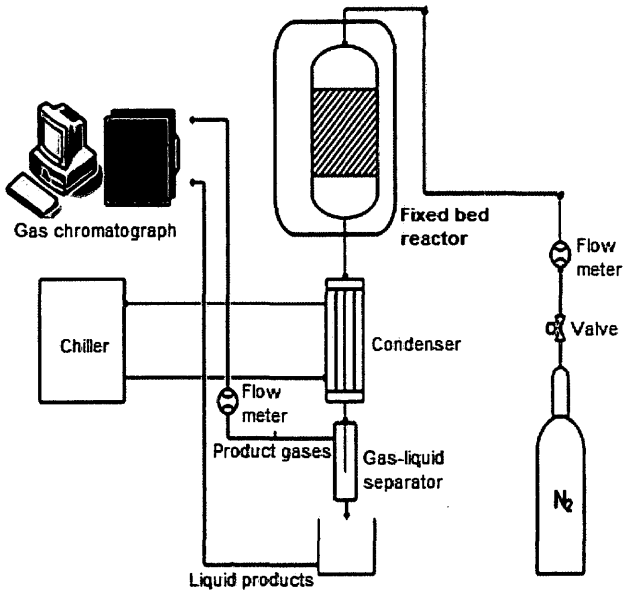

Fig. 4.1 Reactor schematics for slow and high heating rate pyrolysis experiments

The biochars obtained from HHR pyrolysis of pinewood, timothy grass and wheat straw were denoted as HPWB, HTGB and HWSB. Similarly, the SHR biochars for pinewood, timothy grass and wheat straw were named as SPWB, STGB and SWSB. The HHR bio-oils from pinewood, timothy grass and wheat straw were denoted as HPWBL, HTGBL and HWSBL, while the SHR bio-oils from the three feedstocks were represented as SPWBL, STGBL and SWSBL.

4.2.2. Proximate and ultimate analysis

The moisture, ash and volatile matter content of SHR and HHR biochars were determined using the standard procedures described in ASTM D1762-84 (ASTM D1762-84, 2007). Common organic elements such as C, H, N and S in the bio-oils and biochars were determined in an Elementar Vario EL III (Hanau, Germany) elemental analyzer. Analysis for major inorganic elements in biochars was done in a PerkinElmer NexION 300D ICP-MS using the procedures described in section 3.2 of Chapter 3. The calorific values of biochars and bio-oils were theoretically estimated using modified Dulong's formula (see equation 1).

4.2.3. Fourier transform infrared (FT-IR) spectroscopy

FT-IR analysis was carried out to characterize the surface organic functional groups in the biochar and bio-oil samples. For FT-IR of biochars, the KBr pellet method was followed (see section 3.2). For the analysis of bio-oil samples, smears were made between two quartz plates prior to spectroscopy.

4.2.4. Raman spectroscopy

A Renishaw inVia Raman microscope (Renishaw Inc., USA) equipped with 514 nm laser diode and back scattering configuration was used to analyze the biochar samples. The spectral resolution was 4 cm^{-1} with 10% laser power and a total acquisition of 15 was considered. The Raman spectra in the range of 1100-1800 cm^{-1} were curve-fitted using the WiRE Raman software (version 3.2).

4.2.5. Thermal and structural analysis

The thermogravimetric analysis (TGA) as well as X-ray diffractometry (XRD) of HHR and SHR biochar samples was performed to determine their thermal and crystalline nature. The detailed procedures for TGA and XRD analyses are given in Chapter 3 (sections 3.2.6 and 3.2.7).

4.3. Results and discussion

4.3.1. Proximate and ultimate analysis

The SHR pyrolysis of PW, TG and WS resulted in 41-44 wt.% biochars, 18-24 wt.% bio-oils and 24-27 wt.% pyrolysis gases (Fig. 4.2). High bio-oil yield in fast pyrolysis is due to the rapid quenching of biomass components at high heating rates and short residence times that cause liquid intermediate products (e.g., volatile components) to condense before further reactions break down high molecular weight species to gases (Xu et al., 2011b). On the other hand, HHR pyrolysis resulted in yields of 21-24 wt.% biochars, 40-48 wt.% bio-oils and 17-24 wt.% pyrolysis gases from the three biomasses. The relatively high yield of biochars in slow pyrolysis is because of its low heating rates and long residence times which results in secondary coking and re-polymerization reactions (Duman et al., 2011; Xu et al., 2011a).

Atomic H/C and O/C ratios are indices of aromaticity and carbonation of biochar. From the atomic ratios (H/C, O/C and N/C) in Table 4.1, the chemical formulae for HPWB, HTGB and HWSB were established as $CH_{0.6}N_{0.002}O_{0.2}$, $CH_{0.7}N_{0.03}O_{0.4}$ and $CH_{0.6}N_{0.01}O_{0.4}$, respectively. Similarly the chemical formula for SPWB, STGB and SWSB were $CH_{0.4}N_{0.003}O_{0.1}$, $CH_{0.4}N_{0.02}O_{0.3}$ and $CH_{0.4}N_{0.01}O_{0.4}$, respectively. The HHR bio-oils *viz.* HPWBL, HTGBL and HWSBL had their formula as $CH_{1.8}N_{0.02}O_{0.3}$, $CH_{1.8}N_{0.03}O_{0.3}$ and $CH_{1.8}N_{0.02}O_{0.3}$ respectively. The chemical formula for SPWBL, STGBL and SWSBL were $CH_{1.8}N_{0.02}O_{0.3}$, $CH_{1.7}N_{0.03}O_{0.4}$ and $CH_{1.6}N_{0.02}O_{0.3}$, respectively.

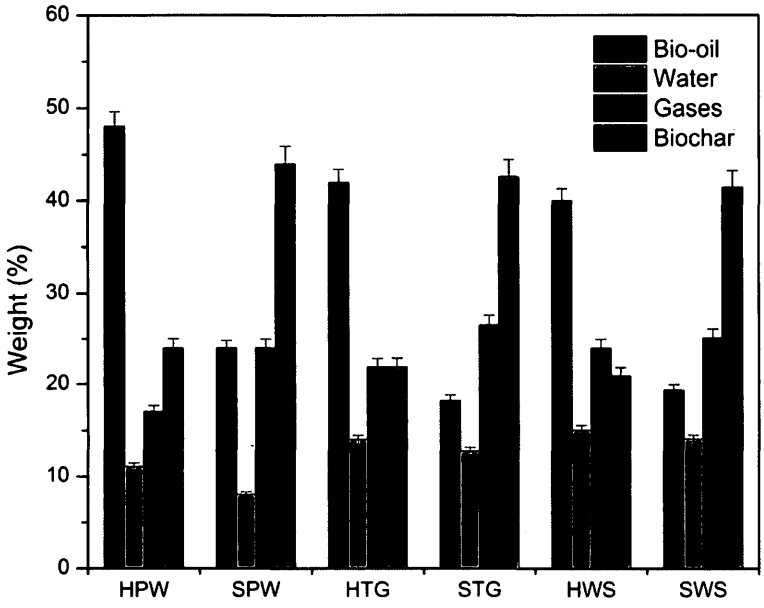

Fig. 4.2 Analysis of product yield from HHR and SHR pyrolysis

Note: HPW, HTG and HWS represent the high heating rate pyrolysis of pinewood, timothy grass and wheat straw; while SPW, STG and SWS represent the slow heating rate pyrolysis for the same feedstocks.

The carbon content was high in HHR bio-oils (62.9-65.4 wt.%) than SHR bio-oils (58.9-61.7 wt.%). The average hydrogen content in HHR bio-oils was higher than that of SHR bio-oils. The high carbon and hydrogen levels in HHR bio-oils signified a higher degree of C–H cross-linking and occurrence of high molecular weight components in the bio-oils compared to SHR bio-oils. The high carbon content in HPWB (75.5 wt.%) and SPWB (81.3 wt.%) was a supporting aspect for making it a good soil carbon enhancing material. The carbon content was higher in the case of SHR biochars than HHR biochars, whereas among bio-oils HHR bio-oils had higher carbon content than SHR bio-oils.

Table 4.1 Proximate and ultimate analysis of biochars and bio-oils produced from HHR and SHR pyrolysis

Feedstock	Proximate analysis (wt.%)				Ultimate analysis (wt.%)					Atomic ratio			HHV
	Moisture	Ash	Volatiles	Fixed C	C	H	N	S	O	H/C	O/C	N/C	(MJ/kg)
High heating rate (HHR) biochars													
HPWB	0.7	4.1	86.3	8.9	75.5	3.7	0.2	0.1	20.5	0.6	0.2	0.002	27.4
HTGB	0.9	3.1	87.7	8.3	63.7	3.6	1.9	0.04	30.8	0.7	0.4	0.03	21.7
HWSB	0.8	3.6	87.9	7.7	64.8	3.1	0.8	0.1	31.2	0.6	0.4	0.01	21.4
Slow heating rate (SHR) biochars													
SPWB	0.8	4.6	86.4	8.2	81.4	3.0	0.3	0.03	15.3	0.4	0.1	0.003	29.2
STGB	0.6	3.5	88.4	7.5	67.5	2.3	1.9	0.1	28.2	0.4	0.3	0.02	21.5
SWSB	0.8	3.9	88.1	7.2	65.2	2.3	0.9	0.1	31.5	0.4	0.4	0.01	20.3
High heating rate (HHR) bio-oils													
HPWBL	-	-	-	-	65.4	9.6	1.6	0.4	23.0	1.8	0.3	0.02	32.0
HTGBL	-	-	-	-	62.9	9.3	2.2	0.9	24.7	1.8	0.3	0.03	30.5
HWSBL	-	-	-	-	64.3	9.4	1.9	0.6	23.8	1.8	0.3	0.02	31.3
Slow heating rate (HHR) bio-oils													
SPWBL	-	-	-	-	61.5	9.1	1.4	0.01	28.0	1.8	0.3	0.02	29.2
STGBL	-	-	-	-	58.9	8.4	1.8	0.5	30.4	1.7	0.4	0.03	27.0
SWSBL	-	-	-	-	61.7	8.2	1.5	0.2	28.4	1.6	0.3	0.02	28.0

Note: All the data are average of replicate measurements with standard deviation less than 5%.

The higher heating value (HHV) of HHR bio-oils (30.5-32 MJ/kg) was comparatively higher than that of SHR bio-oils (27-29.2 MJ/kg). The higher HHV along with greater amount of carbon and hydrogen with low oxygen levels in HHR bio-oils suggested better fuel properties than SHR bio-oils. Pinewood bio-oils had relatively high HHV due to highest levels of C (61.5, 65.4 wt.%) and H (9.1, 9.6 wt.%) contents. HPWB (27.1 MJ/kg) and SPWB (28.6 MJ/kg) represented highest HHVs among HHR and SHR biochars, respectively.

A van Krevelen diagram for biomass and biochars was plotted to compare their atomic ratios (H/C and O/C) and estimate the degree of aromaticity and carbonation (Fig. 4.3). The diagram demonstrated the significance of atomic ratios on the heating value of feedstocks and biochars. From the diagram, it is well-illustrated that biochars had a higher calorific value than that of their feedstocks, which was further confirmed using the Dulong's formula for HHV (see Tables 3.1 and 4.1) SHR biochars demonstrated higher HHVs than those of HHR biochars.

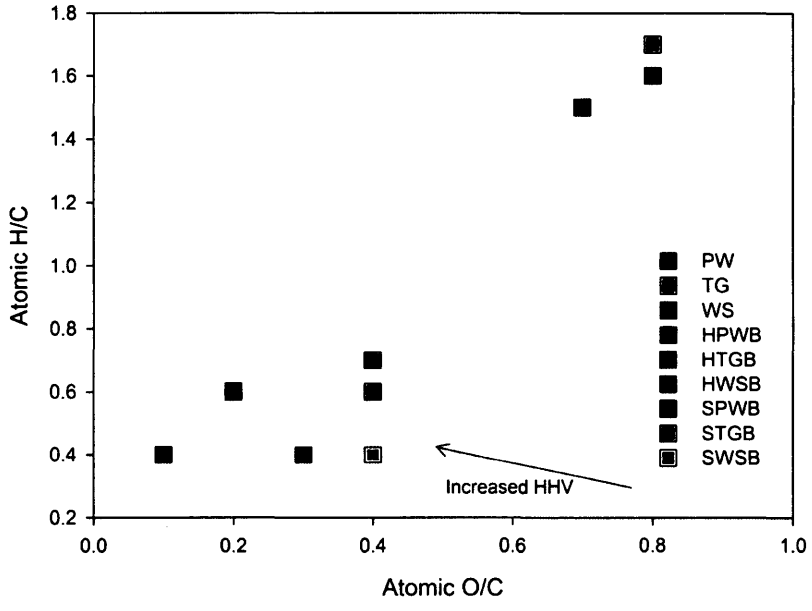

Fig. 4.3 van Krevelen diagram for biomass, HHR and SHR biochars

Abbrev. Pinewood (PW), timothy grass (TG) and wheat straw (WS). HPWB, HTGB and HWSB represent the high heating rate biochars from PW, TG and WS; while SPWB, STGB and SWSB represent the slow heating rate biochars from the same feedstocks.

Table 4.2 ICP-MS analysis for determination of inorganic elements (in ppm) in HHR and SHR biochars

Elements	High heating rate biochars			Slow heating rate biochars		
	HPWB	HTGB	HWSB	SPWB	STGB	SWSB
Macro-elements (g/kg)						
K	1.9	46.4	76.5	2.9	48.3	75.5
Ca	4.7	8.4	11.5	5.8	9.9	10.8
Micro-elements (mg/kg)						
Na	362	164	7879	447	312	8043
Mg	776	5228	2993	865	5894	2998
Al	480	110	270	868	592	487
P	462	4685	3620	567	4933	3505
Cr	208	8	19	125	131	71
Mn	281	149	51	423	179	88
Fe	5367	254	668	3413	497	502
Cu	42	24	13	42	29	80
Zn	75	63	75	126	130	63
Pb	14	8	6	11	5	4
Total alkali metals	8.1	64.8	102.3	10.5	69.4	100.8

Note: All the data are average of replicate measurements. *Abbrev.* HPWB, HTGB and HWSB represent the high heating rate biochars from pinewood, timothy grass and wheat straw; while SPWB, STGB and SWSB represent the slow heating rate biochars from the same feedstocks.

Table 4.2 gives the elemental composition of the biochars produced from HHR and SHR pyrolysis. Biochars derieved from WS and TG had significant amount of elements such as Na, K, Ca and Zn. Calcium was found to be high in STGB (9.9 g/kg) and SWSB (10.8 g/kg) compared to that in HPWB (4.7 g/kg). Calcium is accumulated in the aerial parts of the plants especially in the bark and parenchyma cells of leaves through precipitation of calcium oxalate crystals as

raphides (Werkelin et al., 2005). Since PW used for pyrolysis was without bark, its biochar showed lower amount of Ca than WS and TG biochars.

The combined level of heavy metals such as Cr, Fe and Pb was high in the case of HPWB (5589 mg/kg) and SPWB (3549 mg/kg). Considerable amount of alkaline metals such as Na, Mg, K and Ca in SHR biochars indicate their compatibility as soil amendments for enhancing soil fertility and reducing soil acidity. Among biochars, SWSB had the highest levels of P (3505 mg/kg) and K (75.5 g/kg).

4.3.2. Spectroscopic analysis

The FT-IR spectra of HHR and SHR biochars are shown in Fig. 4.4 (A, B). Different bands in the spectra represented different functional groups in biochar as given in Table 4.3. The band at 3500-3660 cm^{-1} was assigned to –OH stretching. The bands at 1463 and 2940 cm^{-1} were assigned to CH_2 aliphatics in biochars originating from cellulose, hemicellulose, lignin and fatty acids from the biomasses (Himmelsbach et al., 2002). Other bands represented presence of C–O in carboxylic and ester groups (1611 and 1707 cm^{-1}), C–C and C–O in aromatic rings (1590 cm^{-1}), carboxylic bonds (1707 cm^{-1}), C=C stretching (1275 cm^{-1}) and phenolic –OH stretching (777-1235 cm^{-1}).

The FT-IR spectra of bio-oils from HHR and SHR pyrolysis of PW, TG and WS are presented in Fig. 4.4 (C, D). The C=O vibrations between 1680 and 1780 cm^{-1} were from ketones, esters, aldehydes and carboxylic acids, whereas –OH vibrations (3200-3450 cm^{-1}) were from phenols and alcohols. The –OH and C–O vibrations indicated the presence of carboxylic acids and their derivatives in bio-oils. The bands at 1350-1475 cm^{-1} and 2800-3000 cm^{-1} indicated C–H alkanes. Other components present in bio-oils included C–C alkenes (1575-1675 cm^{-1}), C–H alkynes (723, 2852-2963 cm^{-1}), C–C aromatics (1517-1524 cm^{-1}), C–O–C esters (1168 cm^{-1}). The vibrations at 900-1800 cm^{-1} were due to derivatives of structural carbohydrates and lignin in biomass.

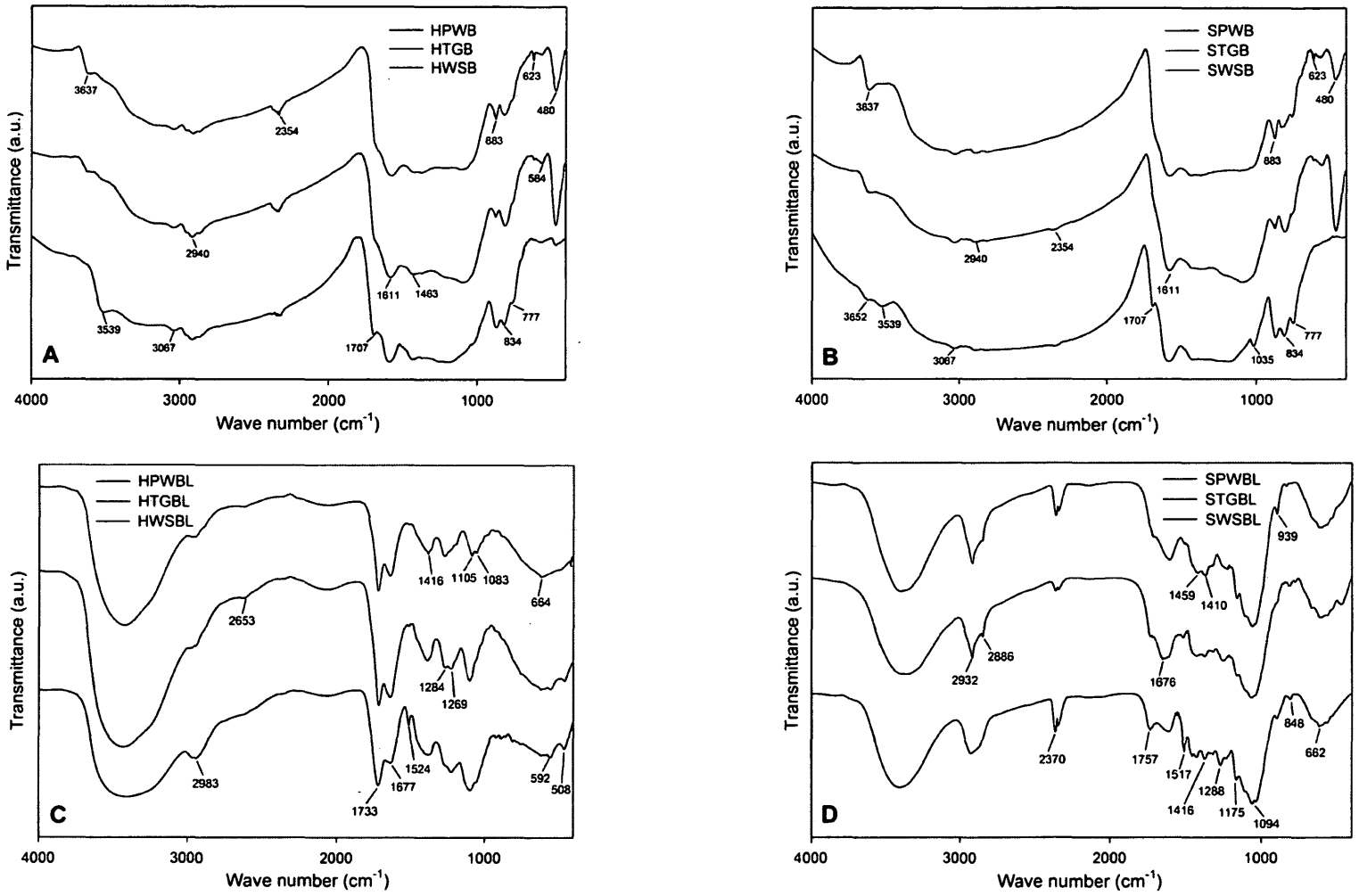

Fig. 4.4 FT-IR spectroscopy of (A) HHR biochars, (B) SHR biochars, (C) HHR bio-oils and (D) SHR bio-oils

Table 4.3 Functional group assignments for different FT-IR bands in HHR and SHR biochars

Wave number (cm^{-1})	Functional groups	Relative band intensity	
		HHR biochars	SHR biochars
623	Alkynes	Strong	Strong
777, 1235, 3500-3660	–OH stretching	Medium	Medium
834, 883	Alkenes	Strong	Strong
1275	C=C stretching	Medium	Weak
1463, 2940, 3067	Alkanes, CH_2 aliphatics	Medium, strong	Weak
1611	Carboxylic acid derivatives	Strong	Strong
1707	Carboxylic acid	Medium	Negligible
2354	Nitriles	Strong	Absent
3539, 3657	Alcohols and phenols	Weak, medium	Strong

Table 4.4 Assignments for different Raman bands in HHR and SHR biochars

Raman shift (cm^{-1})	Band name	Assignment
1700	G_L	C=O carbonyl group
1590	G	C=C alkene
1540	G_R	Amorphous C structure
1465	V_L	Methylene or methyl group
1300	D	C–C
1230	S_L	Aryl-alkyl ether
1185	S	Aliphatic ether

To predict both crystalline and amorphous nature of carbon in HHR and SHR biochars, Raman spectroscopy was used as an analytical tool as it is sensitive to both carbon structures. Deconvolution (curve fitting) of Raman spectra between 1100 and 1800 cm^{-1} resulted in various bands *viz.* G_L, G, G_R, V_L, D, S_L and S (Fig. 4.5). The band names and their assignments have been given in Table 4.4. The nomenclature for Raman bands has been followed according to Keown et al. (2008). The band at 1185 cm^{-1} (S band) and 1230 cm^{-1} (S_L) indicated the strong intensity for aryl-alkyl ether bonding.

The 600-1300 cm^{-1} region was due to aliphatic chains of C=C as found in WS and TG biochars. The bands between 1300 cm^{-1} (D band) and 1465 cm^{-1} (V_L) indicated methylene or methyl groups. The bands at 1550 cm^{-1} (G_R band) and 1700 cm^{-1} (G_L band) were from aromatic compounds, whereas the band specific to 1590 cm^{-1} (G band) was referred to C=C aromatic groups or alkene C=C vibrations (Keown et al., 2008). Other bands such as 1568 and 1634 cm^{-1} indicated aliphatic substitutes and C=N structures, respectively (Agarwal and Ralph, 1997). The D band represented higher aromatic rings ($\leq$ 6 fused rings), while G_R, G_L and V_L represented the amorphous components with smaller fused aromatic rings (Kim et al., 2011).

4.3.3. Structural analysis

From the TGA analysis, weight loss at temperature up to 180°C resulted from absorbed moisture volatilization (Fig. 4.6). The weight loss between 200 and 680°C for all biochars resulted from combustion of their residual organic matter. A shift in exothermicity was found in the case of SHR biochars, which signified maximum heat release and their thermal stability due to the higher weight loss occurring from volatilization of organic components. Within the temperature range of 400-650°C, weight loss in HHR biochars was about 15-20% and in SHR biochars it was about 10-12%.

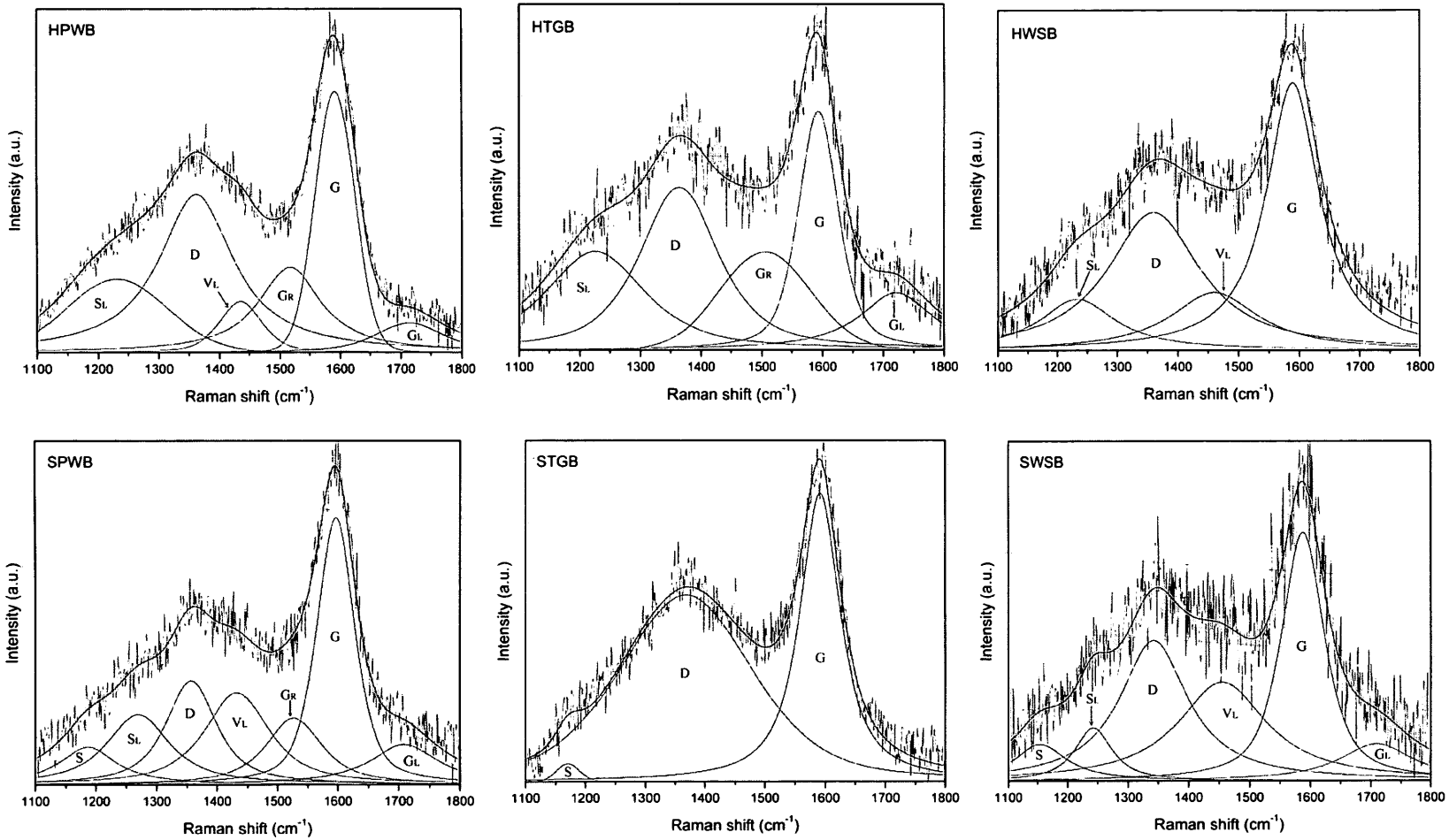

Fig. 4.5 Deconvolution of Raman bands from 1100-1800 cm^{-1} for HHR and SHR biochars

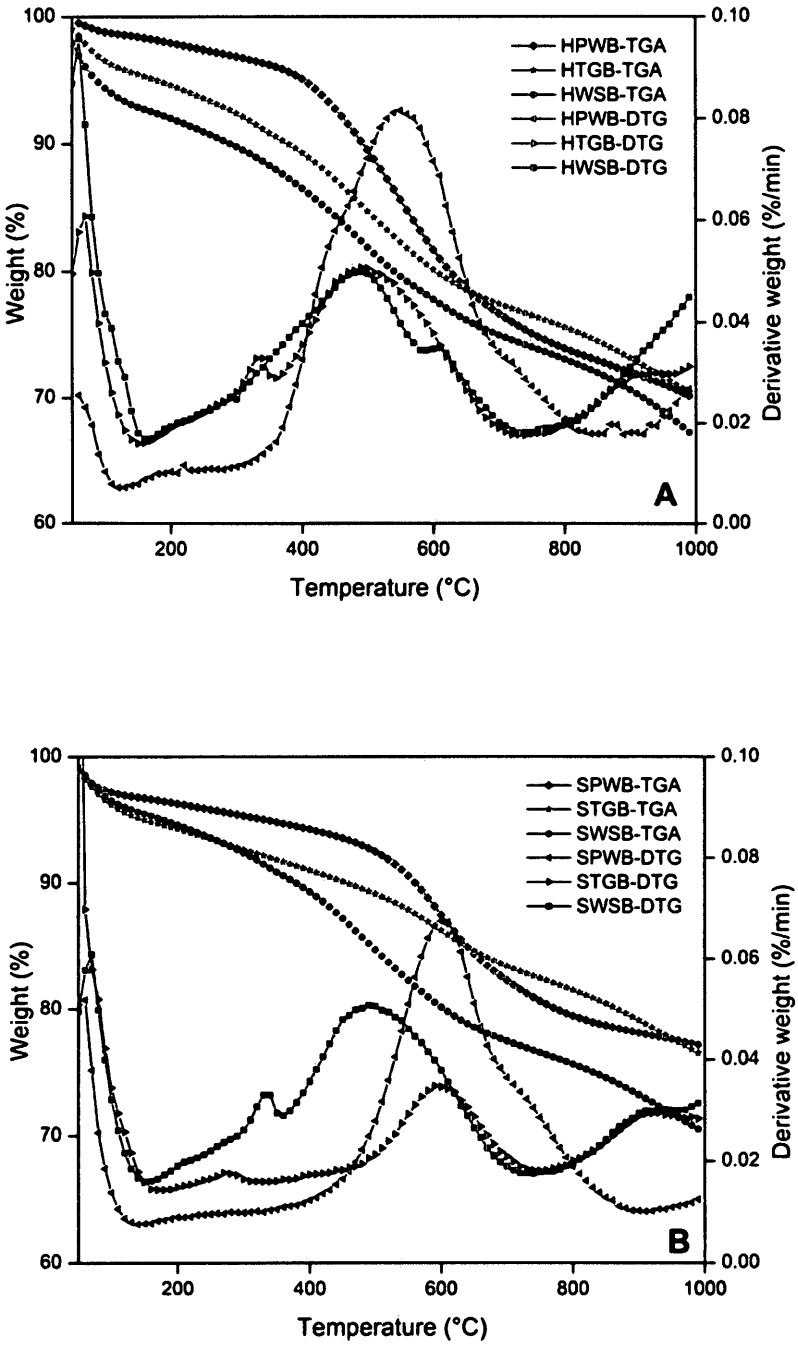

Fig. 4.6 Thermogravimetric analysis of (A) HHR biochars and (B) SHR biochars

Note: TGA in the figure represent the thermogravimetric curves, while DTG represent the differential thermogravimetric curves.

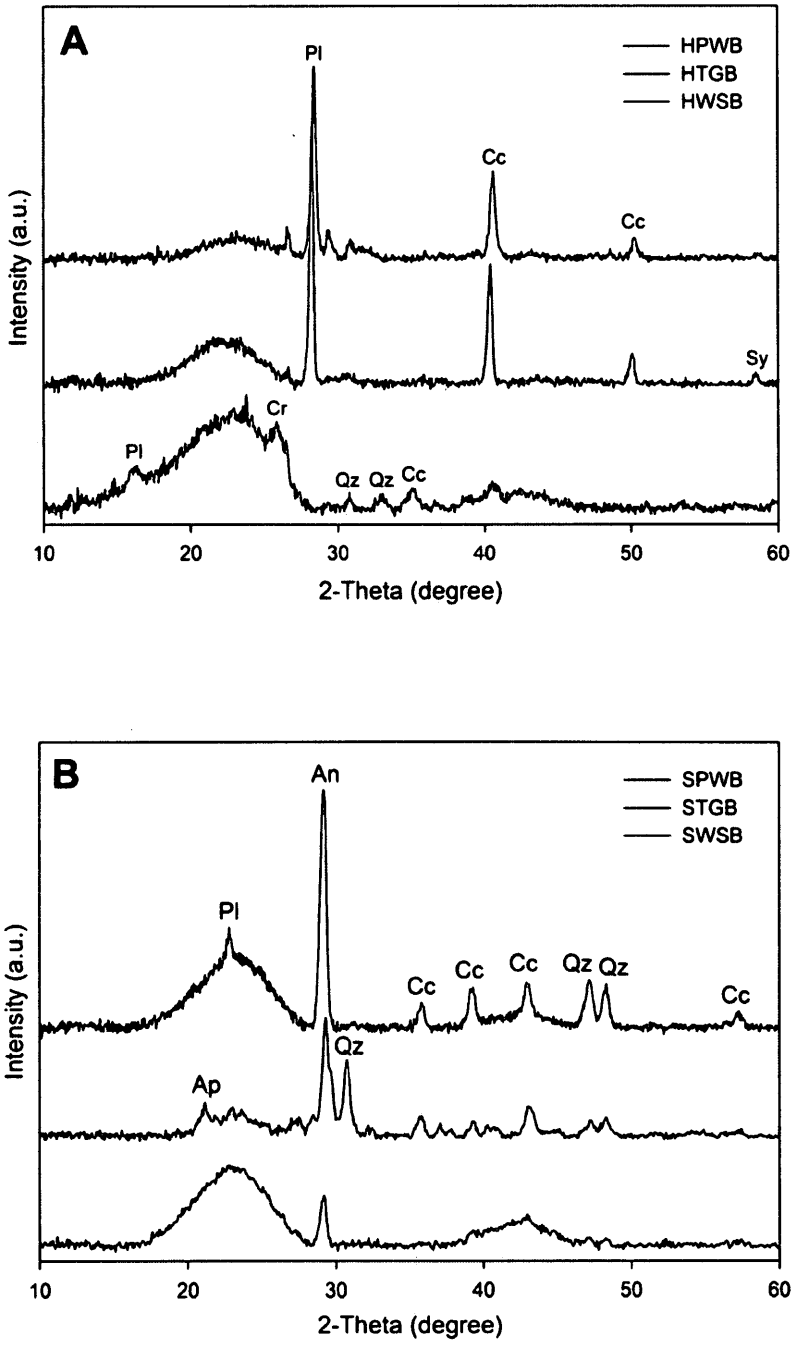

Fig. 4.7 X-ray diffractometry analysis of (A) HHR biochars and (B) SHR biochars

Abbrev. Anhydrite (An), apatite (Ap), calcite (Cc), cristobalite (Cr), plagioclase (Pl), quartz (Qz) and sylvite (Sy)

More degradation in HHR biochars was due to their weaker C–C and C–H bonds than SHR biochars. The stronger C–C and C–H bonds in SHR biochars can be related to their higher amount of carbon and hydrogen than those of HHR biochars (Table 4.1). Among all biochars, SWSB and HWSB were found to be less thermally stable due to their maximum weight loss at higher temperatures.

A number of crystalline and semi-crystalline phases in the biochars close to the XRD detection limit belonged to minerals commonly Na, Mg, Al, Ca, Fe and Mn (Fig. 4.7). The peaks identified in biochars belonged to anhydrite (An), apatite (Ap), calcite (Cc), cristobalite (Cr), plagioclase (Pl), quartz (Qz) and sylvite (Sy). The broad peak at 24.5° (2θ) in most biochars was due to formation of turbostratic carbon crystallites (Kim et al., 2011). This region is characterized with the presence of cellulose polymorphs in biomass (see Fig. 3.4A). Pyrolysis causes dehydration of cellulose components to form carbon crystallites.

The occurrence of carbonate (calcite and anhydrite), phosphate (apatite) and silicates (plagioclase, quartz and cristobalite) in the biochars was due to their presence of large amount of inorganic components as identified through ICP studies. This is a supportive feature for the biochars towards soil applications in rejuvenating the soil's fertility and reducing soil acidity. In contrast to HHR biochars, SHR biochars showed relatively more peaks in the XRD patterns due to their larger amount of inorganic metal composition (see Table 4.2).

4.4. Conclusions

The HHR pyrolysis of pinewood, timothy grass and wheat straw resulted in yields of 21-24 wt.% biochars, 40-48 wt.% bio-oils and 17-24 wt.% pyrolysis gases. On the other hand, SHR pyrolysis resulted in 41-44 wt.% biochar, 18-24 wt.% bio-oil and 24-27 wt.% pyrolysis gas yields. Relatively double-fold increase in the yield of biochars took place in SHR pyrolysis than HHR pyrolysis, whereas similar phenomenon was observed for the higher bio-oil productions from HHR pyrolysis.

In terms of energy content, SHR biochars exhibited a higher HHV than the HHR biochars.

Raman spectroscopy helped to understand the crystalline and amorphous carbonaceous structures present in biochars, especially the graphite and defect carbon structures. Biochars showed the presence of carbonates (calcite), sulphite (anhydrite), phosphate (apatite), silicates (cristobalite, plagioclase, quartz) and chloride (sylvite). The higher amount of alkaline metals found in SHR biochars (Na, Mg, K and Ca) indicated their application as soil amendments for enhancing soil fertility and reducing soil acidity. TGA analysis revealed relatively higher degradation in HHR biochars at higher temperatures due to weaker C–C and C–H bonds. The relatively high thermal stability, alkaline nature and high carbon content of SHR biochars were advantageous for their soil applications, whereas their HHV makes them a better energy product than HHR biochars. In contrast, the high carbon and hydrogen content along with high HHV of HHR bio-oils suggested better fuel values.

Chapter Five: Evolution of lignocellulosic feedstocks during delignification and hydrothermal pretreatment

5.1. Introduction

Lignocellulosic biomass from agriculture, forest, prairies and energy crops are available in surplus with nearly 200 billion tons produced annually worldwide (Zhang, 2008). However, the bioconversion of lignocellulosic biomass to fuel alcohols (ethanol and butanol) requires the breakdown of cellulose and hemicellulose to monomeric sugars for fermentation by microorganisms. The widely used hydrolysis processes for biomass to produce fermentable sugars are hydrothermal, dilute acid or alkaline pretreatment and enzymatic hydrolysis (see Chapter 2).

Lignocellulosic feedstocks are composed of 35-55% cellulose, 20-40% hemicellulose and 10-25% lignin (Sukumaran et al., 2010). The factors that contribute to the recalcitrance of lignocelluloses include the degree of lignification, cellulose crystallinity and its specific surface area, degree of polymerization, acetylated hemicelluloses, lignin-carbohydrate complexes and biomass pore volume (Hu and Ragauskas, 2012). In addition, other features that make lignocelluloses resistant to chemical and enzymatic pretreatments include plant's epidermal tissue (cuticle and epicuticular waxes), arrangement and density of their vascular bundles, relative amount of sclerenchymatous tissues along with structural heterogeneity and complexity of cell wall components such as microfibrils and matrix polymers (Himmel et al., 2007).

Cellulose has a degree of polymerization between 1,510 and 5,500 in plants and primarily occurs in crystalline form (Hallac and Ragauskas, 2011). On the other hand, hemicellulose is amorphous and has a degree of polymerization in the range of 50-200 (Yaman, 2004). The amorphous nature and lower degree of polymerization make hemicelluloses easily hydrolysable than cellulose. Lignin is a three

dimensional, amorphous, cross-linked phenyl propane polymer of guaiacyl, syringyl and *p*-hydroxyphenyl units. Lignin is hydrophobic and fills the spaces in the cell wall (middle lamella in wood) between cellulose and hemicelluloses by covalently binding with hemicelluloses (Kumar et al., 2009). Moreover, the hydrophilic hemicellulose in the cell wall acts as an inter-fiber bonding agent between cellulose microfibrils. This cellular arrangement provides rigidity to the plant cell wall and makes the biomass recalcitrant to acids and enzymes. In addition, lignification provides mechanical strength to the plant in withstanding aggressive environmental conditions and prevents it from microbial or fungal destruction including invasion by pests and pathogens.

There are no known microorganisms that are able to utilize lignin for alcohol production (Zaldivar et al., 2001). Moreover, lignin acts as a barrier against biomass saccharification. Hence, it is essential to denature the polymeric lignin that prevents access of chemicals and enzymes to cellulose and hemicellulose. Due to their reticulation and three dimensional structures, lignin is usually insoluble in solvents, unless it is degraded by chemical treatments. Lignin is almost insoluble in concentrated H_2SO_4, although an alkaline treatment (e.g., NaOH and $NaClO_2$) helps remove lignin from the biomass (Lin et al., 2010). In addition, the evolutionary changes in the feedstock during delignification is least understood today. With this objective, this chapter focuses on the chemical and structural changes in pinewood, timothy grass and wheat straw as a result of delignification and hydrothermal pretreatment.

5.2. Materials and methods

5.2.1. Biomass pretreatment and delignification

The biomasses used in this study were pinewood (PW), timothy grass (TG) and wheat straw (WS). The details of their collection and chemical characterization can be found comprehensively in Chapter 3.

For hydrothermal (HT) pretreatment, 10 g of biomass in 200 mL distilled water (1:20 mass/volume) was autoclaved at 121°C for 1 h. After autoclaving, the hydrothermally treated- pinewood (PWHT), timothy grass (TGHT) and wheat straw (WSHT) were filtrated and oven-dried at 50°C for 24 h before analysis.

Delignification of feedstocks was carried out by mixing 10 g of biomass with 320 mL Milli-Q water, 16 mL 98% CH_3COOH and 8 g $NaClO_2$ (Kristensen et al., 2008). The mixture was placed in a water bath at 80°C for 1 h. The reaction was terminated by cooling to 10°C. The delignified- pinewood (PWDL), timothy grass (TGDL) and wheat straw (WSDL) were recovered by filtration, washed with ice-cold water and oven-dried at 50°C for 24 h before analysis. The untreated, HT treated and delignified biomasses are shown in Fig. 5.1.

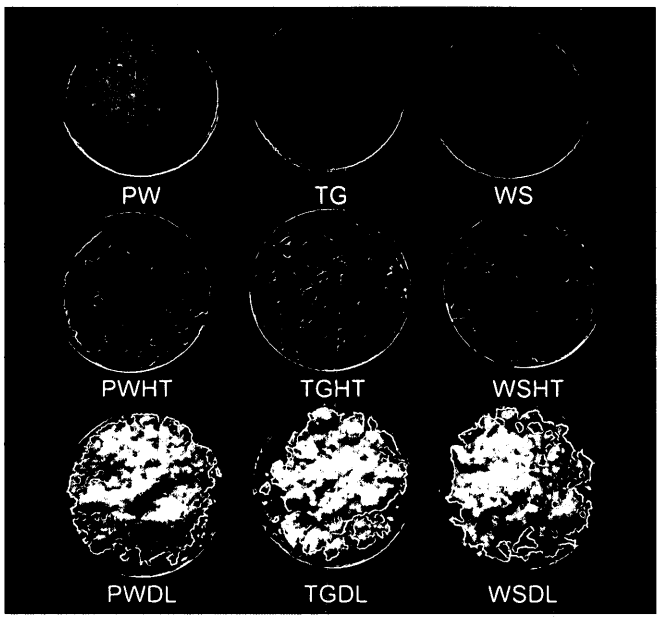

Fig. 5.1 Illustration of untreated biomass (top row), hydrothermally pretreated biomass (middle row) and delignified biomass (bottom row)

Abbrev. Pinewood (PW), timothy grass (TG), wheat straw (WS); hydrothermally pretreated-pinewood (PWHT), timothy grass (TGHT) and wheat straw (WSHT); delignified- pinewood (PWDL), timothy grass (TGDL) and wheat straw (WSDL)

5.2.2. Proximate, ultimate and compositional analysis

The moisture, ash and volatile matter in feedstocks were determined using standard ASTM procedures as described in Chapter 3 (section 3.2.2). The CHNS analysis and calorific value (as higher heating value, HHV) determinations were done using the procedures mentioned in Chapter 3 (sections 3.2.2 and 3.2.3).

The biomass samples were acid hydrolyzed for determination of cellulose, hemicellulose and lignin using the standard NREL method (Sluiter et al., 2008a). As per the method, samples were hydrolyzed with 72% H_2SO_4 at 30°C for 1 h followed by 4% H_2SO_4 at 121°C for 1 h. The hydrolyzed sugars (e.g., arabinose, cellobiose, glucose and xylose) were quantified in an Agilent Series 1100 HPLC (Agilent Technologies Ltd., USA) equipped with a refractive-index detector. The analysis was performed using an Aminex HPX 87H ion-exclusion column (BioRad, USA) with a Cation H micro-guard cartridge (BioRad). 5mM H_2SO_4 was used as the mobile phase with a flow rate of 0.6 mL/min and column temperature of 55°C. The weight percent of sugars in the hydrolysates were determined by comparing with respective sugar standards.

5.2.3. Thermogravimetric analysis (TGA)

TGA was used to determine the devolatilization characteristics of untreated, HT treated and delignified feedstocks in a PerkinElmer Pyris Diamond TG/DTA instrument (PerkinElmer, USA). About 5 mg of biomass was heated from 25 to 500°C at a heating rate of 10°C/min with purge gas (argon) flow rate of 10 mL/min. The rate of weight loss with respect to temperature was recorded.

5.2.4. X-ray diffractometry (XRD)

XRD of untreated and treated feedstocks was carried out using a Bruker D8 Advance X-ray diffractometer (Bruker AXS, Germany) with CuKα radiation at 40 kV, 130 mA, $\lambda = 0.154$ nm and 2θ scanning angle of 10-70° at a scanning speed of 0.2°/min. The degree of cellulose crystallinity (expressed as crystallinity

index, CrI) in the feedstocks was calculated from the diffraction intensities using the Segal method (Segal et al., 1959) as follows:

$$CrI = 100 \times \left[\frac{I_{002} - I_{amorphous}}{I_{002}}\right] \quad \text{(Equation 2)}$$

Where, I_{002} is the intensity for the crystalline portion of cellulose at ~22.0° and $I_{amorphous}$ is the intensity corresponding to the amorphous portion at ~18.0°.

5.2.5. Fourier transform infrared (FT-IR) and Raman spectroscopy

FT-IR analysis was performed using a Smiths Detection IluminatIR FT-IR spectrometer (Smiths Detection Inc., USA) coupled to a Renishaw inVia Raman microscope (Renishaw Inc., USA). FT-IR spectra for biomass samples were collected in the range of 500-4000 cm^{-1} with a co-addition of 64 scans at a 4 cm^{-1} spectral resolution using a 15X ARO objective and a 100 μm aperture. The FT-IR and Raman spectra were collected from the same sample spot for accuracy and uniformity in analysis.

Raman measurements were acquired using the Renishaw inVia Raman microscope equipped with Renishaw 785 nm laser diode and a CCD (charge-couple device) detector. Raman spectra for biomass samples were collected at a resolution of 4 cm^{-1} using a 20X objective with 10 s exposure time and 8 accumulations. Raman maps for untreated, HT treated and delignified feedstocks were acquired for studying their in-situ distribution of lignin (1580-1620 cm^{-1}) and plant waxes (2800-3000 cm^{-1}). Renishaw WiRE software (version 3.4) was used for the spectral analysis and mapping. The Renishaw CCD camera was used to capture optical images of the sample spot for Raman maps.

5.2.6. Scanning electron microscopy (SEM)

SEM imaging for the feedstocks was performed using a FEI Quanta 3D FEG DualBeam microscope (FEI Company, USA) operated in high vacuum mode

and 5 kV of voltage. Prior to analysis, the samples were gold coated in a Denton Desk V Sputter coater (Denton Vacuum, USA).

5.2.7. Atomic force microscopy (AFM)

AFM imaging was performed in an Agilent 4500 AFM microscope (Agilent Technologies Ltd., USA) operating in intermittent contact mode. A silicon cantilever (AppNano, USA) with a curvature radius < 6 nm was used at a force constant of 48 N/m and a resonant frequency of 190 kHz. All analyses were done at a scanning rate of 0.5 line/s and a set-point oscillation amplitude to free air oscillation of 0.7-0.8 with resonant amplitude of 2-3V. The images were processed using Scanning Probe Image Processor 5.1.5 (Image Metrology, Denmark).

5.3. Results and discussion

5.3.1. Proximate, ultimate and compositional analysis

The proximate and ultimate analyses together with compositional analysis of untreated, HT treated and delignified feedstocks are presented in Table 5.1. The fraction of ash increased in the order: $Ash_{Untreated} < Ash_{HT\ treated} < Ash_{Delignified}$. On an average basis, the ash level increased by 56.3% in the HT treated samples and by 84.5% in the delignified samples than that of untreated samples. The increasing trend of ash in HT treated and delignified feedstocks indicated the increase in crystallinity of the samples.

PW samples exhibited relatively higher amount of C and H than those in TG and WS samples, due to their woody nature. The delignified samples showed a 17% decrease in C content compared to the untreated feedstocks. The H/C and O/C ratios in delignified samples showed a gradual increase of 22.6 and 34.5%, respectively than untreated samples.

Table 5.1 Proximate, ultimate and compositional analysis of untreated, hydrothermally treated and delignified biomass

Analyses	PW	TG	WS	PWHT	TGHT	WSHT	PWDL	TGDL	WSDL
Moisture (wt.%)	6.8 ± 0.2	5.6 ± 0.3	5.2 ± 0.3	7.2 ± 0.4	5.9 ± 0.3	6.6 ± 0.3	6.5 ± 0.3	5.7 ± 0.2	5.9 ± 0.3
Volatiles (wt.%)	71.7 ± 1.5	78.2 ± 2.1	70.1 ± 1.2	70.5 ± 0.9	74.2 ± 1.3	75.3 ± 1.1	69.7 ± 0.9	73.2 ± 1.0	72.4 ± 0.9
Fixed carbon (wt.%)	19.2	12.6	20.3	17.8	14.4	12.0	17.1	14.9	15.6
Ash (wt.%)	2.3 ± 0.1	3.6 ± 0.3	4.4 ± 0.2	4.5 ± 0.2	5.5 ± 0.2	6.1 ± 0.3	6.7 ± 0.3	6.2 ± 0.1	6.1 ± 0.2
C (wt.%)	48.9	43.4	44.1	46.3	43.4	44.8	40.3	35.7	37.3
H (wt.%)	6.2	6.1	6.0	6.7	6.7	8.0	6.6	5.9	6.3
N (wt.%)	0.1	1.3	0.4	0.1	1.0	0.2	0.02	0.3	0.1
S (wt.%)	0.1	0.1	0.01	0.2	0.1	0.004	0.1	0.02	-
O (wt.%)	42.5	45.5	45.0	42.3	43.4	40.9	46.3	51.9	50.2
Atomic H/C	1.5	1.7	1.6	1.7	1.8	2.1	2.0	2.0	2.0
Atomic O/C	0.7	0.8	0.8	0.7	0.8	0.7	0.9	1.1	1.0
Atomic N/C	0.001	0.03	0.01	0.002	0.02	0.004	0.0003	0.01	0.002
HHV (MJ/kg)	18.1 ± 1.2	15.9 ± 1.5	15.6 ± 1.3	18.2 ± 1.1	17.1 ± 0.9	17.9 ± 0.9	15.4 ± 0.6	12.1 ± 0.4	13.6 ± 0.6
Compositional analysis (wt.%)									
Cellobiose	2.5	1.9	2.4	3.5	3.6	4.8	6.2	5.1	5.9
Glucose	48.2	44.1	49.5	62.2	57.6	59.1	75.8	72.3	74.6
Xylose	19.5	22.7	16.7	4.1	4.6	3.7	8.4	8.1	7.8
Arabinose	3.3	6.9	6.9	0.3	6.1	5.2	1.7	7.5	4.9
Lignin	24.2	20.8	20.1	25.4	22.6	21.1	1.2	0.8	0.7

Note: All the data are average of replicate measurements with standard deviation less than 5%.

From the atomic ratios, the chemical formulae for PW, TG and WS were established as $CH_{1.5}O_{0.7}N_{0.001}$, $CH_{1.7}O_{0.8}N_{0.03}$ and $CH_{1.6}O_{0.8}N_{0.01}$, respectively. Correspondingly, the formulae for PWHT, TGHT and WSHT were determined as $CH_{1.7}O_{0.7}N_{0.002}$, $CH_{1.8}O_{0.8}N_{0.02}$ and $CH_{2.1}O_{0.7}N_{0.004}$. Similarly, PWDL, TGDL and WSDL had their formula as $CH_2O_{0.9}N_{0.0003}$, $CH_2O_{1.1}N_{0.01}$ and $CH_2ON_{0.002}$, respectively.

The high calorific values (MJ/kg) of PW (18.1), PWHT (18.2) and PWDL (15.4) were due to the woody and ligneous nature of PW. Lignin has a HHV of 23.3-25.6 MJ/kg, which is about 30% higher than that of holocellulose (Novaes et al., 2010). The high lignin content (24.2 wt.%) in PW along with its higher C (48.9 wt.%) and H (6.2 wt.%) contents resulted in its high HHV. The average calorific value in the delignified samples showed a decline of 17.1 wt.% than that of untreated samples. This was because of lignin removal in delignified feedstocks.

The compositional analysis for cellulose and hemicellulose sugars in the feedstocks was performed following the standard NREL procedures. Assuming a complete conversion, the composition of glucose and cellobiose was recognized as cellulose, whereas xylose and arabinose together indicated hemicellulose (Lenihan et al., 2010). The percent composition of cellulose and hemicellulosic sugars as well as lignin is given in Table 5.1. The cellulose occurrence was in the order: $Cellulose_{Untreated}$ (46-51.9 wt.%) < $Cellulose_{HT\ treated}$ (61.2-65.7 wt.%) < $Cellulose_{Delignified}$ (77.4-82 wt.%). On an average, cellulose increased by a factor of 28.4% in HT treated feedstocks and by 61.4% in delignified feedstocks. On the other hand, hemicellulose showed a reverse order of occurrence as: $Hemicellulose_{Untreated}$ (22.8-29.6 wt.%) > $Hemicellulose_{Delignified}$ (10.1-15.6 wt.%) > $Hemicellulose_{HT\ treated}$ (4.4-10.7 wt.%). Hemicellulose decreased by a factor of 49.5% in delignified samples and by 68.4% in HT treated samples.

As hemicellulose is relatively easy to hydrolyze than cellulose because of its amorphous nature, lower degree of polymerization and molecular weight less

than 30,000 (Huber et al., 2006), it was found to decrease in HT treated and delignified samples. A decrease in lignin fraction by 95.9% was achieved in delignified feedstocks. The lignin occurrence was in the order: $Lignin_{HT\ treated}$ (21.1-25.4 wt.%) > $Lignin_{Untreated}$ (20.1-24.2 wt.%) > $Lignin_{Delignified}$ (0.7-1.2 wt.%).

5.3.2. Thermal and structural analysis

The devolatilization process for the untreated feedstocks started at 240-280°C with the maximum weight loss in the range of 300-360°C (Fig. 5.2). The initial devolatilization temperature for PW was ~260°C, whereas for PWHT and PWDL it was ~280 and 240°C, respectively (Fig. 5.2A). TG started degrading at ~280°C, whereas for TGHT and TGDL it was ~270 and 240°C, respectively (Fig. 5.2B). Similarly, the devolatilization temperature for WS, WSHT and WSDL were ~270, 295 and 250°C (Fig. 5.2C). The decrease in the devolatilization temperature of delignified samples was due to removal of lignin and their modified cellular structure. Cellulose and hemicellulose degrade at 250-350°C and 200-300°C, respectively while lignin degrades at a wide temperature range of 200-500°C (Carrier et al., 2011).

In the XRD pattern of all feedstocks (Fig. 5.3), the major maximum at 21.7° (d-space ~3.96 Å) and minor maximum at 15.5° (d-space ~5.51 Å) were due to the occurrence of Cellulose I and Cellulose II, respectively (Vassilev et al., 2012). The halo at 34.5° (d-space ~2.59 Å) represented the presence of hemicellulose. Cellulose is known to have six crystalline forms, namely Cellulose I, Cellulose II, Cellulose III_1, Cellulose III_2, Cellulose IV_1 and Cellulose IV_2 (Correa et al., 2010) Among all forms, Cellulose I and II are predominantly found in nature. Cellulose I has two crystalline polymorphs: (i) Cellulose I_α which is triclinic, metastable and dominant to lower plants and herbaceous species, and (ii) Cellulose I_β which is monoclinic, stable and dominant for higher plants and woody species (Vassilev et al., 2012).

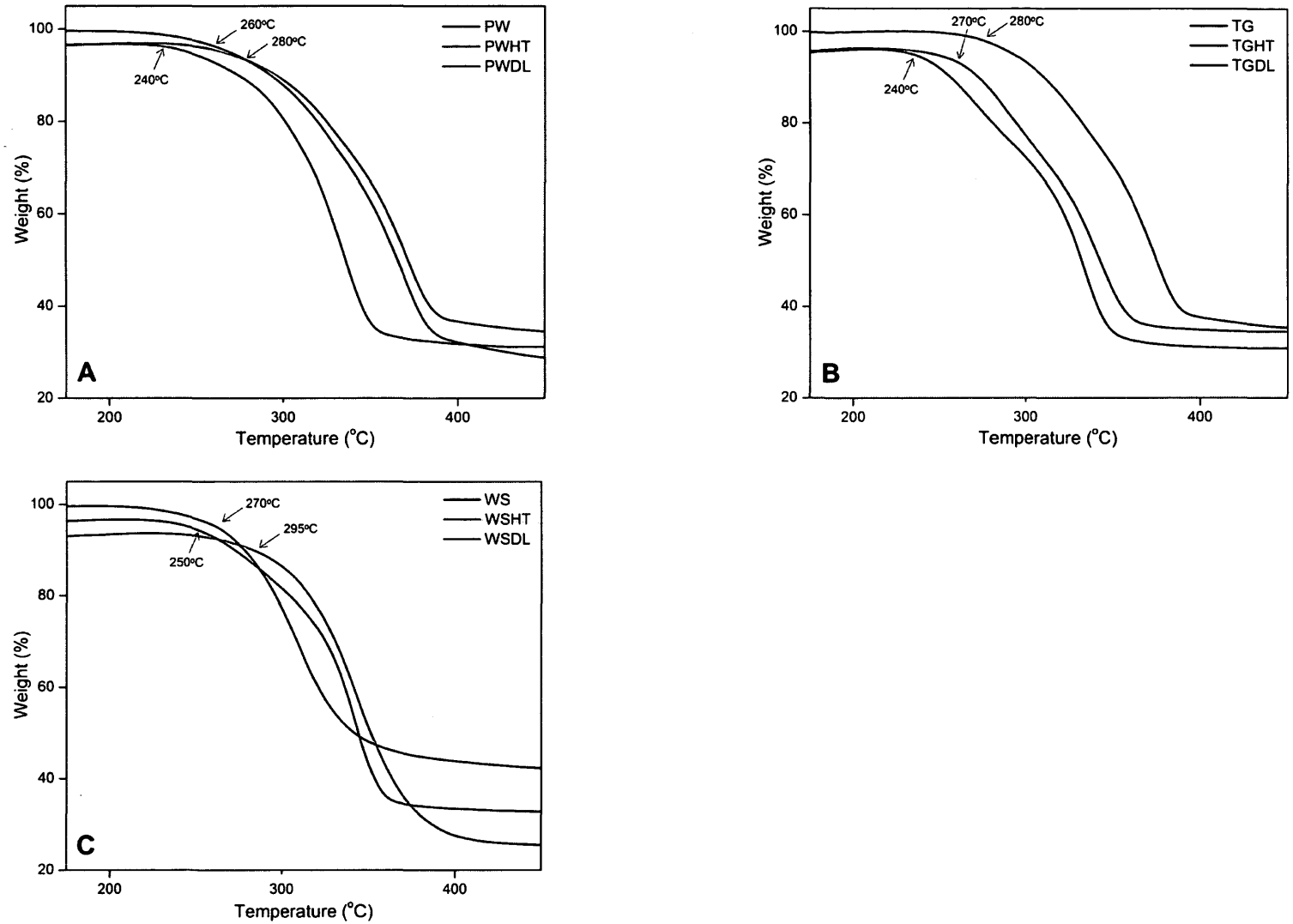

Fig. 5.2 Thermogravimetric analysis of untreated, HT treated and delignified (A) PW, (B) TG and (C) WS biomass

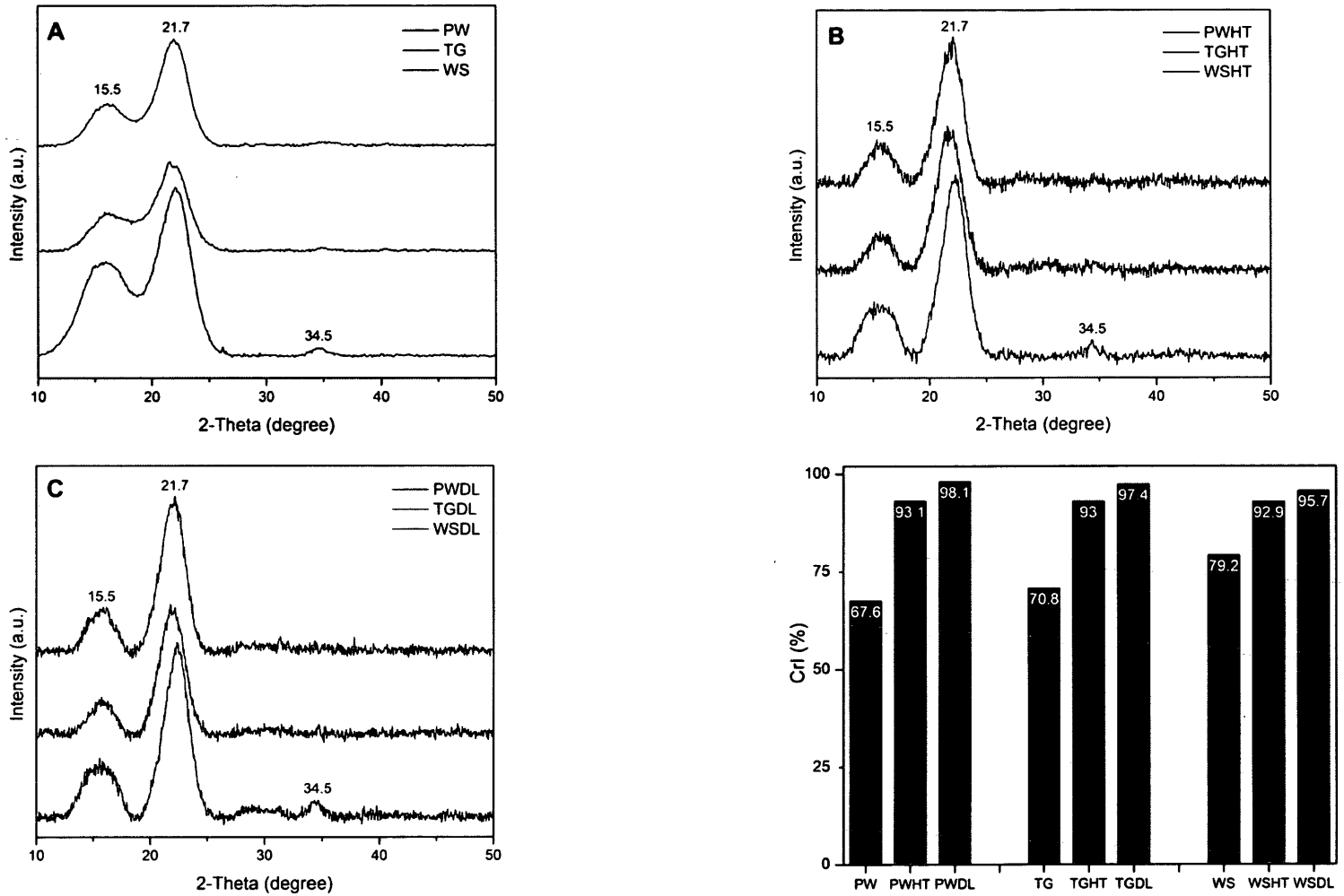

Fig. 5.3 X-ray diffractometry analysis for (A) untreated biomass, (B) HT treated biomass, (C) delignified biomass and (D) crystallinity index (CrI) determination

The crystallinity index, CrI (Fig. 5.3D) for the biomasses calculated using Segal method varied as $CrI_{Untreated}$ (67.6-79.2%) < $CrI_{HT\ treated}$ (92.0-93.1%) < $CrI_{Delignified}$ (95.7-98.1%). The increase in the crystallinity of cellulose was evident from the XRD patterns of HT treated and delignified biomass which showed considerably narrow and intense peaks at 15.5° and 21.7°. The reason for narrowing of these peaks could be explained as high temperature water act as a catalyst in penetrating the crystalline and amorphous regions of cellulose and releasing free water molecule from biomass causing re-crystallization (Biswas et al., 2011). WS, PWHT and PWDL demonstrated maximum CrI of 79.2, 93.1 and 98.1% among untreated, HT treated and delignified feedstocks.

5.3.3. Spectroscopic analysis

The FT-IR spectra of feedstocks were studied to determine their surface organic functional groups (Fig. 5.4). The spectra revealed the most prominent broad peak at 3300-3400 cm^{-1} originating from –OH stretching vibration. The peaks at 2850-2916 cm^{-1} were due to CH_2 and CH_3 asymmetric and symmetric vibrations from long chain organic compounds such as plant waxes, fatty acids, fatty esters, high molecular mass aldehydes or ketones (Himmelsbach et al., 2002). The peak at 1380 cm^{-1} was due to aliphatic CH_3 deformation. The 1040-1260 cm^{-1} stretch was due to alcohols, ethers, carboxylic acids and esters. The peaks at 1428 and 1641 cm^{-1} indicated C–H alkanes and C=C alkenes, respectively.

The peaks at 900-1428 cm^{-1} represented amorphous and crystalline forms of cellulose (Oh et al., 2005). The bands due to C–O–C aliphatic (1097 cm^{-1}) and C–O alcohol (1175 cm^{-1}) were from oxygenated functional groups of cellulose. The increasing intensities of these peaks were observed with treatments which corresponded to the compositional analysis (Table 5.1). The cumulative intensities of these cellulose peaks in HT treated and delignified feedstocks were because of the higher concentration of cellulose due to removal of hemicellulose and lignin.

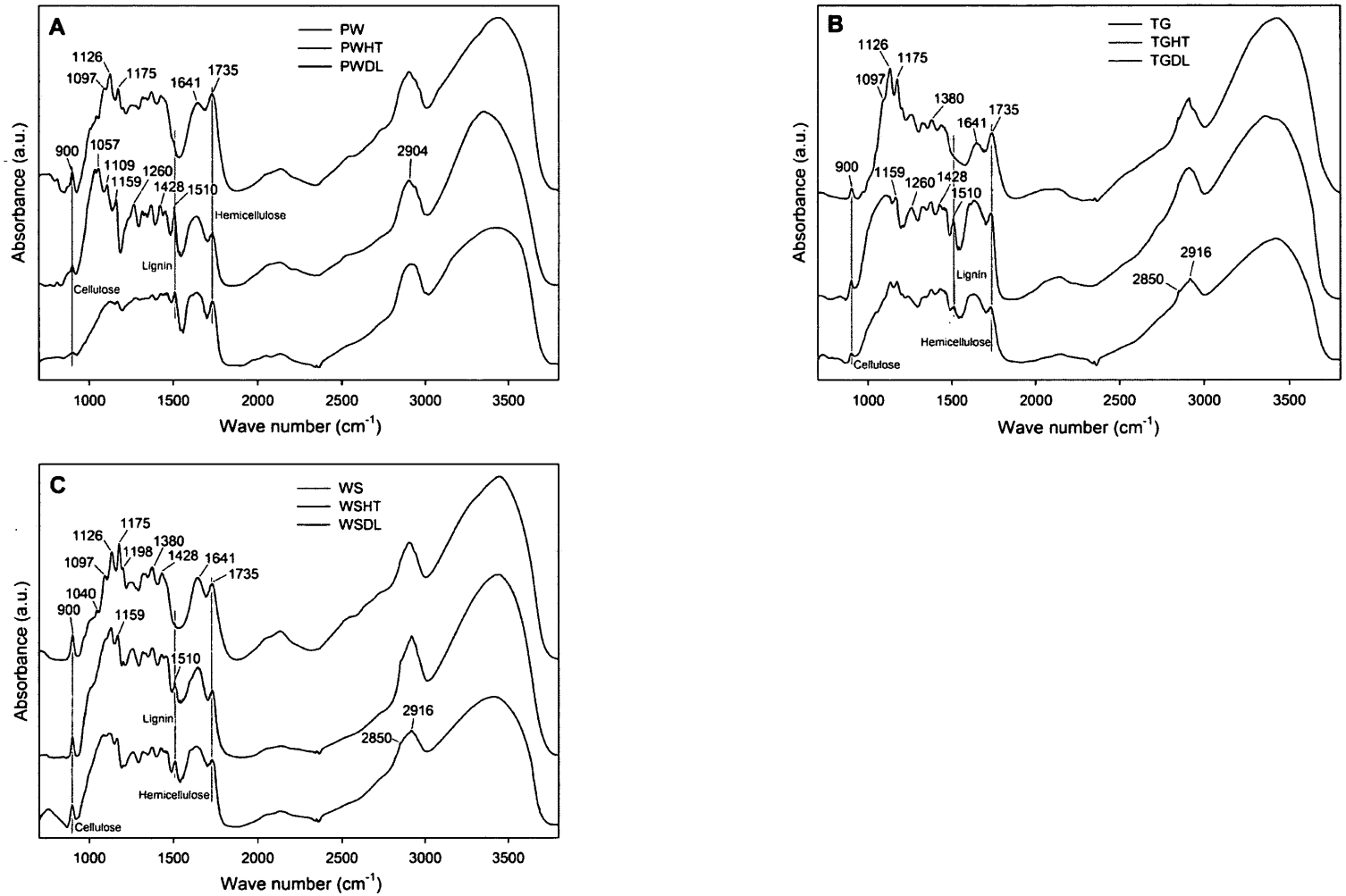

Fig. 5.4 FT-IR spectroscopy of untreated, HT treated and delignified (A) PW, (B) TG and (C) WS biomass

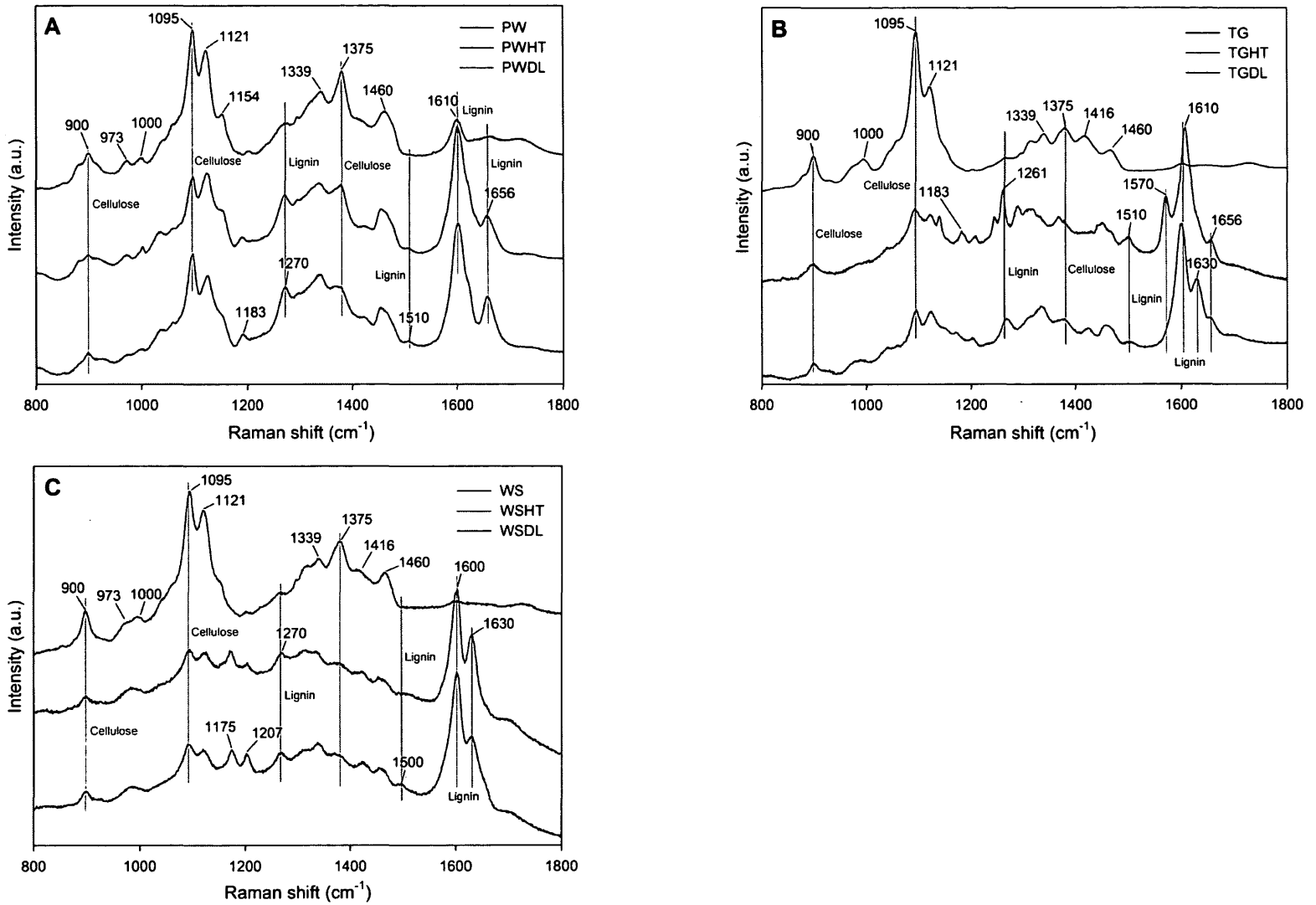

Fig. 5.5 Raman spectroscopy of untreated, HT treated and delignified (A) PW, (B) TG and (C) WS biomass

The C=O carbonyl band at 1735 cm^{-1} was ascribed to hemicellulose (Kristensen et al., 2008). The hemicellulose peak appeared to decrease in the HT samples suggesting a decrease in their occurrence as quantitatively observed in Table 5.1. The peak at 1510 cm^{-1} represented aromatic C–C stretch. The relative intensity of the lignin peak was enhanced in the HT treated feedstocks versus the untreated samples. The reason for increase in lignin intensity in HT treated samples was due to the hemicellulose removal. The absence of any peaks at 1510 cm^{-1} in delignified samples suggested lignin removal through alkaline treatment.

Raman spectroscopy is an analytical tool widely used to evaluate the structural features of carbonaceous materials as it is sensitive to both crystalline and amorphous structures. As seen from Fig. 5.5, the cellulosic and hemicellulosic components occurred in the spectral range of 900-1183 cm^{-1} (Agarwal and Ralph, 1997). The peaks at 1339, 1375 and 1460 cm^{-1} represented C–H deformation in cellulose. The peak at 1416 cm^{-1} was ascribed to hemicellulose and its reduced intensity in HT treated samples explained its removal. The Raman peaks at 900 and 1095 cm^{-1} represented amorphous and crystalline cellulose.

Similar to FT-IR findings, these cellulose peaks demonstrated a steady increase in HT treated and delignified feedstocks. This not only explained the crystallinity of cellulose as measured through XRD CrI (Fig. 5.3D) but also confirmed its increasing concentrations as estimated through compositional analysis (Table 5.1). The increasing crytallinity of the samples reduced the peak widths for cellulose components, whereas the hemicellulose features remained amorphous causing peak widths to broaden.

Major vibrations in the Raman spectra (Fig. 5.5) at 1261, 1270 and 1510-1656 cm^{-1} were due to lignin with the most distinctive bands at 1600 and 1610 cm^{-1} (Agarwal, 2006). A minor peak at 1610 cm^{-1} was found in PWDL suggesting traces of residual lignin which was quantified as 1.2 wt.% (Table 5.1). This could be because of the release of lignin during delignification and further re-deposition on the biomass surface.

Raman spectroscopy was used to generate chemical maps for lignin and plant waxes in PW, TG and WS samples (Figs. 5.6-5.8). In Figs. 5.6-5.8: (A, B, C); (D, E, F) and (G, H, I) represent the Raman maps for untreated, HT treated and delignified samples, respectively. In order to study the in-situ lignin distribution, chemical maps was generated from the spectral region of 1580-1620 cm^{-1}, whereas the 2800-3000 cm^{-1} region was selected for plant waxes. In Figs. 5.6-5.8: B, E and H represent the lignin maps, while C, F and I represent the maps for plant waxes. The optical microscopic images of the sample spots for mapping are shown in Figs. 5.6-5.8: A, D and G.

The intensity scale bar (counts) in the figures with color gradient explains the change in lignin and wax distribution in the feedstocks with respect to HT and delignification treatment. As lignin is known to glue the fibrous components in plants, it could be clearly seen encrusting the cell walls and binding the cells together in Fig. 5.6 (D, E). In the cell walls, lignin is enriched mostly in the middle lamella between adjacent cell walls (Vassilev et al., 2012). This sheath of lignin acts as a shield to protect the plant cells from acids, enzymes and other stress conditions. A comparison between sub-figures B and E (Figs. 5.6-5.8) indicated a delocalization of the lignin sheath. A few vacuoles in the lignin matrix of PWHT were observed (Fig. 5.6B), which could be explained as the HT pretreatment led the steam under pressure to penetrate the plant's cellular structure and alter the lignin arrangement.

The magnitudes of lignin and waxes were found to significantly decrease in delignified samples. The approximate counts for lignin in PWDL were ~160, which showed a significant decline from the native feedstock (PW: ~9000 counts). This suggested nearly 98.2% lignin removal which corresponded to the compositional analysis (Table 5.1). Similarly, from the counts for waxes in PW samples there was a reduction of about 77.3% in PWHT and 89.1% in PWDL. TGHT, TGDL and WSDL showed a decrease in intensities by nearly 86.7%, 97.3% and 87.7%, respectively.

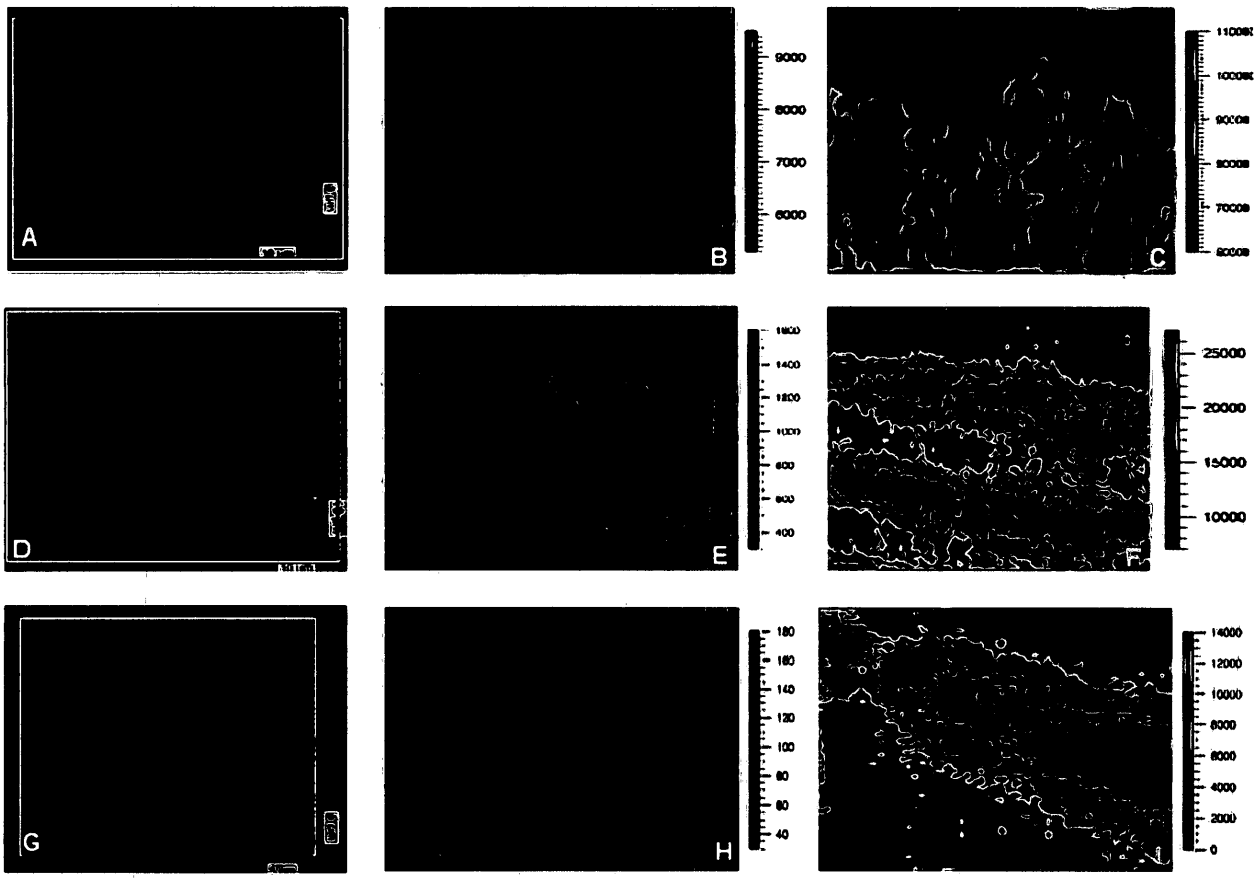

Fig. 5.6 Chemical maps for PW (A, B, C), PWHT (D, E, F) and PWDL (G, H, I). Optical images of the sample spot (A, D, G); lignin maps (B, E, H); wax maps (C, F, I)

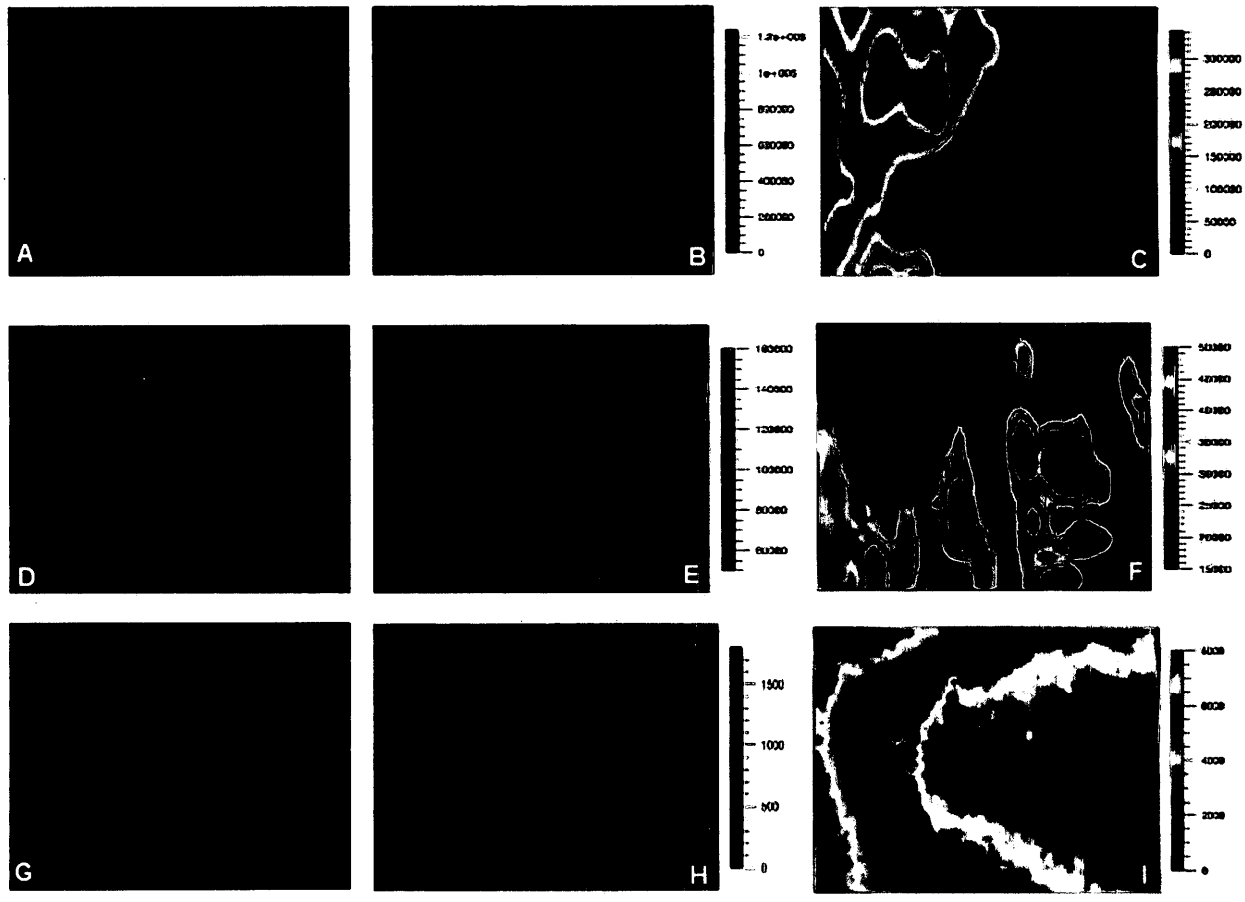

Fig. 5.7 Chemical maps for TG (A, B, C), TGHT (D, E, F) and TGDL (G, H, I). Optical images of the sample spot (A, D, G); lignin maps (B, E, H); wax maps (C, F, I)

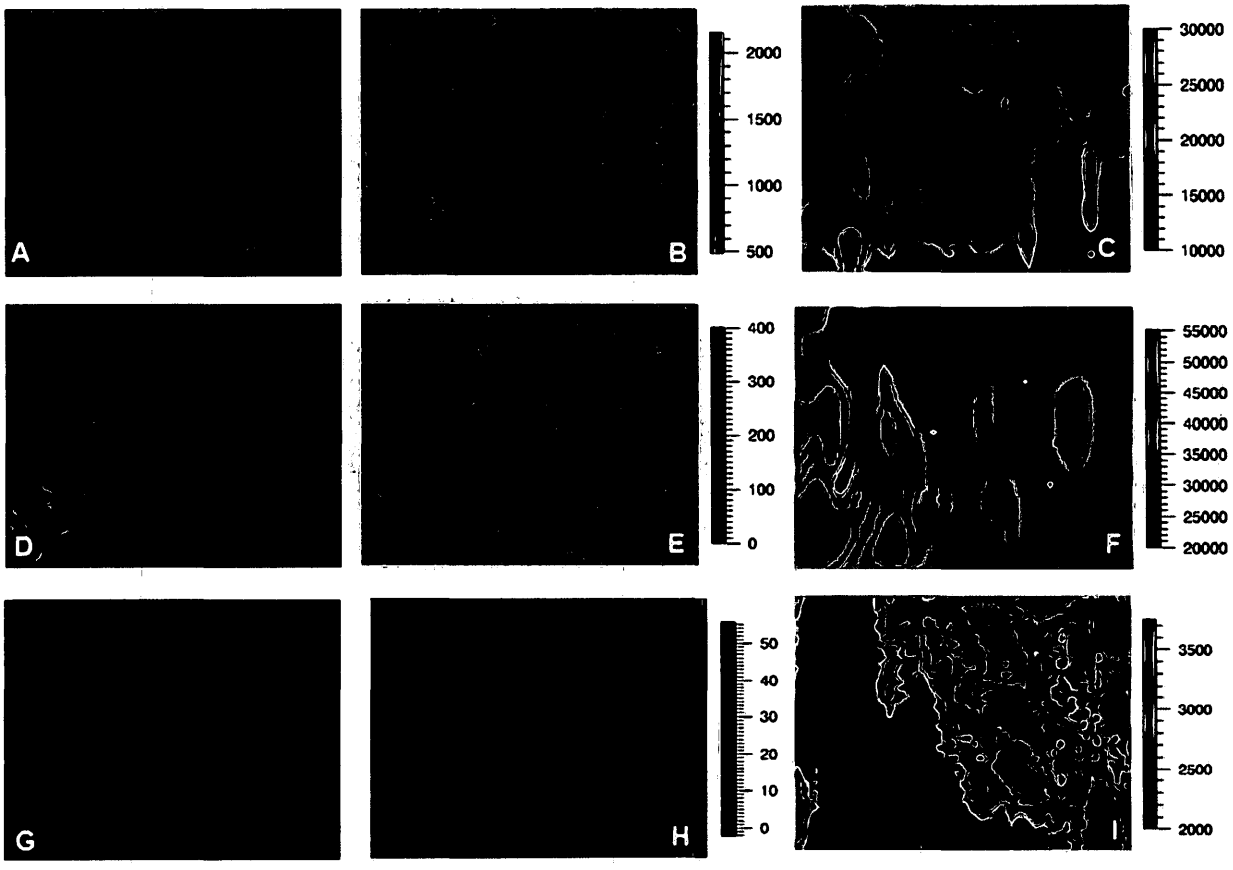

Fig. 5.8 Chemical maps for WS (A, B, C), WSHT (D, E, F) and WSDL (G, H, I). Optical images of the sample spot (A, D, G); lignin maps (B, E, H); wax maps (C, F, I)

5.3.4. Morphological analysis

SEM and AFM were used to study the biomass morphology effected by to the HT pretreatment and delignification. From the SEM images, PW samples (Fig. 5.9) appeared to have dense and fibrous structures compared to TG (Fig. 5.10) and WS samples (Fig. 5.11). This was because of its woody nature, unlike the porous and fragile structures of herbaceous feedstocks. Compared to the HT treated (Figs. 5.9-5.11: D, E, F) and delignified (Figs. 5.9-5.11: G, H) samples, untreated biomass (Figs. 5.9-5.11: A, B) exhibited a more compact and rigid structure. This was because the untreated samples were largely lignified and the cellulose microfibrils embedded in hemicellulosic polymers were supported by the lignin network (Kristensen et al., 2008). The removal of lignin and hemicellulose after HT and alkaline treatment caused extensive changes in the sample morphology suggesting enhanced accessibility of enzymes for saccharification.

The untreated feedstocks showed their surface being covered with a thin layer of debris and fragmented crusts. These crusts and debris were from plant waxes, mucilage and other biomass extractives from middle lamella (Vassilev et al., 2012). The existence of the broken crusts and debris indicating sample roughness were also evident from the AFM topography images (Figs. 5.9-5.11: C). AFM is useful in imaging the sample surface directly through the probe allowing quantitative estimations such as surface roughness, expressed as root-mean-square roughness (RRMS). The RRMS for 5 μm × 5 μm areas on untreated samples was assessed from AFM which varied as: TG (558 nm) > PW (391 nm) > WS (206 nm). This relationship corresponded well with the SEM observations which revealed TG to contain larger amount of debris and uneven texture.

A partial defibration and separation of individual fibres in TGHT and WSHT was noticed, which was induced by the HT treatment. The defibration was relatively insignificant in PW because of its ligneous nature that helped its fibres to bind firmly with each other.

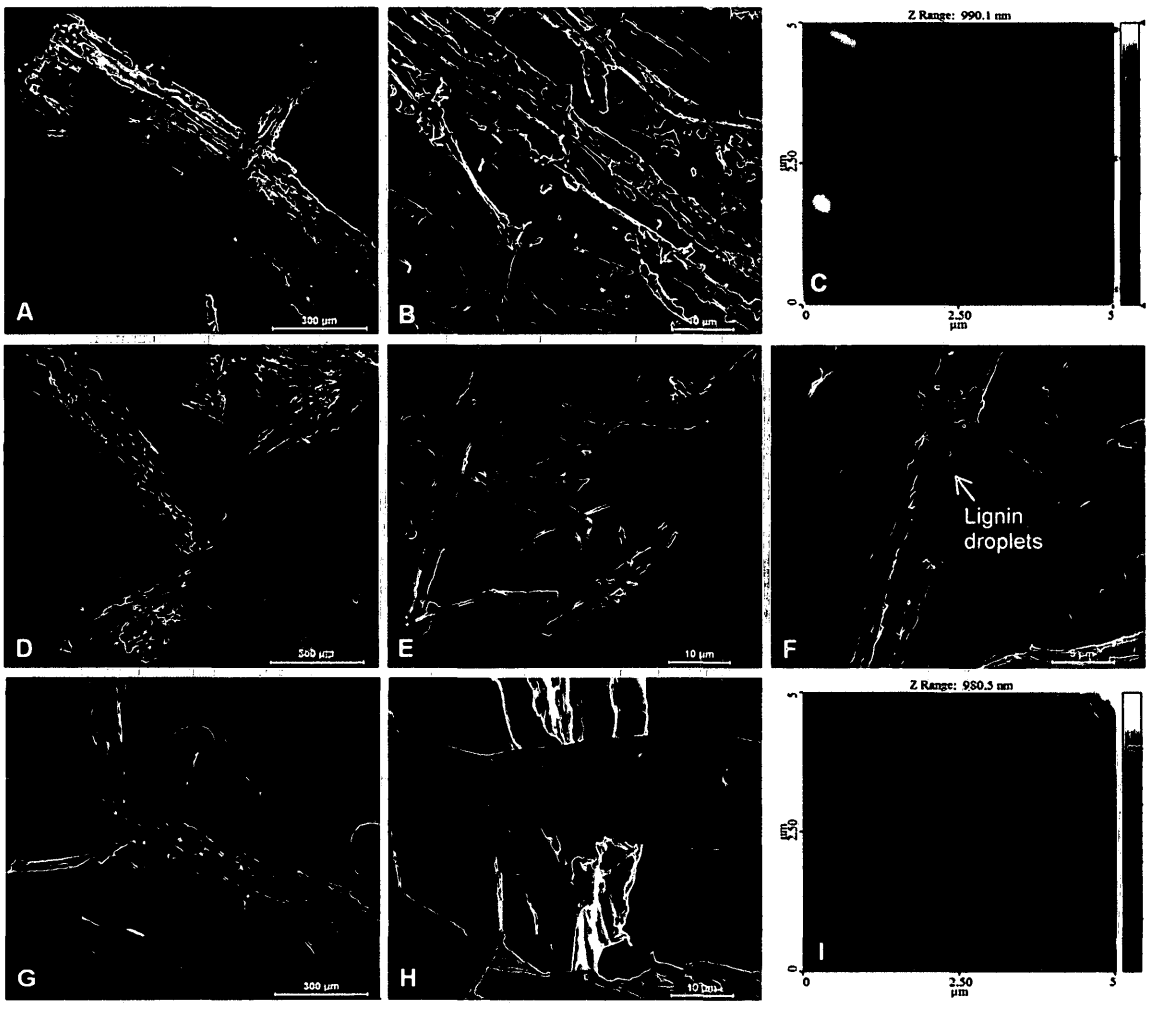

Fig. 5.9 SEM and AFM (C, I) images of PW (A, B, C), PWHT (D, E, F) and PWDL (G, H, I)

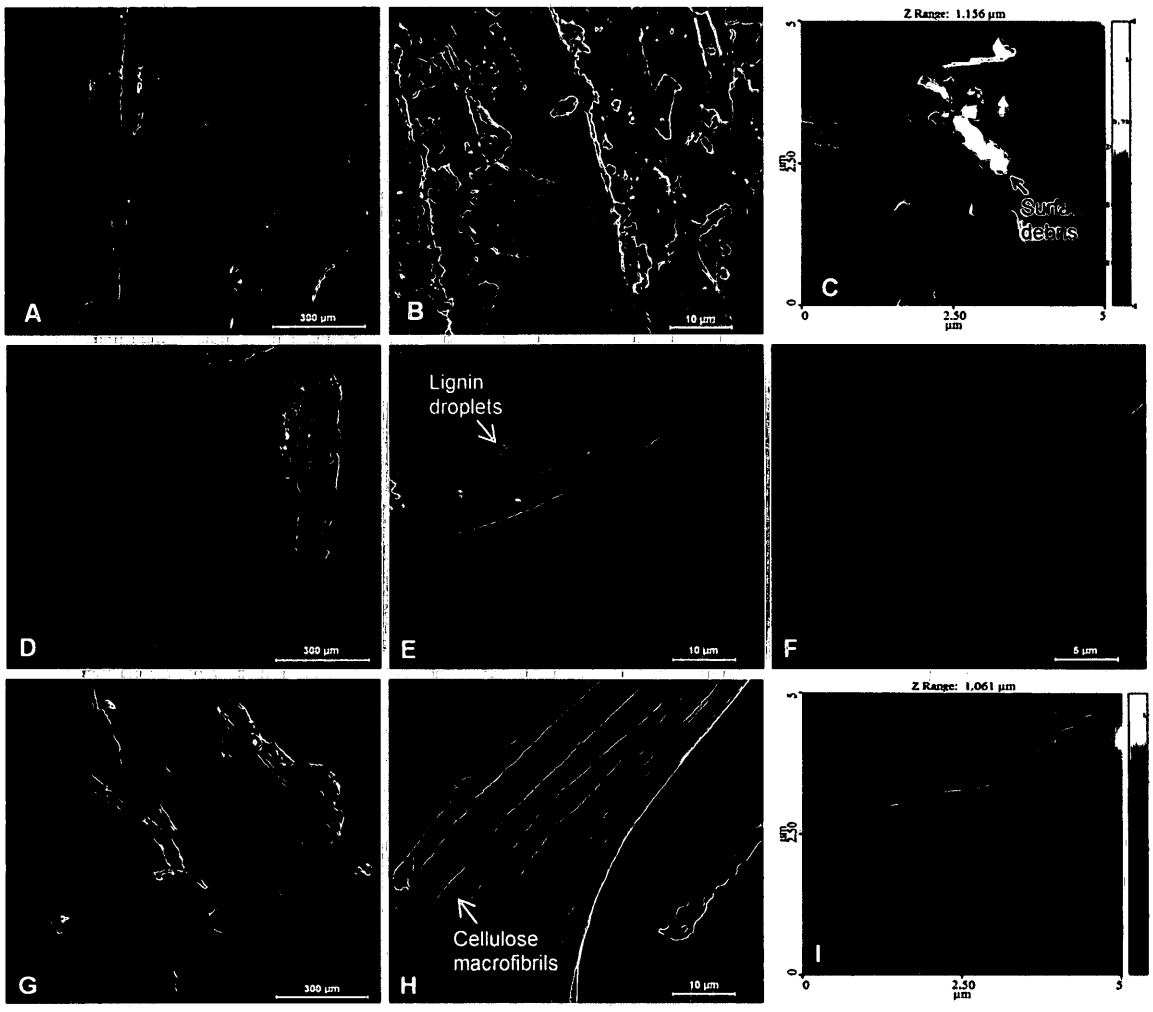

Fig. 5.10 SEM and AFM (C, I) images of TG (A, B, C), TGHT (D, E, F) and TGDL (G, H, I)

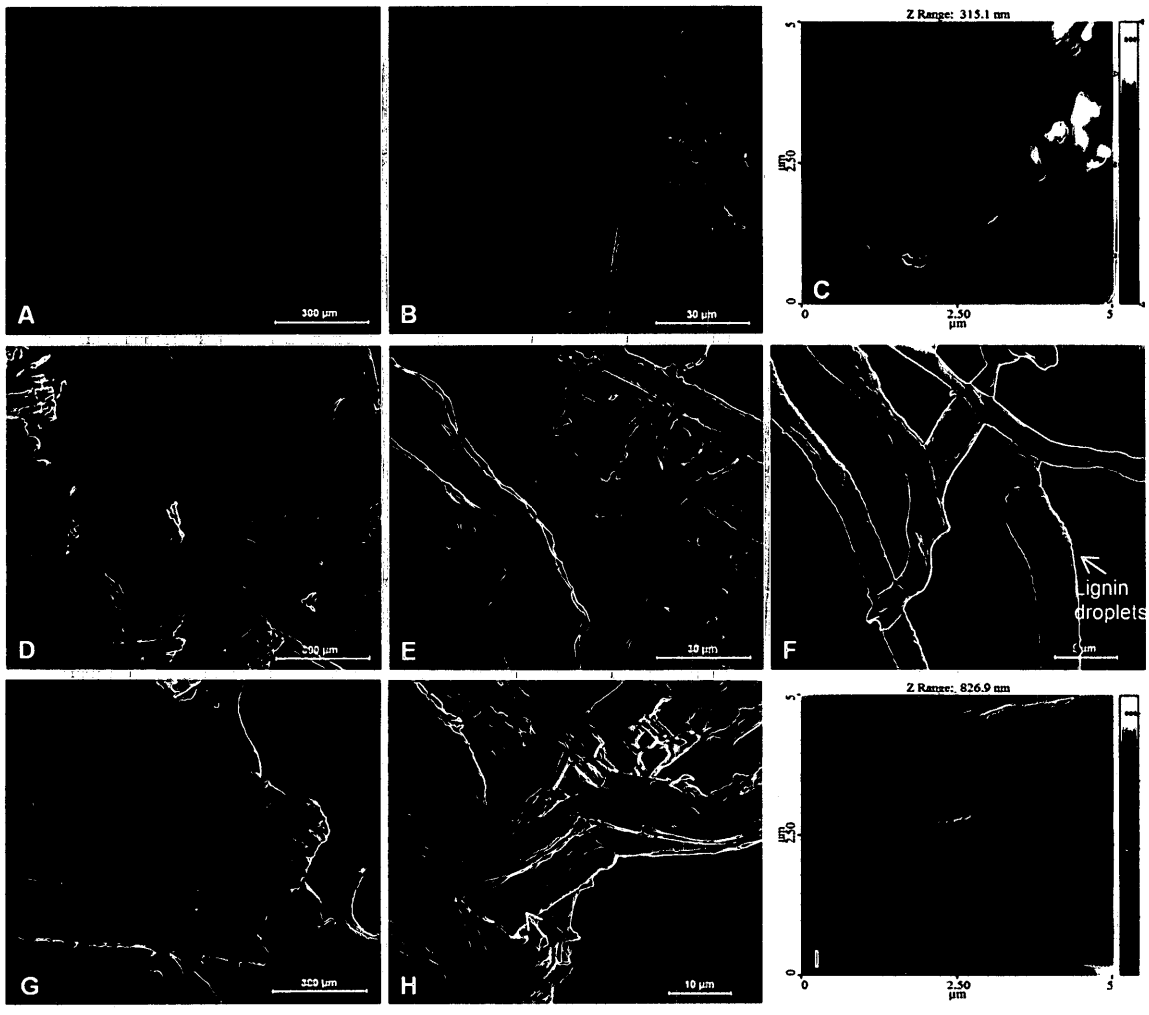

Fig. 5.11 SEM and AFM (C, I) images of WS (A, B, C), WSHT (D, E, F) and WSDL (G, H, I)

The defibration effect in TGHT (Fig. 5.10D) and WSHT (Fig. 5.11D) could induce biomass hydrolysis by presenting an increased surface area for the action of acids and enzymes. With closer observations on HT treated fibres, spherical and globular deposits appearing like droplets were found to cover their surface (Figs. 5.9-5.11: E, F). The occurrence of these droplets was due to lignin deposits (Kristensen et al., 2008). This phenomenon was in accordance with the spectroscopic findings on higher lignin concentrations in HT treated samples.

The delignified samples appeared fragmented although the extent of defibration was less because of the hemicellulose content of the middle lamella that holds the cellulose microfibrils together. The delignified feedstocks showed no visible incidence of spherical deposits indicating lignin removal (Figs. 5.10-5.11: G, H). In an exception, PWDL had a few uneven debris and deposits from lignin, reflecting some residual lignin (1.2 wt.%, Table 5.1). At higher magnifications, the delignified feedstocks presented a reasonably smooth surface exposing a few vein-likes structures which were presumably due to cellulose macrofibrils (Figs. 5.10-5.11: H). The cellulose macrofibrils displayed various interwoven structure which were uncovered due to the removal of lignin and hemicelluloses.

AFM images (Figs 5.9-5.11: I) of delignified samples resolved strand-like structures of cellulose macrofibrils. The RRMS for delignified samples decreased in the order: TGDL (1323 nm) > PWDL (1061 nm) > WSDL (422 nm), which was in the similar sequence as untreated samples. AFM imaging is relatively sensitive to rough surfaces. Successful imaging for HT treated samples was not achieved due to their roughness created by the lignin droplets as viewed through SEM. The SEM and AFM observations on delignified feedstocks displayed no cracks, pores or any major perforations that compromised with the crystallinity of cellulose macrofibrils. In contrast, the exposure of macrofibrils indicated enhanced crystallinity of cellulose that supported the compositional, structural and spectroscopic findings.

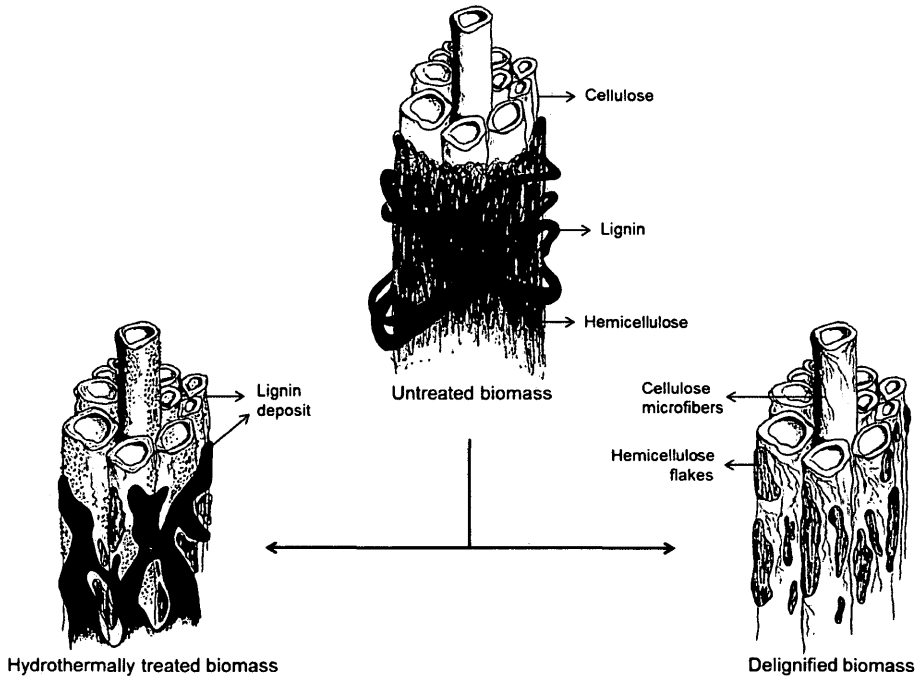

Fig. 5.12 Artistic portrait of lignocellulosic network modifications during hydrothermal pretreatment and delignification *(Portrait by Sonil Nanda)*

The physico-chemical, thermal and structural analysis of untreated, hydrothermally treated and delignified biomasses helped to better understand the lignocellulosic chemistry and modifications in the plant cell wall during the biomass pretreatments. An artistic portrait of the plant cellular evolutions during the hydrothermal and chemical treatments has been shown as Fig. 5.12. It can be seen from the three dimensional portrait that in a lignocellulosic feedstock, the hemicelluloses encrust cellulosic fibres. Lignin acts as a binding agent to hold the cellulose-hemicellulose network intact. As hemicellulose is easy to hydrolyse at higher temperatures, the hydrothermal treatment caused their extensive removal from the feedstock. The hot water treatment also caused the polymeric lignin to alter its normal orientation and re-localize on the cellulosic fibres as droplets. Furthermore, delignification resulted in the removal of both lignin and hemicelluloses, therefore exposing the cellulosic fibres.

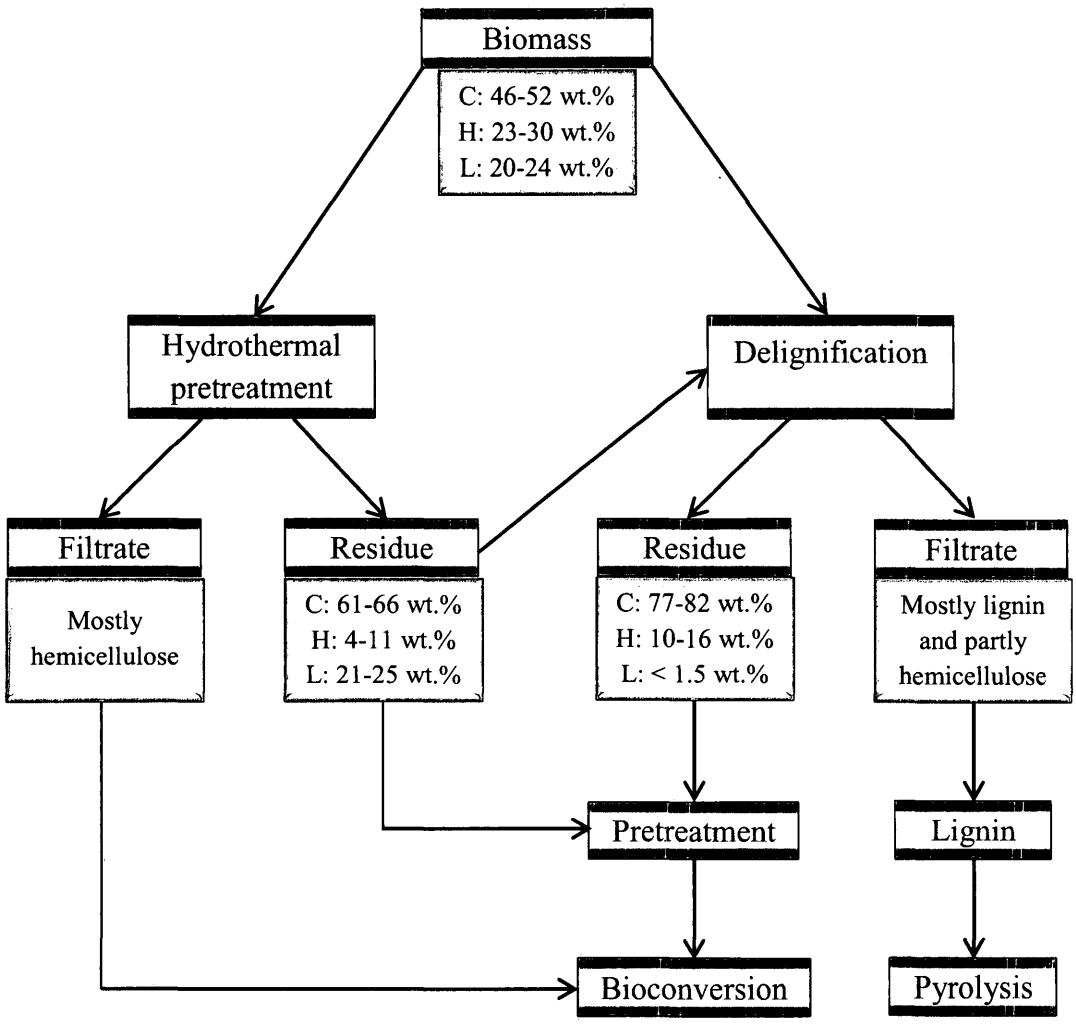

Fig. 5.13 Mechanistic model of delignification and product utilization

Abbrev. Cellulose (C), hemicellulose (H) and lignin (L)

The overall process of delignification is illustrated in a mechanistic model (see Fig. 5.13). For recovering the fermentable sugars from biomass the two approaches of biomass pretreatment have been mentioned i.e., hydrothermal pretreatment and delignification. Since, hemicellulose is easy to hydrolyze because of its lower degree of polymerization than cellulose it is easy hydrolyzed during hydrothermal pretreatment. The hydrothermal pretreatment not only

releases hemicellulose but also re-localizes lignin on to the cell surface without removing it. With an efficient lignin removal (> 1.5 wt.% final concentration) and increased cellulose level (77-82 wt.%), the delignified biomass acts as a suitable feedstock for bioconversion. Furthermore, the aqueous solution obtained during biomass delignification (rich in dissolved lignin) could be harvested for purification of lignin. The purified lignin has potentials to be used in pyrolysis for high quality bio-oil and bio-chemical production.

5.4. Conclusions

Pinewood, timothy grass and wheat straw were hydrothermally treated and delignified using acidified sodium chlorite to study the changes in distribution of lignin and plant waxes. The TGA results demonstrated a decrease in the decomposition temperature (240-250°C) of delignified samples due to their modified cellular structure and removal of lignin. The compositional analysis confirmed the loss of lignin in the delignified residues (0.7-1.2 wt.%) as compared to the untreated feedstocks (20.1-24.2 wt.%). A minor increase in the lignin levels (21.1-25.4 wt.%) was observed in hydrothermally treated feedstocks due to delocalization of lignin and its re-deposition on the biomass surface as spherical droplets. A considerable rise in the cellulose levels was found in delignified (77.4-82 wt.%) and hydrothermally treated (61.2-65.7 wt.%) samples than the native feedstocks (46-51.9 wt.%) because of the gradual removal of hemicelluloses and lignin. As hemicelluloses are hydrophilic and easy to hydrolyse in liquid hot water, their concentration was relatively low in hydrothermally treated biomass (4.4-10.7 wt.%). The increase in cellulose levels was reflective in the XRD patterns with intensification of peaks for Cellulose I (21.7°) and Cellulose II (15.5°). In addition, the crystallinity index for cellulose was higher in delignified samples (~98.1%) and HT treated samples (~93.1%).

The absence of lignin peaks in FT-IR (1510 cm^{-1}) and Raman (1261, 1270, 1510-1656 cm^{-1}) spectra in delignified samples suggested their removal. The

occurrence and distribution of lignin and waxes in the biomasses were studied through chemical maps generated using Raman mapping technique. The formation of vacuoles in the lignin matrix in hydrothermally treated feedstocks explained the alteration of lignin arrangement due to penetration of steam under pressure into the plant cellular structure.

Chapter Six: Bioconversion of lignocellulosic biomass to ethanol and butanol

6.1. Introduction

Lignocellulosic residues are attractive renewable resources for the production of next generation biofuels. With their vast availability, they are considered to be a suitable alternative to the diminishing fossil fuels. The major components of lignocellulosic biomass are cellulose, hemicellulose and lignin. Cellulose is composed of glucose polymers which are largely insoluble and exist in crystalline microfibrils making the sugars difficult to extract. Hemicellulose, which comprises of various pentose and hexose sugars, is attached to the cellulose microfibrils. On the other hand, lignin is a phenyl propane polymer which forms a complex network cross-linking the cellulose and hemicellulose together. In order to break the lignocellulosic framework and extract the fermentable sugars for bioconversion to higher fuel alcohols, a pretreatment method prior to conversion is required.

A number of pretreatment methods available for biomass are dilute acid, alkali, hot water, ammonia fiber explosion, carbon dioxide explosion and organic solvent (Kumar et al., 2009). Among all, dilute sulfuric acid pretreatment is the widely used commercial process in the pilot scale. An ideal pretreatment should have the following properties: (i) degrade the lignin and hemicellulose complex with cellulose, (ii) improve the sugar yield as a result of hydrolysis of cellulose and hemicellulose, and (iii) prevent excessive degradation or loss of carbohydrate. Dilute sulfuric acid pretreatment solubilizes the hemicelluloses and thereby disrupts the lignocellulosic composite linked by covalent bonds, H-bonds and van der Waals forces.

During the past few decades there has been a significant interest in the production of fermentation derived fuel such as ethanol from agriculture-based substrates (e.g., corn). Recently, butanol has emerged as a superior fuel than ethanol

that can be efficiently produced from lignocellulosic feedstocks. A few known butanol producing bacteria are *Clostridium acetobutylicum* and *C. beijerinckii*. These clostridia can produce butanol through anaerobic ABE (acetone-butanol-ethanol) fermentation of both pentose (xylose) and hexose (glucose) sugars in the biomass hydrolysate. These are advantageous over the ethanol producing *Saccharomyces cerevisiae* that mostly use hexose sugars leaving behind pentoses (Qureshi and Ezeji, 2008).

As a fuel, butanol can be used in pure form or blended in gasoline in any concentration unlike ethanol that can be blended only up to 85% (Durre, 2007). In addition, the energy content of butanol is 29.2 MJ/L, which is 30% higher than that of ethanol (21.2 MJ/L) and is much closer to gasoline (32.5 MJ/L). Also, butanol's low vapor pressure, hydroscopic nature, less volatility and less flammability facilitates its blending and supply in existing gasoline channels and pipelines (Qureshi and Ezeji, 2008). However, production of butanol has many drawbacks such as its low final titer levels, culture toxicity due to low butanol tolerance by clostridia and purification issues (Zheng et al., 2009).

This chapter describes the bio-production of ethanol and butanol from pinewood, timothy grass and wheat straw. These feedstocks are least explored in terms of their butanol and ethanol producing potentials. In addition, a dilute sulfuric acid pretreatment followed by enzymatic hydrolysis of these lignocellulosic residues is developed for higher sugar yields, as discussed in this chapter. Furthermore, the biomass hydrolysates with cellulosic and hemicellulosic components are fermented for the production of ethanol and butanol.

6.2. Materials and methods

6.2.1. Lignocellulosic biomass and compositional analysis

The biomass samples used in this study were pinewood (PW), timothy grass (TG) and wheat straw (WS). A comprehensive characterization of these three feedstocks can be found in previous chapters. The compositional analysis (cellulose-

hemicellulose-lignin) of the feedstocks was performed using the standard NREL method (Sluiter et al., 2008a; b). The details of the operating procedures can be found in Chapter 5 (section 5.2.2).

6.2.2. Dilute acid pretreatment

For dilute acid pretreatment, 50 g of biomass (dry basis) was mixed well with 500 mL of 0-2.5% (v/v) H_2SO_4 to distilled water in a 1 L conical flask. The flask was cotton plugged and covered with aluminum foil prior to autoclaving at 121°C for 1 h. After autoclaving, the hydrolysates were cooled to room temperature and neutralized to pH 5.0 with 10 M NaOH (Qureshi et al., 2010). The sugar (i.e., glucose and xylose) levels in the biomass hydrolysates were quantified through HPLC using an Aminex HPX 87H column (operating conditions given in Chapter 5, section 5.2.2).

6.2.3. Enzymatic hydrolysis

About 6 mL/L each of cellulase, β-glucosidase and xylanase (Sigma-Aldrich, Canada) were added to the neutralized biomass hydrolysates and incubated at 45°C for 72 h with agitation at 80 rpm (Qureshi et al., 2010) in a New Brunswick Scientific Excella E24 benchtop shaker (Fisher Scientific, Canada). After 72 h of enzymatic hydrolysis, the mixture was centrifuged at 3300×g to remove the biomass residues. The supernatant liquid containing hydrolyzed sugars were recovered and filter sterilized by passing through a 0.2 μm filter disc (Fisher Scientific, Canada). The sterilized hydrolysates were stored in sterilized screw capped Pyrex bottle at 4°C prior to the fermentation experiments. The sugar levels in the hydrolysates were quantified through HPLC as mentioned earlier. The hydrolysate with greater sugar yields was used in fermentation for ethanol and butanol production.

6.2.4. Fermentation for ethanol production

Saccharomyces cerevisiae ATCC 96581 (Cedarlane, Canada) was used for ethanol production. The inoculum for fermentation was maintained in ATCC

1245 YPD broth medium containing yeast extract (10 g/L), peptone (20 g/L) and dextrose (20 g/L) for 24 h at 30°C, pH 5.6 with 150 rpm.

For ethanol production, 100 mL of biomass hydrolysate was supplemented with yeast extract (1.5 g/L), peptone (1 g/L), ammonium sulfate (1 g/L), dipotassium phosphate (0.5 g/L), magnesium sulfate (0.5 g/L) and manganese(II) sulfate (0.5 g/L) at pH 5.6 (Govumoni et al., 2013). About 6 mL of actively growing *S. cerevisiae* ATCC 96581 was added to the medium and incubated for 60 h at 30°C with agitation at 150 rpm in a New Brunswick Scientific Excella E24 benchtop shaker (Fisher Scientific, Canada). Ethanol production from glucose as the control substrate was studied at levels varying from 50-150 g/L. The specified concentrations of glucose solutions were supplemented with the abovementioned nutrients. About 1.5 mL of sample was drawn every 12 h for ethanol and residual sugar determinations in an HPLC. Prior to all measurements, the liquid samples were filtered through 0.2 μm filter discs to remove any sediment.

6.2.5. Fermentation of butanol production

Clostridium beijerinckii B-592 (NRRL, USA) was used for butanol production. The dried clostridia spores were rejuvenated in a sterilized ATCC 2107 modified reinforced clostridial broth medium (Cedarlane, Canada) in an anaerobic chamber (New Bruinswick Scientific Galaxy 170R CO_2 incubator, Eppendorf Canada). About 6 mL of actively growing *C. beijerinckii* B-592 culture was transferred to a 100 mL of freshly prepared pre-sterilized ATCC 2107 media in a 250 mL screw-capped Pyrex bottle for inoculum development. The ATCC 2107 modified reinforced clostridial broth contained peptone (10 g/L), beef extract (10 g/L), yeast extract (3 g/L), dextrose (5 g/L), NaCl (5 g/L), starch (1 g/L), L-cysteine HCl (0.5 g/L), sodium acetate (3 g/L) and 0.025% resazurin (4 mL/L). The inoculum was allowed to grow for 16-18 h at 35°C prior to inoculation into the fermentation media.

Butanol production was studied with glucose as the control substrate at levels varying from 50-150 g/L. About 2.5 mL of 40 g/L yeast extract was added to 100 mL of glucose solutions (50-150 g/L) and sterilized at 121°C for 15 min followed by cooling to room temperature. After cooling, 6 mL of the *C. beijerinckii* B-592 (grown in ATCC 2107) was added to the medium and incubated for 72 h at 35°C.

Similarly, 100 mL of filter sterilized biomass hydrolysate (pH 6.5) was transferred to a 250 mL pre-sterilized screw-capped Pyrex bottle. About 2.5 mL of 40 g/L sterilized yeast extract solution was added to the hydrolysates followed by inoculation with 6 mL of the actively growing *C. beijerinckii* B-592 (in ATCC 2107) as described above. During all fermentations, 1.5 mL of liquid sample was taken every 12 h and filtered with 0.2 μm filter discs for ABE and residual sugar determinations in an HPLC. For measuring the levels of acetic acid and butyric acid, an Aminex HPX 87P column (BioRad) was used with Milli-Q water as the mobile phase at a flow rate of 0.6 mL/min.

All the analyses mentioned above such as compositional analysis, acid/enzymatic hydrolysis as well as ethanol and butanol fermentation processes were performed in triplicates with standard deviation less than 5%.

6.3. Results and discussion

6.3.1. Compositional analysis

Prior to the dilute acid and enzymatic pretreatments, the compositional analysis of PW, TG and WS was performed to quantify the lignocellulosic components along with extractives and ash. About 90% of dry matter in lignocellulosic biomass comprises of cellulose, hemicellulose and lignin, whereas the remaining consists of extractives and ash (Balat, 2011). The exhaustive extraction process of feedstocks using water, ethanol and hexane led to the removal of extractives. Table 7 gives the compositional analysis of the three lignocellulosic feedstocks. The yield of total extractives in PW, TG and WS were

15.7, 16.5 and 19.2 wt.%, respectively. The high amount of total extractives in WS indicated higher amount of water, ethanol and hexane soluble components such as terpenes, terpenoids, tannins, resins, waxes, lipids and organic acids.

On the other hand, the cellulose concentration in the three feedstocks ranged between 34.2 and 39.1 wt.%, with WS demonstrating highest levels. The hemicellulose levels were highest (30.1 wt.%) in TG and lowest (23.6 wt.%) in PW. This was due to the fact that fast-growing plants are abundant in hemicellulose that aids in conducting and concentrating tissue for mineralized solutions rich in sulphates, chlorides, nitrates and silicic acid in plants (Vassilev et al., 2012). PW showed utmost levels of lignin (20.4 wt.%) compared to the herbaceous feedstocks (TG and WS).

6.3.2. Acid and enzymatic hydrolysis

Figure 6.1 illustrates the sugar yields from PW, TG and WS as a result of different H_2SO_4 concentrations ranging from 0 to 2.5% and enzymatic hydrolysis (denoted as 'E' in Fig. 6.1). Enzymatic hydrolysis resulted in higher sugar yields from all feedstocks than the dilute acid hydrolysis. The enzymatic hydrolysis resulted in an increase of 66.5, 65.7 and 60% in total sugar (glucose and xylose) yield from PW, TG and WS, respectively. Among all feedstocks, PW showed maximum fermentable sugar yields of 68.5 g/L at a 2% H_2SO_4 hydrolysis and enzymatic pretreatment. On the other hand, a 1.5% H_2SO_4 hydrolysis and enzymatic pretreatment led to the production of 57.4 and 63.6 g/L of sugars from TG and WS, respectively.

The trend of sugar yields (PW > WS > TG) from the feedstocks could be related to their carbon, hydrogen and oxygen contents which also varied in the similar way. The carbon, hydrogen and oxygen levels of PW (97.6 wt.%), TG (94.9 wt.%) and WS (95.1 wt.%) has been previously discussed in Chapter 3, and they are of significant relation in the sugar yields as they occur as carbohydrates in plants and hydrocarbons in fuels.

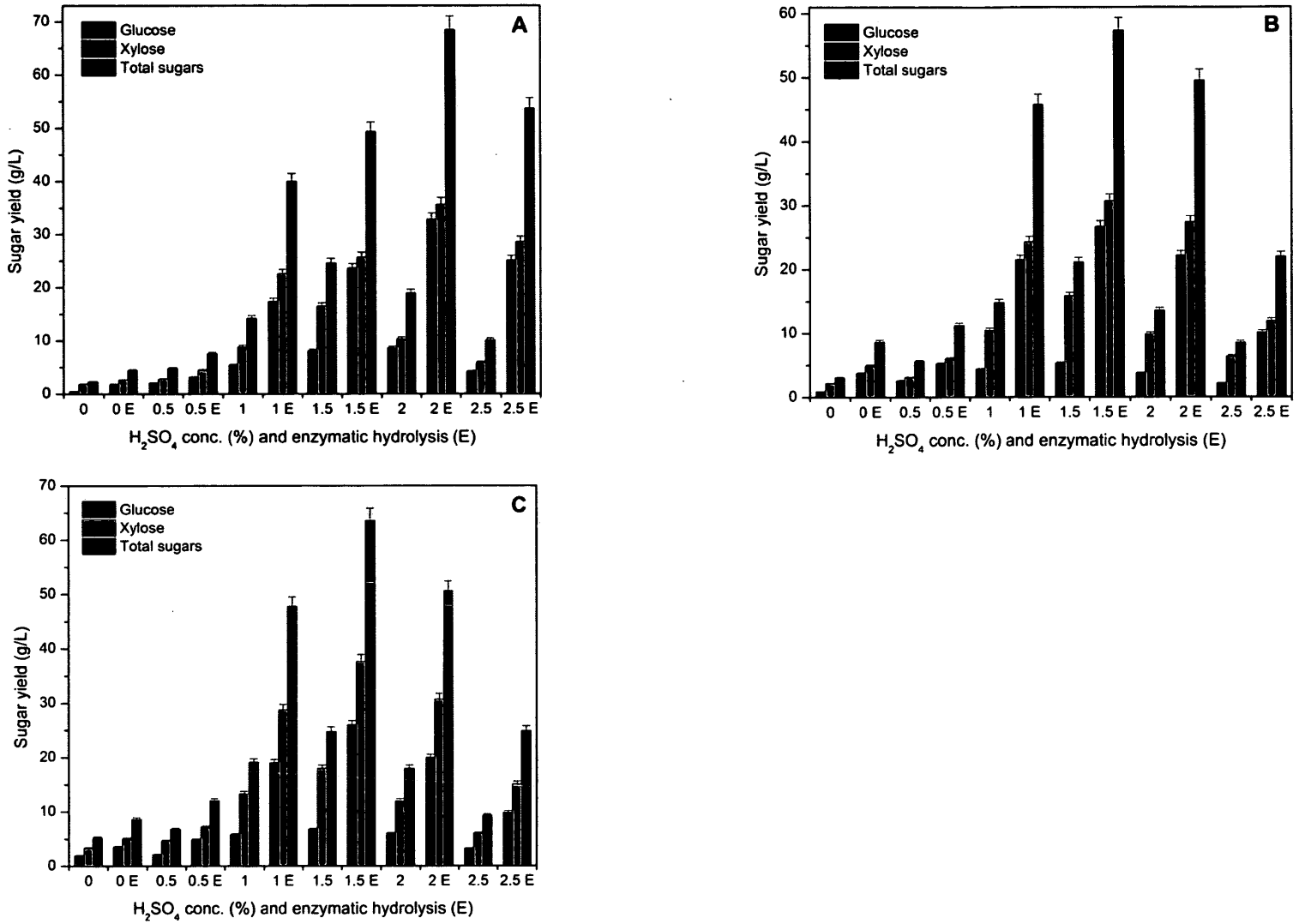

Fig. 6.1 Sugar yields from (A) PW, (B) TG and (C) WS at varying (0-2.5% H_2SO_4) concentrations and enzymatic hydrolysis

As a result of dilute H_2SO_4 pretreatment for all feedstocks, there was a significant increase in the xylose yields compared to that of glucose. In contrast to glucose, xylose yield increased by 37.6, 60.3 and 54.7% in the dilute acid hydrolysates of PW, TG and WS, respectively. This was due to the fact that hemicelluloses (primarily xylose) are easily hydrolysable in dilute acid than cellulose (glucose) because of their amorphous nature and lower degree of polymerization (Hu and Ragauskas, 2012). Compared to dilute acid pretreatment, enzymatic hydrolysis resulted in an increase in glucose concentration (g/L) by 72.3, 78.8 and 68.9% in PW, TG and WS, respectively. Correspondingly, xylose levels (g/L) increased by 61.4, 54.7 and 54% in the enzymatic hydrolysates of PW, TG and WS.

This escalation of glucose and xylose levels was due to the activity of cellulase, β-glucosidase and xylanase. Cellulases (e.g., endoglucanases and cellobiohydrolases) hydrolyze the β-(1,4)-glycosidic linkages of cellulose releasing cellobiose molecules (Perez et al., 2002). Cellobiose comprises of cellulose chains with repeats units of D-glucose established through β-(1,4)-glycosidic linkages. Further, β-glucosidases break down cellobiose molecules releasing two glucose subunits. On the other hand, xylanases hydrolyze the β-(1,4) bond in the xylan backbone, producing short xylooligomers and xylose (Shallom and Shoham, 2003). Xylan is a polysaccharide carbohydrate made from xylose units.

However, dilute H_2SO_4 pretreatment is necessary prior to enzymatic hydrolysis as it could lead to high reaction rates and significantly improve cellulose hydrolysis (Kumar et al., 2009). The removal of majority of hemicelluloses (xylose) enhances cellulose (glucose) recovery by exposing the cellulose fibers to enzymes for catalysis. The highest total sugar yield from the enzymatic hydrolysis of PW (68.5 g/L) was found at a 2% H_2SO_4, whereas for TG (57.4 g/L) and WS (63.6 g/L) it was at 1.5% H_2SO_4. The digestibility of cellulose in biomass is influenced by the physicochemical, structural and compositional

factors (Kumar et al., 2009). The woody and fibrous nature of PW along with its high amount of lignin (20.4 wt.%) led to the requirement of a relatively higher H_2SO_4 concentration than that of TG and WS. In contrast to PW, herbaceous feedstocks such as TG and WS were found to be porous and fragile with low lignin (16.3-18.1 wt.%) necessitating lower H_2SO_4 concentration for hydrolysis.

A gradual decrease in glucose and xylose yields was found with increase in H_2SO_4 concentrations. There was a notable decrease in the total sugar yields of 21.5, 61.7 and 60.8% in the enzymatic hydrolysis of PW, TG and WS, respectively at 2.5% H_2SO_4 treatment. This was because of the undesired conversion of sugars to furfurals and hydroxymethylfurfurals (HMF), which are obtained from the dehydration of sugars at higher acid levels (Kumar et al., 2009). In addition, higher dilute acid treatment is generally corrosive, hazardous and requires corrosion-resistant reactors which increase the process expenditures.

6.3.3. Ethanol production

The evaluation of ethanol yields from *S. cerevisiae* ATCC 96581 was performed on glucose medium at different substrate levels varying from 50 to 150 g/L (Fig. 6.2). The final ethanol concentrations of 19.3, 31.5 and 47.1 g/L were obtained from *S. cerevisiae* at 50, 100 and 150 g/L glucose levels, respectively in 60 h of fermentation. Maximum ethanol concentration of 48.3 g/L was obtained from 150 g/L glucose medium (Fig. 6.2C) in 36 h. However, the high ethanol concentrations in 50 and 100 g/L glucose levels were 20.3 and 32.9 g/L.

High sugar and ethanol contents in the fermentation broth inhibit growth and the rate of product formation by yeast. The specific growth rate (per hour) for yeast is found to decrease from 0.61 at 50 g/L glucose to 0.51 at 140 g/L glucose (Ghose and Tyagi, 1979). As a result of substrate inhibition, the residual glucose was relatively high (41.4 g/L) in the 150 g/L glucose medium at 60 h of fermentation. Similarly, the unutilized glucose content in 50 and 100 g/L glucose media were 12.6 and 18.1 g/L, respectively.

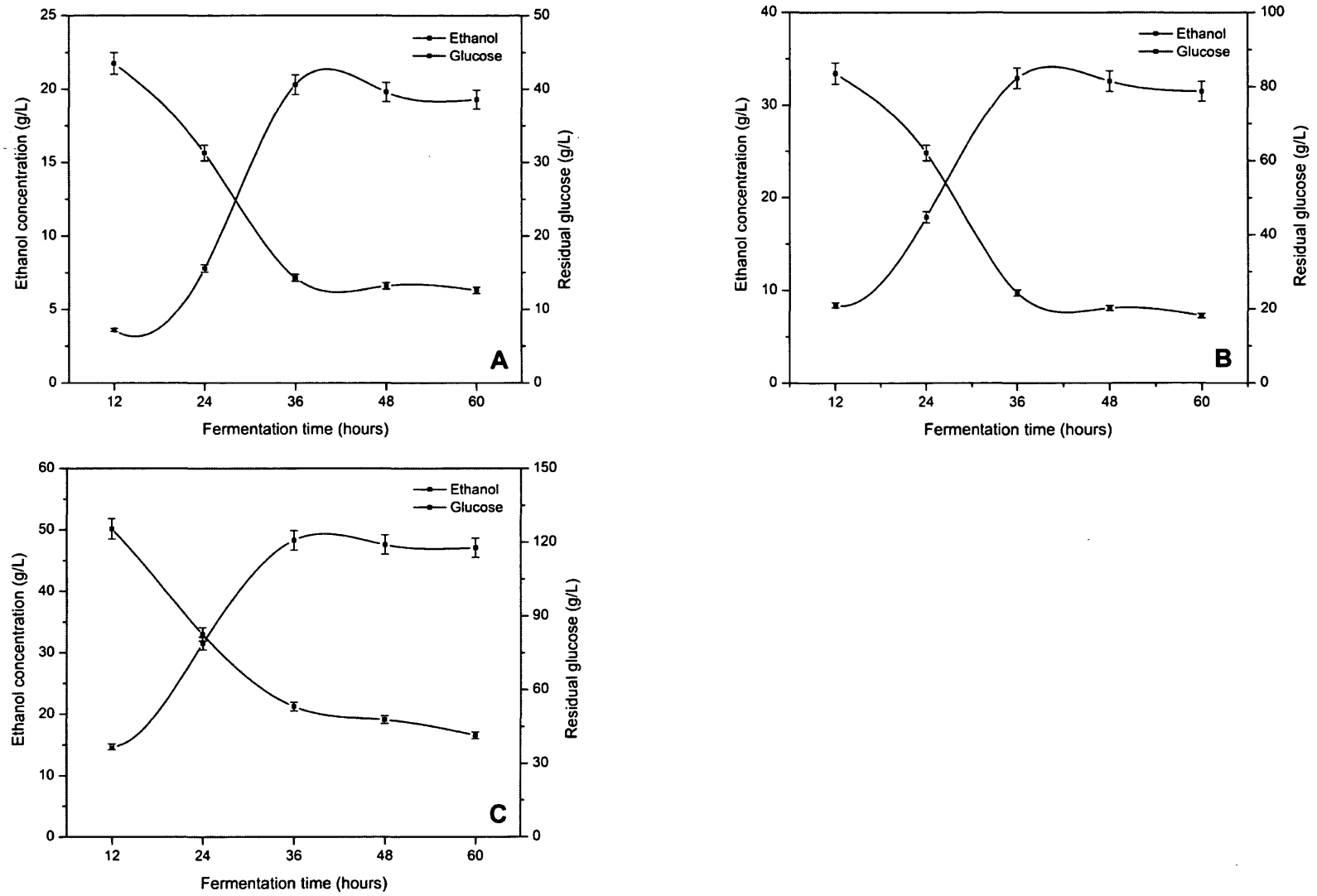

Fig. 6.2 Ethanol production using *S. cerevisiae* ATCC 96581 from (A) 50, (B) 100 and (C) 150 g/L glucose substrates

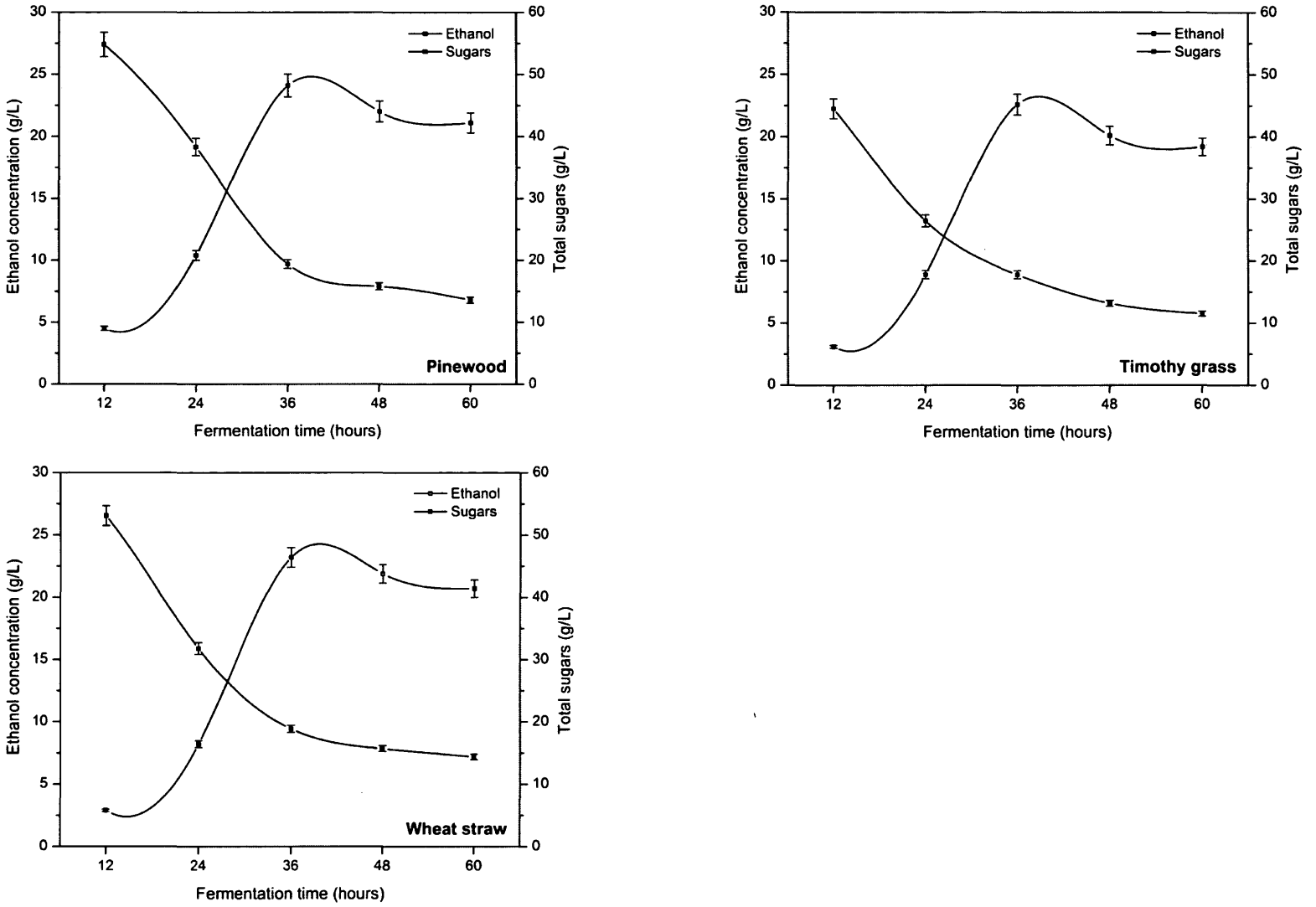

Fig. 6.3 Ethanol production using *S. cerevisiae* ATCC 96581 from pinewood, timothy grass and wheat straw hydrolysates

Furthermore, ethanol at a level of 90 g/L is completely inhibitory (no growth) to *S. cerevisiae*, although the inhibition is initiated at 24 g/L ethanol. Ethanol at higher concentrations can alter the composition, structure and function of the microbial cell membranes as well as inhibit cell division and decrease cell viability, thus reducing metabolic activity (Liu and Qureshi, 2009). However, cell organelles such as mitochondria and vacuoles and cellular metabolism such as sugar transport systems are found to play a vital role in ethanol tolerance mechanism for yeasts.

Following the glucose control fermentations, the biomass hydrolysates were fermented using *S. cerevisiae* to evaluate their ethanol yields. The bioconversions were performed on PW, TG and WS hydrolysates with initial sugar (glucose and xylose) concentrations of 68.5, 57.4, and 63.6 g/L, respectively (Fig. 6.3). The ethanol levels in all hydrolysates were found to be high (22.6-24.1 g/L) at 36 h of fermentation at 30°C. PW hydrolysate demonstrated highest levels of ethanol (24.1 g/L) compared to TG and WS (Fig. 6.3A). The residual total sugar levels at 60 h of fermentation were found to be 13.6, 11.5 and 14.4 g/L for PW, TG and WS, respectively.

Two significant phases were observed in the ethanol production for glucose and biomass hydrolysates. The first phase was characterized with a marked increase in ethanol yields between 12 and 36 h, whereas the second phase showed a significant decrease in the sugar levels within the same period. This could be explained through the yeast metabolism. *S. cerevisiae* started metabolizing the sugars for ethanol at 12-36 h of fermentation and as the level reached up to 24.1 g/L in hydrolysates and 25.5 g/L in glucose media, an inhibition mechanism restricted the yeast to further multiply and produce ethanol.

6.3.4. Butanol production

Figure 6.4 illustrates the trend of butanol production from glucose substrates with concentrations ranging from 50-150 g/L. Butanol production by

Clostridium spp. is characterized based on two major classes of products, namely solvents (acetone, ethanol and butanol) and organic acids (acetic acid and butyric acid) (Zheng et al., 2009). The levels of acetone, butanol and ethanol along with acetic and butyric acid were recorded up to 72 h of fermentation. Maximum butanol concentration of 11.9 g/L was found in 100 g/L glucose media at 60 h of fermentation (Fig. 6.4B). Similarly, the levels of acetone (6.1 g/L), ethanol (1.9 g/L) were high in 100 g/L glucose media at 60 h. Acetic acid (4.5 g/L) and butyric acid (2.5 g/L) levels were higher in 100 g/L glucose media at 72 h of the fermentation. The total amount of ABE was high (17.9 g/L) in 100 g/L glucose medium compared to those of 50 and 150 g/L glucose media.

With an increase in the substrate (glucose) level, there was an increase in the residual glucose concentration. The residual glucose contents in 50, 100 and 150 g/L glucose media were 18.2, 28.3 and 53.8 g/L, respectively at 72 h. This large amount of remaining glucose in the fermentation media was due to the substrate inhibition and butanol toxicity. Glucose concentration of 161.7 g/L has been found to cause substrate inhibition for clostridia in butanol fermentation process, resulting in a lag phase of approximately 40 h (Ezeji et al., 2004).

A typical ABE fermentation by clostridia occurs in two phases i.e., acidogenic and solventogenic phase as discussed in Chapter 2 (section 2.4.2). The acidogenic phase is the initial growth phase that results in H_2, CO_2, acetic and butyric acid (Jones and Woods, 1986). Due to the formation of acids, the pH of the medium lowers and the bacteria enters stationary growth stage. This shifts the bacterial metabolism towards the production of solvents (ABE) in the second fermentation phase i.e., solventogenic phase. These two phases of clostridial metabolism were evident from the trend analysis of ABE fermentation (Figs. 6.4 and 6.5). As the acidogenic phase occurs early in the fermentation, producing acids, the yields of acetic and butyric acid were high at 24 h followed by a sharp decrease in the yield at 36 h. On the other hand, there was a noticeable increase in the acetone and butanol yields in the later fermentation hours, particularly in 60 h.

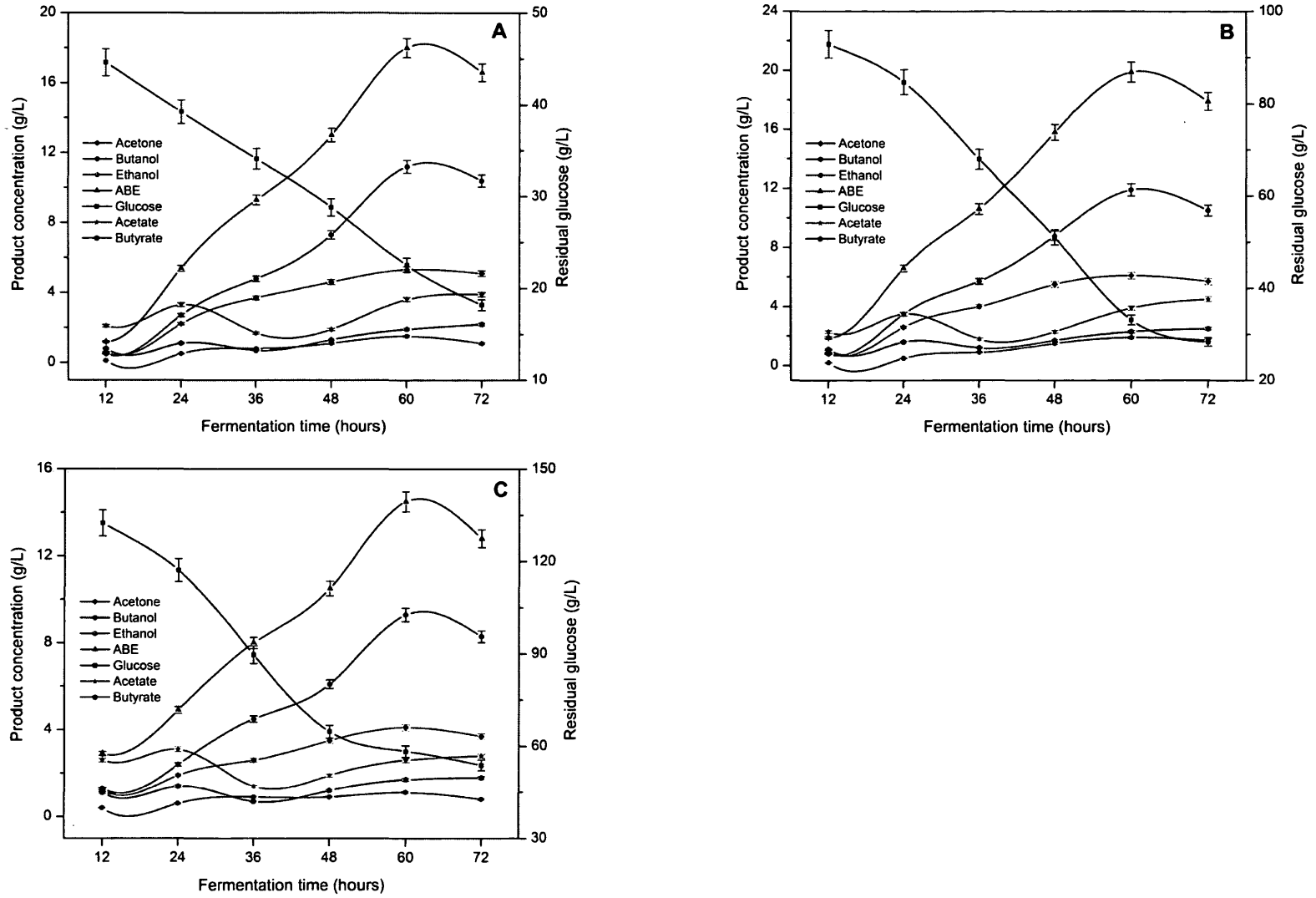

Fig. 6.4 Butanol production using *C. beijerinckii* B-592 from (A) 50, (B) 100 and (C) 150 g/L glucose substrates

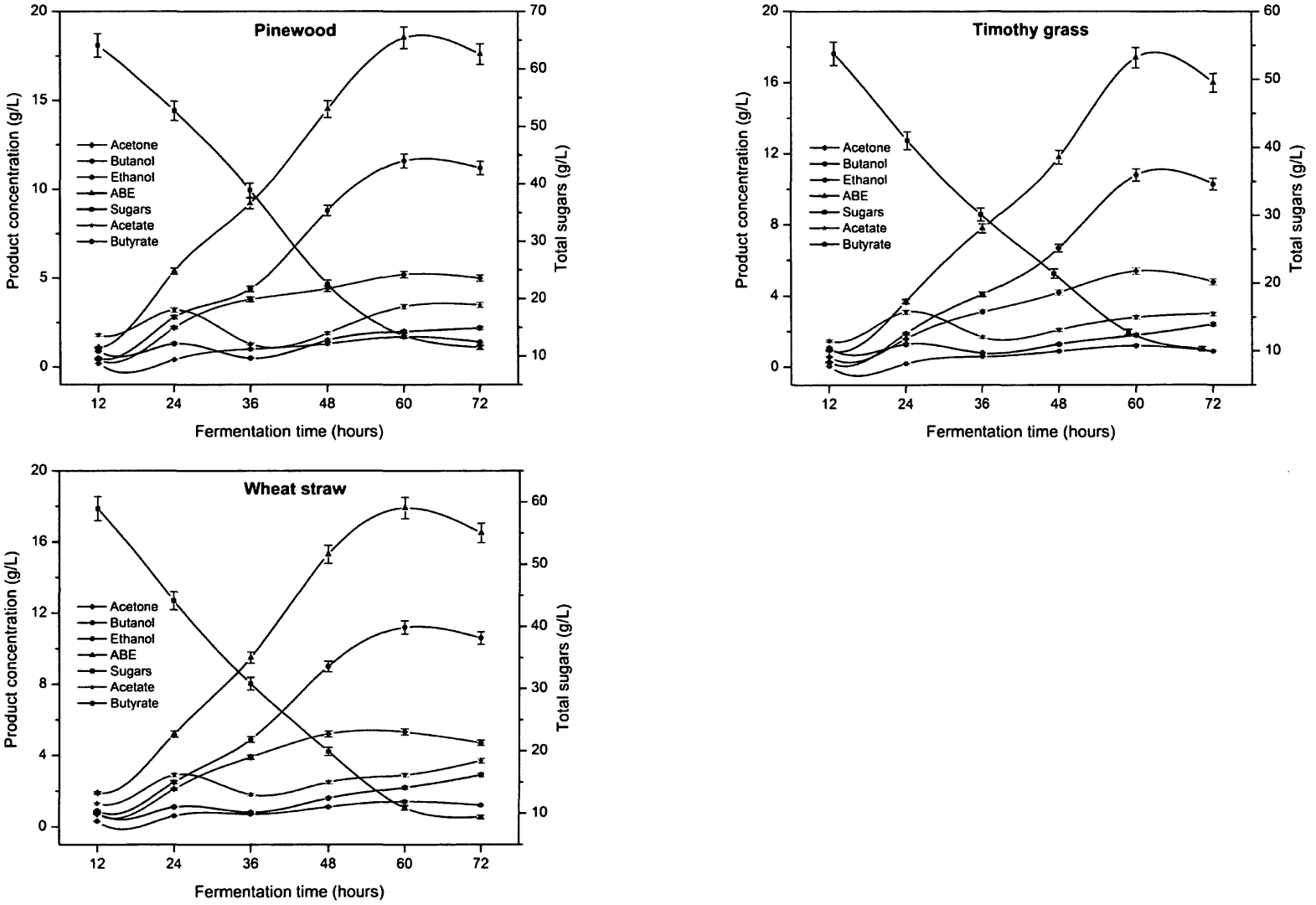

Fig. 6.5 Butanol production using *C. beijerinckii* B-592 from pinewood, timothy grass and wheat straw hydrolysates

The fermentation of biomass hydrolysates was performed by *C. beijerinckii* B-592 to have a comparative yield analysis for ABE and organic acid (Fig. 6.5). The total amount of ABE in the three hydrolysates were in the order: PW (18.5 g/L) > WS (17.9 g/L) > TG (17.4 g/L) at 60 h of fermentation. Among all feedstock hydrolysates, PW exhibited highest butanol (11.6 g/L) and ethanol (1.7 g/L) levels, whereas highest acetone level (5.4 g/L) was found in the case of TG. The average concentration of solvents in the three feedstocks was in the order: butanol (5.7-6.6 g/L) > acetone (3.3-3.7 g/L) > ethanol (0.6-1.0 g/L). This was due to the fact that a typical ABE fermentation by *Clostridium* spp. yields acetone, butanol and ethanol in the ratio of 3:6:1 (Zheng et al., 2009).

Compared to ethanol fermentation, ABE fermentation resulted in lower final butanol levels, which was because of butanol toxicity. Butanol at a level of 12 g/L is inhibitory to *C. beijerinkii* (Westhuizen et al., 1982). Moreover, a maximum butanol production of 19.6 g/L has been reported by *C. beijerinckii* BA101 (Liu and Qureshi, 2009). Butanol as a solvent enters in to the bacteria's cytoplasmic membranes and changes the membrane structures resulting in membrane fluidity (Durre, 2008). This significantly interferes with the normal metabolic functions of the bacteria. For instance, a 20-30% increase in the membrane fluidity was noticed in *C. acetobutylicum* in response to 1% butanol exposure during fermentation.

A few advancements such as fed-batch fermentation, gas stripping, perstraction, pervaporation and membrane separation have shown to reduce butanol toxicity (Zheng et al., 2009). However, these features considerably add to the overall costs of the bioconversion process. Furthermore, substantial research is underway in the development of genetically modified butanol producing microorganisms. These microorganisms are desired to have better stress responsive proteins and membrane fatty acid composition and structure to resist membrane fluidity that is involved in alcohol tolerances.

6.4. Conclusions

Pinewood, timothy grass and wheat straw were pretreated using dilute H_2SO_4 at varying doses of 0-2.5% followed by enzymatic hydrolysis for the production of fermentable sugars. The compositional analysis for PW, TG and WS showed the presence of 38.8, 34.2 and 39.1 wt.% cellulose; 23.6, 30.1 and 24.1 wt.% hemicellulose; and 20.4, 18.1 and 16.3 wt.% lignin, respectively. The highest levels of glucose (32.9 g/L) and xylose (35.6 g/L) were recovered from PW with 2% H_2SO_4 and enzymatic hydrolysis. In contrast, 1.5% H_2SO_4 pretreatment with enzymatic hydrolysis resulted in 26.7 and 26 g/L glucose and 30.7 and 37.6 g/L xylose yields from TG and WS hydrolysates, respectively.

Maximum ethanol concentrations of 20.3, 32.9 and 48.3 g/L were obtained using *S. cerevisiae* ATCC 96581 from 50, 100 and 150 g/L glucose levels, respectively in 36 h. Among the feedstock hydrolysates, PW demonstrated high ethanol levels (24.1 g/L) followed by WS (23.2 g/L) and TG (22.6 g/L). ABE fermentation using *C. beijerinckii* B-592 led to utmost butanol levels of 11.2, 11.9 and 9.3 g/L from 50, 100 and 150 g/L glucose substrate in 60 h. The butanol concentrations obtained from the biomass hydrolysates decreased as: PW (11.6 g/L) > WS (11.2 g/L) > TG (10.8 g/L). Furthermore, the total ABE levels from PW, TG and WS hydrolysates were found to be 18.5, 17.4 and 17.9 g/L, respectively in 60 h of fermentation.

Chapter Seven: Pyrolysis of hydrolyzed biomass: Production of valuable biochars, bio-oils and gases

7.1. Introduction

Lignocellulosic biomass is a significant storehouse of renewable carbon and has enormous potentials for supplying renewable energy. Recently, lignocellulosic feedstocks are used for the production of fuel ethanol and butanol through fermentation in order to restrict the use of food grains for fuel. The complex nature of lignocellulose makes it indispensable to hydrolyze its native cellulose to produce reducing sugars for fermentation to ethanol and butanol. In order to disrupt the lignocellulosic crystallinity, remove lignin, increase pore volume and solubilize cellulose and hemicellulose to fermentable sugars, pretreatment technologies involving dilute acids and enzymes are necessary. Although the lignocellulosic material in itself is economical, but the high cost of hydrolysis and pretreatment technologies makes ethanol and butanol production process relatively expensive.

Dilute-acid hydrolysis is one of the widely used cost effective and efficient pretreatments that removes and recovers most of the hemicellulose as dissolved sugars and increases glucose yields from cellulose after hemicellulose removal (Kumar et al., 2009). It also has a tendency to improve enzymatic hydrolysis of the biomass to release monomeric sugars. Hydrolysis residue is a major byproduct of biomass hydrolysis and pretreatment. In the hydrolysis of woody biomass, about 40-45 wt.% of the feedstock is obtained as residue (Huang et al., 2012). This residual biomass is concentrated in recalcitrant carbon, as most of its cellulose and hemicellulosic components are released in the hydrolysate during dilute acid and enzymatic pretreatments (Nanda et al., 2013a). In contrast to distillers grains, the hydrolysis residues cannot be used as livestock feed due to its relatively low nutrition value (Wang et al., 2012). Currently, hydrolysis residues are primarily used in combustion for power generation (Kim and Dale, 2004), managed by landfill

disposal or direct land applications. Furthermore, fermentation residues from ethanol refineries are also used for co-firing in a coal-fired power plant to reduce CO_2 emissions (Kern et al., 2012).

Effective utilization of these hydrolysis residues towards value-added compounds through pyrolysis could significantly balance the high cost related in the industrial production of fuel alcohols (Nanda et al., 2013a). Pyrolysis results in a thermal decomposition of these residues to gaseous fuels from which liquid fuels and chemicals can be generated (Mohanty et al., 2013). Moreover, the hydrolysis residues differ in both composition and structure than the indigenous biomass. Hence, it is vital to explore their pyrolytic behavior in order to provide practical insights for their industrial application. In a study by Yao et al. (2011), biochar produced from the pyrolysis of anaerobically digested sugarcane bagasse demonstrated desirable characteristics for soil amelioration, contaminant remediation and water treatment.

However, the research in this field is rare at present. Therefore, this chapter aims to investigate the pyrolysis of lignocellulosic hydrolysis residues for environmental remediation and value-added compounds. Hydrolysis residues obtained from the dilute acid and enzymatic pretreatment of pinewood, timothy grass and wheat straw are pyrolysed in a fixed-bed reactor at slow heating rate to understand the properties of their pyrolysis products (e.g., biochar, bio-oil and pyrolysis gas). The biochars are characterized to suggest their soil applications, whereas bio-oils and gaseous products are studied for their energy potentials.

7.2. Materials and methods

7.2.1. Hydrolysis residues

Three kinds of hydrolysis residues examined in this study were pinewood residue (PWR), timothy grass residue (TGR) and wheat straw residue (WSR). These residues were obtained as major byproducts from ethanol and butanol

fermentation processes. The details of biomass collection, characterization and hydrolysis can be found in sections 3.2 and 6.2 of Chapters 3 and 6, respectively.

The hydrolysis residues (PWR, TGR and WSR) were harvested from a dilute H_2SO_4 hydrolysis process (2% H_2SO_4 for PW, 1.5% H_2SO_4 for TG and WS) at 121°C for 1 h followed by an enzymatic hydrolysis involving a mixture of cellulase, β-glucosidase and xylanase at 45°C for 72 h. The detailed procedures of hydrolysis are given in the preceding Chapter 6 (sections 6.2.2 and 6.2.3). Prior to enzymatic pretreatment the acid hydrolyzed feedstocks were neutralized to pH 5.0 with 10 M NaOH (Qureshi et al., 2010). The residues after hydrolysis were vacuum filtered, thoroughly washed with Milli-Q water until pH 7.0 was reached and dried at 60°C before analysis. For all sample analysis, average values were calculated from $n = 3$ replicate measurements with standard deviation $< \pm 5\%$.

7.2.2. Pyrolysis of hydrolysis residues

The pyrolysis of hydrolysis residues was carried out in a fixed-bed tubular furnace pyrolysis reactor made of inconel tubing with outer diameter 25.4 mm and inner diameter of 22.0 mm. The details of the reactor set-up for pyrolysis could be found in Fig. 4.1 of Chapter 4 (section 4.2.1). Pyrolysis was carried out under an inert gas atmosphere created by argon at a flow rate of 70 mL/min. The temperature for pyrolysis was 600°C with a slow heating rate of 5°C/min and a residence time of 4 h. About 10 g of hydrolysis residues were pyrolyzed for each batch run.

Volatile components generated during the thermal decomposition were transferred to an ice-cooled condenser to collect the liquid products. The bio-oils after pyrolysis were separated into organic and aqueous phases using diethyl ether extraction process (Azargohar et al., 2013). Subsequently, the solvent was removed from organic phase using a rotary evaporator at 25°C. The extracted bio-oil was used for further chemical analysis. The gaseous products were collected in gas sampling bags for analysis in a gas chromatograph (GC).

The biochars obtained from pinewood residue, timothy grass residue and wheat straw residue were denoted as PWB, TGB and WSB; while their bio-oils were represented as PWBL, TGBL and WSBL. Similarly, the pyrolysis gases from the same feedstocks were expressed as PWG, TGG and WSG.

7.2.3. Proximate, ultimate and calorific value determinations

The proximate and ultimate analyses of biochars and bio-oils (ultimate only) were performed using the standard ASTM procedures as described in section 3.2.2 of Chapter 3. Analysis for major inorganic elements in biochars was performed in a PerkinElmer NexION 300D ICP-MS (PerkinElmer, USA) using the procedures described in section 3.2 of Chapter 3.

The calorific value (high heating value or HHV) of biochars and bio-oils were determined using a static bomb calorimeter (see Chapter 3, section 3.2.3). For the pyrolysis gases, the calorific value was calculated as lower heating value (LHV) using the following equation (Lv et al., 2004), where CO, H_2, CH_4 and C_nH_m are the molar concentrations of gaseous products:

$$\text{LHV (KJ/m}^3) = [(30 \times CO) + (25.7 \times H_2) + (85.4 \times CH_4) + (151.3 \times C_nH_m)] \times 4.2$$

7.2.4. pH and electrical conductivity (EC)

Biochar (particle size < 2 mm) was soaked with deionized water at a biochar to water ratio of 1:5 for 24 h with intermittent mixing (Song and Guo, 2012). The biochar-water slurry was then analyzed for pH and EC using an Accumet AP85 Portable pH/conductivity meter (Fisher Scientific, Canada).

7.2.5. Porosity measurement

Brunauer-Emmett-Teller (BET) surface area and total pore volume of biochar samples were determined by an automated gas adsorption analyzer ASAP 2020 (Micromeritics Instruments Corp., USA). Prior to N_2 adsorption-desorption

isotherms measurements at −196°C, biochars were degassed at 300°C under vacuum of 550 μmHg.

7.2.6. Thermogravimetric analysis (TGA)

TGA analysis was used to determine the devolatilization characteristics of hydrolysis residues in a PerkinElmer Pyris Diamond TG/DTA instrument (PerkinElmer, USA). About 0.5 g of biochar was subjected to a temperature program of 50-600°C (heating rate 10°C/min) with purge gas (argon) flow rate of 10 mL/min. The rate of weight loss with respect to temperature was recorded.

7.2.7. X-ray diffractometry (XRD)

XRD of hydrolysis residues and biochars was perfromed using a Bruker D8 Advance X-ray diffractometer (Bruker AXS, Germany) following the procedures described in Chapter 5 (section 5.2.4). The degree of crystallinity (expressed as crystallinity index, CrI) in the hydrolysis residues was calculated using the Segal method (equation 2).

7.2.8. Scanning electron microscopy (SEM)

SEM analysis for the hydrolysis residues and their biochars was performed using a FEI Quanta 3D FEG DualBeam microscope (FEI Company, USA) operated in high vacuum mode and 5 kV voltage. Prior to analysis, the biochars were gold coated in a Denton Desk V Sputter coater (Denton Vacuum, USA).

7.2.9. Fourier transform infrared (FT-IR) and Raman spectroscopy

The FT-IR and Raman spectroscopy for hydrolysis residues, biochars and bio-oils were performed following the methods discussed in Chapter 4 (sections 4.3.2 and 4.3.4). Raman spectrum in the range of 800 to 1800 cm^{-1} was collected for hydrolysis residues, whereas spectrum from 1100 to 1800 cm^{-1} was acquired for biochars and deconvoluted using the WiRE Raman software.

7.2.10. Nuclear magnetic resonance (NMR) analysis

NMR of the bio-oil samples obtained at 600°C from the hydrolysis residues was performed in a Bruker Advance 500 MHz NMR spectrometer (Bruker BioSpin, Canada) equipped with a 5 mm inverse triple resonance TXI probe for ^{1}H and ^{13}C analysis. Bio-oils were diluted with $CDCl_3$ for analysis.

7.2.11. Gas chromatography-mass spectrometry

GC analysis for bio-oils was performed in a Varian CP-3800 GC (Varian Inc., USA) equipped with a flame ionization detector (FID) and a 30 m/0.25 mm DB-5 column (Agilent Technologies Inc., Canada) with 0.25 μm film thickness. Helium was used as the carrier gas at a flow rate of 1.2 mL/min at a column pressure of 22 KPa. Compound separation was achieved following a linear temperature program of 50-250°C (ramp rate 5°C/min) with a total run time of 45 min. The mass composition was calculated using the peak normalization method. The GC-MS analysis for bio-oils was carried out in a Varian Saturn 2000 GC-MS (Varian Inc., USA) fitted with the same column and temperature program as mentioned above. The mass spectroscopy parameters followed were ionization voltage (EI) 70 eV, peak width 2 s, mass range 40-500 amu and detector voltage 1.5 V. Peak identification was carried out by comparison of the mass spectra available on NIST-I and NIST-II libraries.

For pyrolysis gas, GC analysis was performed in an Agilent 7890A GC (Agilent Technologies Inc., USA) equipped with one FID for hydrocarbons and two thermal conductivity detectors (TCD) for gases such as H_2, CO, N_2 and CO_2. The total run time of the samples was 13.5 min.

7.3. Results and discussion

7.3.1. Proximate and ultimate analysis

Prior to elemental analyses, the hydrolysis residues were expressed in a moisture and ash free basis. During sample analysis, care was taken for

reproducibility in duplicates with standard deviation less than ±5%. Figure 7.1 illustrates the product yields from slow pyrolysis of PWR, TGR and WSR at 600°C. The yield of biochar, bio-oil and gases from the residues ranged between 38.9-41.7, 18.6-22.3 and 24.9-28.8 wt.%, respectively. The gas yields (wt.%) were calculated from the difference of biochars and bio-oils. The oil phases in the case of PWR, TGR and WSR were 66.8, 58.9 and 56.3% of their respective total liquid product yields from pyrolysis.

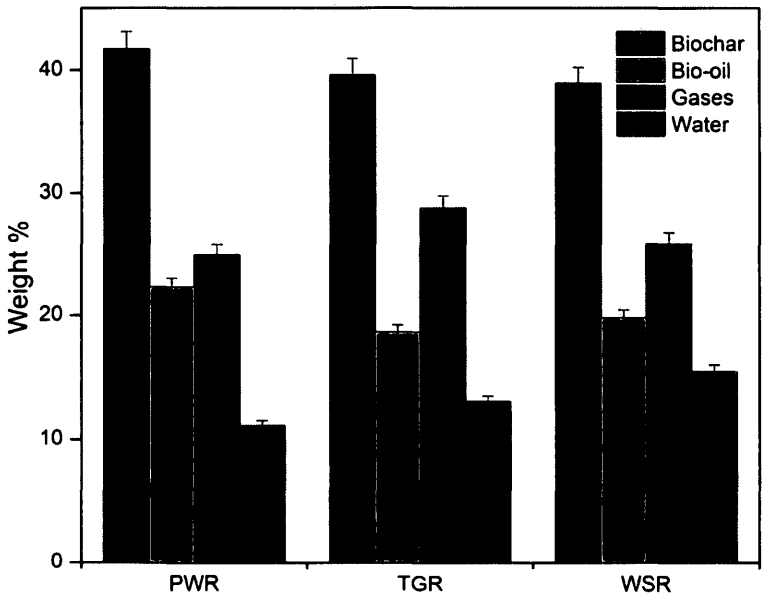

Fig. 7.1 Analysis of product yield from the pyrolysis of hydrolysis residues

The proximate and ultimate analyses together with calorific values of residues, biochars and bio-oils are presented in Table 7.1. The level (wt.%) of ash in the residues was in the order: PWR (1.6) < TGR (1.9) < WSR (2.3), with same trend in the case of biochars as pinewood biochar, PWB (3.7) < timothy grass biochar, TGB (7.6) < wheat straw biochar, WSB (8.7). The high amount of ash indicated the presence of higher amount of inorganic components.

The yield and composition of pyrolysis products depend on the composition of the feedstock. PWR demonstrated a high yield of biochar (41.7

wt.%) and bio-oil (22.3 wt.%), whereas TGR produced a considerable amount of gases (28.8 wt.%). The high yield of biochar and bio-oil from PWR was because of its woody and fibrous nature. Compared to hydrolysis residues, an increment of 70-80% in the fixed carbon content was found in the respective biochars. The high carbon content (87.6 wt.%) in PWB is a supporting feature for making it a good soil-carbon enhancing material.

The nitrogen concentration in TGR (1.1 wt.%) was significantly higher than that of PWR (0.1 wt.%) and WSR (0.5 wt.%). A similar variation in nitrogen levels (wt.%) was also found in the raw untreated feedstocks (Table 3.1) as: TG (1.3 wt.%) > WS (0.4 wt.%) > PW (0.1 wt.%). As nitrogen is related to the plant metabolism, short-lived and fast-growing species such as grasses contain more nitrogen than long-lived and slower-growing species such as trees (Mattson, 1980). High levels of nitrogen in the biochars (0.4-2.0 wt.%) and bio-oils (1.9-4.3 wt.%) were attributed from their feedstocks. On the average basis, sulfur levels showed nearly 54% increase in the biochars and about 72% decrease in the bio-oils than that of the hydrolysis residues. Emission-related (SO_2 and SO_3) problems from timothy grass bio-oil (TGBL) and wheat straw bio-oil (WSBL) were expected as their sulfur concentrations were above 0.2 wt.%. However, hydrodesulfurization helps in removing sulfur from bio-oils to reduce potential SO_2 emissions from their combustion.

The gradual decrease in H/C and O/C ratios in the biochars implied their high aromaticity and carbonaceous nature due to the loss of O-containing species and substitution groups from dehydration, decarboxylation and decarbonylation (Fu et al., 2012). From the atomic ratio data, the chemical formula for PWR, TGR and WSR were established as $CH_{1.7}O_{0.7}N_{0.002}$, $CH_{1.8}O_{0.8}N_{0.02}$ and $CH_{1.8}O_{0.9}N_{0.01}$, respectively. Similarly, the formula for PWB, TGB and WSB were determined as $CH_{0.2}O_{0.1}N_{0.003}$, $CH_{0.3}O_{0.3}N_{0.03}$ and $CH_{0.3}O_{0.2}N_{0.03}$, respectively. Pinewood bio-oil (PWBL), timothy grass bio-oil (TGBL) and wheat straw bio-oil (WSBL) had their formula as $CH_{1.4}O_{0.4}N_{0.03}$, $CH_{1.5}O_{0.3}N_{0.1}$ and $CH_{1.4}O_{0.3}N_{0.05}$.

Table 7.1 Proximate and ultimate analysis of hydrolysis residues, biochars and bio-oils

Analyses	PWR	TGR	WSR	PWB	TGB	WSB	PWBL	TGBL	WSBL
Proximate analysis (wt.%)									
Moisture	5.3 ± 0.2	5.0 ± 0.2	3.4 ± 0.1	0.8 ± 0.02	0.7 ± 0.04	0.5 ± 0.04	-	-	-
Volatile matter	75.7 ± 0.6	71.6 ± 1.1	69.2 ± 0.9	10.6 ± 0.4	8.7 ± 0.3	9.1 ± 0.4	-	-	-
Fixed carbon	17.4	21.5	25.1	84.9	83.0	81.7	-	-	-
Ash	1.6 ± 0.04	1.9 ± 0.1	2.3 ± 0.1	3.7 ± 0.2	7.6 ± 0.04	8.7 ± 0.1	-	-	-
Ultimate analysis (wt.%)									
C	47.1 ± 0.9	42.6 ± 1.0	40.5 ± 0.7	87.6 ± 1.2	65.2 ± 1.2	66.7 ± 1.7	57.2 ± 0.9	63.6 ± 1.0	61.5 ± 1.1
H	6.5 ± 0.1	6.3 ± 0.2	6.0 ± 0.1	1.6 ± 0.1	1.5 ± 0.1	1.5 ± 0.1	6.9 ± 0.3	7.9 ± 0.04	7.1 ± 0.4
N	0.1	1.1 ± 0.02	0.5 ± 0.01	0.4 ± 0.03	2.0 ± 0.3	2.0 ± 0.2	1.9 ± 0.1	4.3 ± 0.3	3.5 ± 0.2
S	0.3	1.1 ± 0.03	1.6 ± 0.03	0.9 ± 0.03	2.0 ± 0.1	3.7 ± 0.2	0.01	0.4 ± 0.01	0.7
O	44.3	46.9	49.2	5.9	21.8	17.4	34.0	23.8	27.3
Atomic ratio									
H/C	1.7	1.8	1.8	0.2	0.3	0.3	1.4	1.5	1.4
O/C	0.7	0.8	0.9	0.1	0.3	0.2	0.4	0.3	0.3
N/C	0.002	0.02	0.01	0.003	0.03	0.03	0.03	0.1	0.05
HHV (MJ/kg)	18.5 ± 0.9	15.8 ± 0.6	14.2 ± 0.5	31.1 ± 1.1	20.1 ± 0.7	22.2 ± 0.4	23.9 ± 0.6	29.3 ± 1.0	25.9 ± 0.5
pH	-	-	-	10.2 ± 0.3	10.8 ± 0.2	11.3 ± 0.2	-	-	-
EC (mS/cm)	-	-	-	8.6 ± 0.1	9.3 ± 0.2	11.1 ± 0.1	-	-	-

Using the atomic H/C and O/C ratios, a van Krevelen diagram was constructed to estimate the degree of aromaticity and carbon content in the hydrolysis residues and biochars (Fig. 7.2). The diagram also demonstrated the significance of atomic ratios on the heating value of feedstocks and biochars. It is well-illustrated that biochars had heating values higher than those of their residues, which was further explained from calorimetric studies. The HHV of PWR (18.5 MJ/kg) and PWB (31.1 MJ/kg) were higher compared to their respective residues and biochars, while TGBL exhibited the highest HHV (29.3 MJ/kg) among bio-oils. The biochars and bio-oils had higher HHV than that of residues because of greater amount of carbon and hydrogen, which indicated more energy content in C–C bonds than in C–O and C–H bonds.

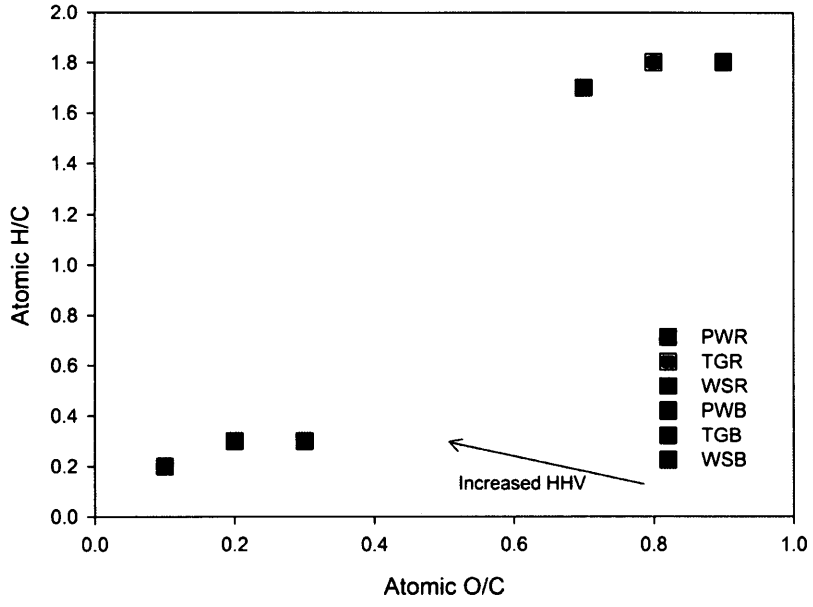

Fig. 7.2 van Krevelen diagram for hydrolysis residues and their biochars

The total carbon balance was calculated for the hydrolysis residues and pyrolysis products as given in Table 7.2. This is based on the CHNS data for biochars and bio-oils along with gas analysis. Among all products, biochars contained large amount of carbon compared to bio-oils and gases in the range of

60.6-77.6%. This was because of their higher yields (38.9-41.7 wt.%) from the pyrolysis. Furthermore, total carbon balance was in the range of 91-105.6%. The deviation of total carbon balance from 100% was due to the loss of some light hydrocarbons during solvent removal step of bio-oil separation and mass balance for gas phase which was based on gas sampling procedures.

Table 7.2 Carbon balance for hydrolysis residues and pyrolysis products

Biomass	Carbon yields (%)			Total carbon balance (%)
	Biochar	Bio-oil	Gas	
PWR	77.6	27.1	1.0	105.6
TGR	60.6	27.8	2.7	91.0
WSR	64.1	30.1	1.3	95.4

Note: All the data are average of replicate measurements

The pH and EC of the biochars increased in the order: PWB < TGB < WSB, similar to ash trend (Table 7.1). However, the higher pH range (10.8-11.3) in TGB and WSB indicated their alkaline nature and presence of greater extent of alkaline metals which could reduce soil acidity caused by inorganic fertilizers. Similarly, TGB and WSB exhibited a higher range of EC (9.3-11.1 mS/cm) than PWB. Moreover, EC > 4 mS/cm indicate salinity on application to sandy soils which may inhibit the plant growth to certain extent due to higher Na levels (Rhoades et al., 1999). However, proper irrigation, tillage and addition of plant growth-promoting rhizobacteria (PGPR) to such soil could potentially reduce salinity and stimulate plant growth by facilitating plant intake of N, P, K, Fe and other essential elements along with phytohormones from biochar-amended soil (Mayak et al., 2004).

The inorganic metal composition of the biochars is given in Table 7.3. In contrast to K that decreases the ash melting point, Ca and Mg usually tend to increase it (Obernberger et al., 2006). As a solid fuel, the impact of ash melting

could be masked in case of TGB and WSB as the combined concentration of Ca and Mg (4366 ppm in TGB and 5728 ppm in WSB) is lower than their K levels (12124 ppm in TGB and 17046 ppm in WSB). However, ash melting could be pertinent in the case of PWB that revealed a higher amount of Ca and Mg (2086 ppm) than K (303 ppm). Calcium was found to be high in WSB (4667 ppm) and TGB (2915 ppm) which is inherited from their feedstocks (elemental composition of feedstocks is given in Table 3.1).

Table 7.3 ICP-MS analysis for determination of inorganic elements (in ppm) in biochars

Elements	PWB	TGB	WSB
Na	22743	43414	70374
Mg	316	1451	1061
Al	143	151	381
P	248	1688	1082
K	303	12124	17046
Ca	1770	2915	4667
Cr	226	86	128
Mn	47	50	18
Fe	274	132	151
Ni	5	11	11
Cu	13	33	22
Zn	13	44	23

Note: All the data are average of replicate measurements

Among the major and minor elements detected, alkali and alkaline elements (Na, Mg, K and Ca) comprised of about 96.2% in PWB, 96.4% in TGB and 98.1% in WSB, respectively. WSB had utmost levels of Na (70374 ppm), K (17046 ppm), Ca (4667 ppm) and Al (381 ppm), whereas TGB showed maximum

extent of Mg (1451 ppm), P (1688 ppm), Mn (50 ppm), Cu (33 ppm) and Zn (44 ppm). On the other hand, the concentrations of Cr (226 ppm) and Fe (274 ppm) were high in PWB which is a characteristic feature of their woody nature as they contain more heavy metals in their tissues than herbaceous biomass due to longer lifetime of biomass in forests. Sodium was detected in elevated levels (22743-70374 ppm) in the biochars which could be due to the feedstocks' treatment conditions. The neutralization of acid hydrolyzed feedstocks by 10 M NaOH prior to enzymatic treatment resulted in this higher Na concentrations in the biochars.

Substantial amount of alkaline metals found in all biochars is an indication of their compatibility as soil amendments for enhancing soil fertility, increasing soil organic carbon and reducing soil acidity. Basic plant nutrients such as N, P, K, Ca and Mg were predominant in herbaceous biochars. Moreover, Na and K are known to catalyze the pyrolysis of cellulose by lowering the decomposition temperature and increasing the overall reaction rate and biochar yield (Das et al., 2008). Conversely, calcium acts as a catalyst for hemicellulose pyrolysis.

7.3.2. Porosity and morphological analysis

The SEM analysis (Fig. 7.3) indicated that PWB had a relatively smoother surface than TGB and WSB. More pore development was found in biochars due to devolatilization of organic components during pyrolysis. The surface of TGB and WSB appeared more porous which was due to the parenchyma tissues and loosely packed vascular bundles (xylem and phloem) in their feedstocks. The vascular bundles act as conductive tissues and help in the exchange of gases and metabolites during photosynthesis. In contrast, the densely packed fibers in PW contributed to a relative firm and less fragmented biochar.

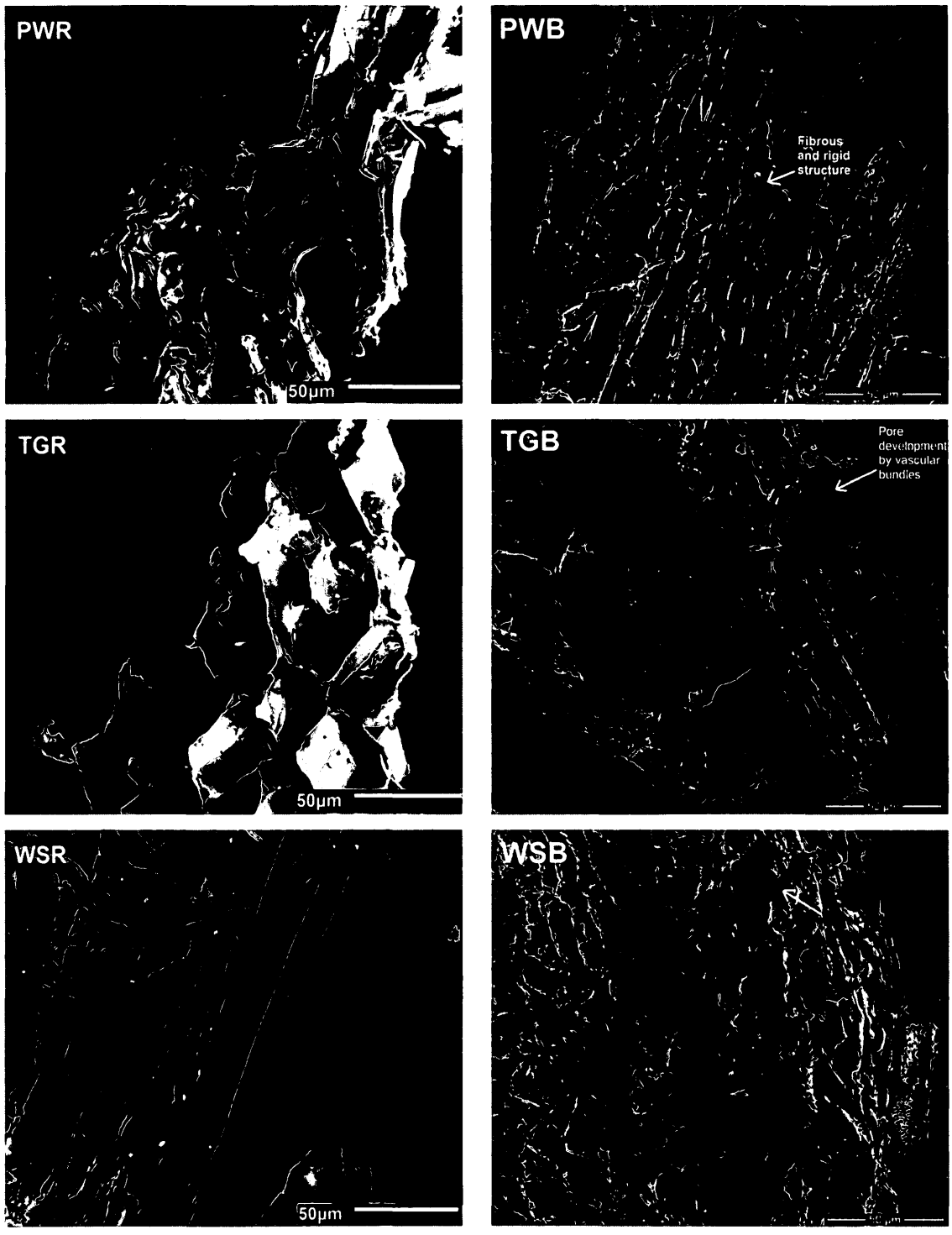

Fig. 7.3 SEM images of hydrolysis residues and their biochars

The porosity analysis showed that the BET surface area and total pore volumes were less than 5 m^2/g and 0.007 cm^3/g, respectively for all biochars. However, the large carbon content in biochars (65.2-87.6 wt.%) and their relatively low ash content (3.7-8.7 wt.%) suggested their suitability for activation process in developing porous materials and activated carbons. These valuable products from biomass pyrolysis can be used as adsorbent, catalyst and catalyst support for various chemical reactions (Azargohar and Dalai, 2008). The porous nature of biochars enhances the formation of fungal hyphae as networks between their cracks and pores. This not only helps to transfer growth promoters and nutrients from soil to plants but also aids in holding the soil particles in proximity to plant roots preventing soil erosion (Lehmann et al., 2011).

7.3.3. Thermal and structural analysis

The thermal decomposition of TGR and WSR started at around 200°C, whereas for PWR it was around 240°C (Fig. 7.4). The maximum weight loss for all residues occurred between 350 and 400°C. This stage is termed active pyrolysis zone which is featured by loss of moisture and light volatile compounds causing a sharp drop in the sample weight. Further, a slight change in the mass loss curves was observed with a slow weight loss until 500°C, indicating the passive pyrolysis zone. The active pyrolysis zone is characterized by the degradation of residual hemicellulose (200-300°C) and cellulose (250-350°C), whereas the passive pyrolysis zone is considered for slow degradation of lignin (200-500°C) over a wide temperature range (Jeguirim and Trouve, 2009).

The primary degradation of TGR and WSR at ~200°C could be due to the high calcium content in the initial feedstocks that has a tendency to catalyze the hemicellulose breakdown occurring at 200-300°C. Maximum degradation was observed in the case of WSR and TGR due to weaker C–C and C–H bonds. Comparatively, PWR was thermally stable with relatively less mass loss due to its stronger C–C and C–H bonds attributed by its higher C and H content (Table 7.1).

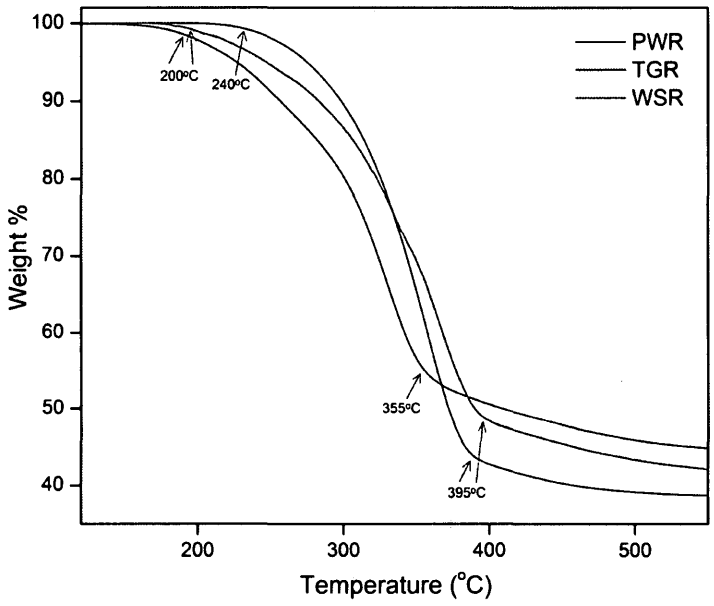

Fig. 7.4 Thermogravimetric analysis of hydrolysis residues

The XRD patterns of hydrolysis residues and the resulting biochars are shown in Fig. 7.5. In the XRD pattern of hydrolysis residues, the peaks at 15.5° (d-space ~5.51 Å), 21.7° (d-space ~3.96 Å) and 34.5° (d-space ~2.59 Å) were assigned to Cellulose I, Cellulose II and hemicellulose, respectively (Fig. 7.5A). The crystallinity index (CrI) for the hydrolysis residues decreased in the order: PWR (94.1%) > WSR (93.3%) > TGR (90.5%). The degree of crystallinity of biomass materials at 13-17° and 20-23° was due to polymorphism of cellulose. The development of broad peaks around 24.5° (d-space ~3.62 Å) and 43.5° (d-space ~2.12 Å) in PWB (Fig. 5B) indicated the formation of turbostratic carbon crystallites (Kim et al., 2011).

The diffraction peaks at 14.7° (d-space ~5.91 Å) and 33.7° (d-space ~2.63 Å) were due to weddelite, while the peak at 16.0° (d-space ~5.51 Å) indicated whewellite. Whewellite (calcium oxalate monohydrate) and weddelite (calcium oxalate dihydrate) are soluble in acidic water solutions (Vassilev et al., 2012), and their appearance in the residues is due to H_2SO_4 treatment during hydrolysis.

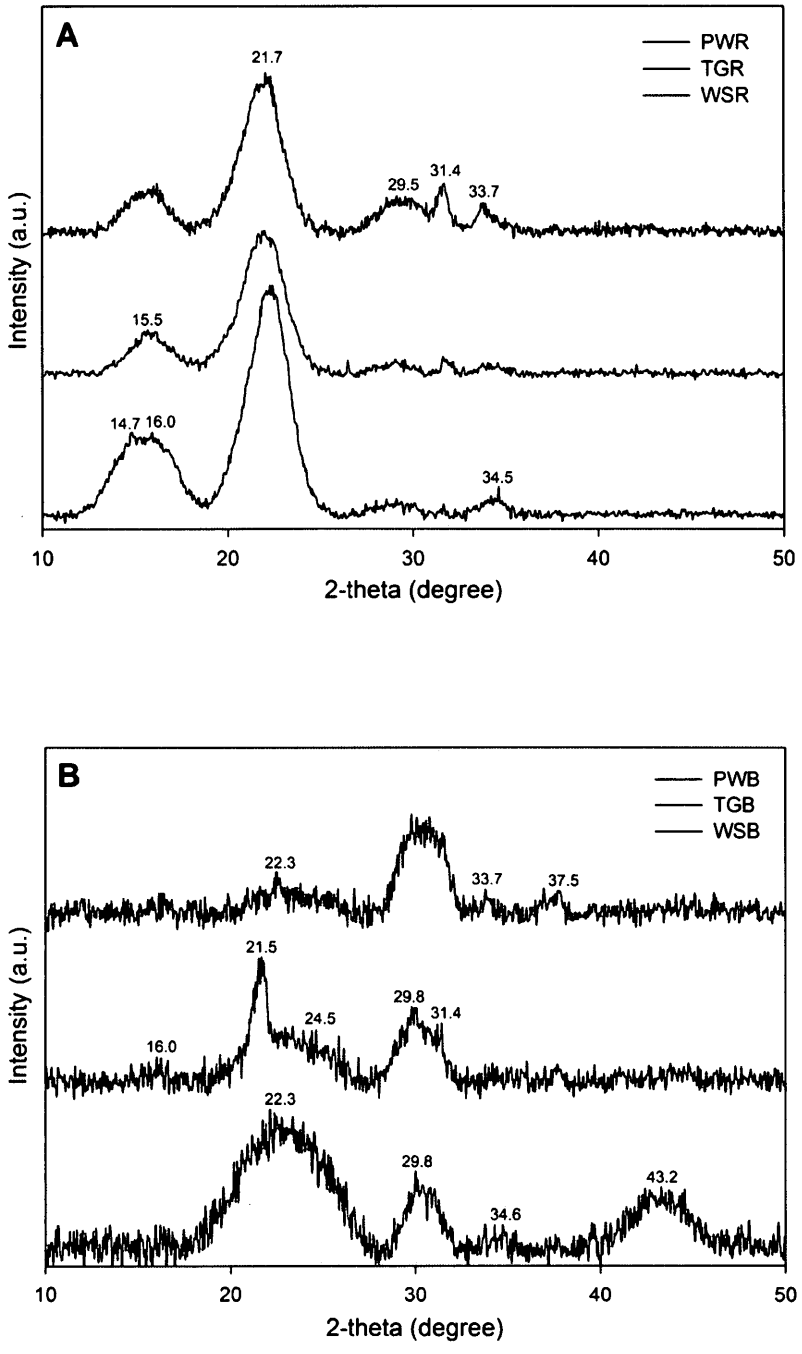

Fig. 7.5 X-ray diffractometry analysis of (A) hydrolysis residues and (B) biochars

Nitrate peak was observed at 31.4° (d-space ~2.81 Å) in the case of WS and TG residues and biochars. This is because for the higher amount of nitrogen in these herbaceous residues and their resulting biochars (Table 7.1). The sulphate peaks at 29.5° (d-space ~2.99 Å) and 29.8° (d-space ~2.96 Å) were due to the presence of anhydrite, while 24.5° (d-space ~3.61 Å) represented gypsum. These Ca sulphates are not typical to biomass or biochars, however their presence in the XRD patterns could be attributed to the higher amounts of Ca present in feedstocks and their H_2SO_4 pretreatment.

The gypsum and anhydrite content in biochars could act as soil conditioner for enhancing soil fertility. The diffraction peaks at 34.6° (d-space ~2.59 Å) and 43.2° (d-space ~2.19 Å) were detected as calcite, whereas apatite peak was found at 37.5° (d-space ~2.38 Å). These common carbonate (calcite) and phosphate (apatite) minerals occur in biomass as debris from soil contaminants. As a bioremediation supplement, the carbonate in biochars could aid in neutralizing the acidic conditions of both soil and water.

A few silicate (opal) peaks were detected in the biochars at 21.5° (d-space ~4.04 Å) and 22.3° (d-space ~3.95 Å). As the silicic acid is adsorbed by the plants from the soil solution, it flocculates in cell structures, undergo polymerization and deposit in the plant cells resulting in the formation of silica hydrate or opal (Vassilev et al., 2012). The presence of chloride (sylvite) peak was also noticed in the XRD patterns of biochars at 33.7° (d-space ~2.63 Å). The origin of sylvite in feedstocks is due to the precipitation and evaporation of mineral solution in the plants. The presence of nitrate, phosphate and chloride in the biochars suggests their soil applications in enhancing crop productivity.

7.3.4. Spectroscopic analysis

The FT-IR spectra of hydrolysis residues, their biochars and bio-oils are shown in Fig. 7.6. The major peaks of interest and their assignments are tabulated in Table 7.4. The spectra of hydrolysis residues in the region 3300-3400 cm^{-1}

represented –OH stretching vibrations (Fig. 7.6A). Intense peaks for hydrolysis residues in at 1630-1745 cm^{-1} originated from carbonyls mainly ketones and esters. These bands could be predicted from some residual waxes, fatty acids, fatty esters, high molecular weight aldehydes or ketones. The CH_2 bands at 2860-2928 cm^{-1} were due to the presence of waxes.

Vibrations at 1000-1280 cm^{-1} in the residues were due to alcohols, ethers, carboxylic acids and esters. The C–O stretch (1175 cm^{-1}) signifying alcohols and carboxylic acids represented oxygenated functional groups of cellulose and hemicellulose, whereas the band at 1516 cm^{-1} was assigned to C=C aromatic rings indicating lignin (Chen et al., 2008). Nitrile components were found in TGR and WSR at 2368 and 2397 cm^{-1} which correlates to their significant nitrogen content (Table 7.1).

The FT-IR spectra of biochars (Fig. 7.6B) showed the removal of O- and H-containing functionalities as compared to the feedstocks due to their higher production temperatures of 600°C. The absence of these functional groups in biochars indicates the evolution of CO_2, CH_4 and H_2 from the pyrolysis of residual cellulose, hemicelluloses and lignin at temperatures above 400°C. During pyrolysis, CO_2 is released by cracking and reforming of C=O bonds, while CO is generated from cracking of C–O–C and C–O bonds, and H_2 is produced by the breaking of C–H bonds and formation of H–H bonds (Siengchum et al., 2013).

Major organic components present in hydrolysis residues at 903-1745 cm^{-1} diminished upon heating to 600°C. Due to thermal degradation of cellulose and lignin, aromatic C–C compounds (499 cm^{-1}), C–H alkynes (625 cm^{-1}), C–H alkene (907 cm^{-1}), C–H alkanes (1460, 2882, 2950 cm^{-1}) and C–N amines (1137, 1234 cm^{-1}) were exposed. The increased nitrogen levels in biochars contributed to the appearance of C–N amines.

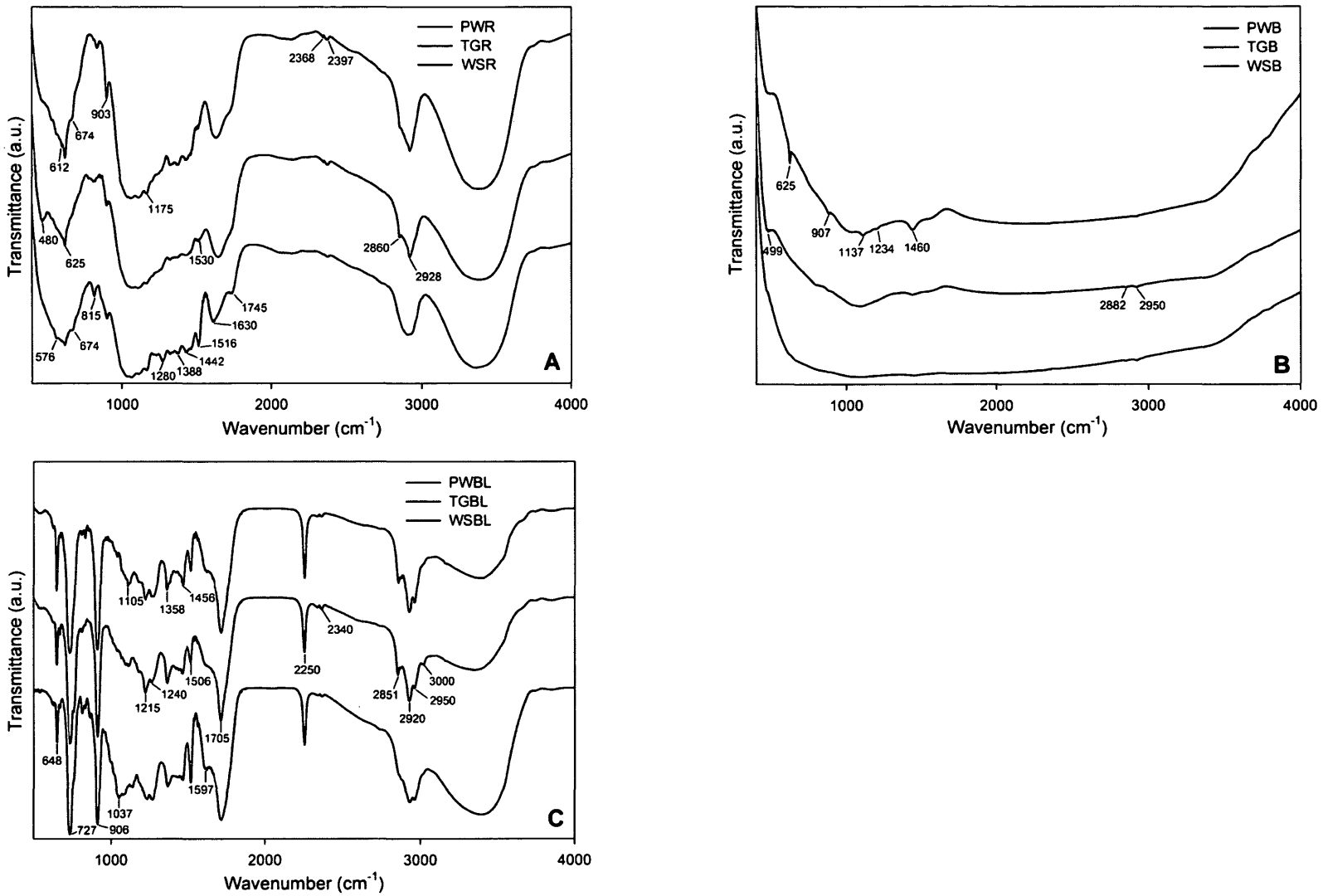

Fig. 7.6 FT-IR spectroscopy of (A) hydrolysis residues, (B) biochars and (C) bio-oils

Table 7.4 Functional group assignments for different FT-IR bands in hydrolysis residues, biochars and bio-oils

Wave number (cm^{-1})	Assignments
Hydrolysis residues	
480, 576	C–C aromatic rings
612, 625, 674	C–H alkynes
815, 903	C–H alkenes
1175, 1280	C–O alcohols, ethers, carboxylic acids, esters
1388, 1442, 2860, 2928	C–H alkanes
1516, 1530	C=C aromatic rings
1630, 1745	C=O aldehydes, ketones, carboxylic acids, esters
2368, 2397	C≡N nitriles
Biochars	
499	C–C aromatic rings
625	C–H alkynes
907	C–H alkenes
1137, 1234	C–N amines
1460, 2882, 2950	C–H alkanes
Bio-oils	
648	C–H alkynes
727, 906	C–H phenyl rings
1037, 1105, 1215	C–N amines
1240, 1358, 1506, 1597	NO_2 nitro compounds
1705	C=O aldehydes, ketones, carboxylic acids, esters
2250, 2340	C≡N nitriles
2851, 2920, 2950	C–H alkanes
3000	C–H aromatic rings

The FT-IR spectra of bio-oils are shown in Fig. 7.6C. The broad peak at 3300-3600 cm^{-1} originated from H-bonds available with alcohols or phenols. The CH_2 and CH_3 asymmetric and symmetric vibrations were observed at 2920-2950 cm^{-1}. These vibrations originated from derivatives of cellulose and hemicellulose. An intense band at 1705 cm^{-1} in the bio-oils was due to C=O aldehydes, ketones, carboxylic acids and esters (Ozcimen and Ersoy-Mericboyu, 2010). Similarly, strong phenyl ring bands were observed at 727 and 906 cm^{-1}. TGBL and WSBL showed the presence of alkanes at 2851-2950 cm^{-1} at comparatively higher intensity. The significant level of nitrogen in bio-oils was evident in the FT-IR spectra with occurrence of various nitro compounds, nitriles and amines.

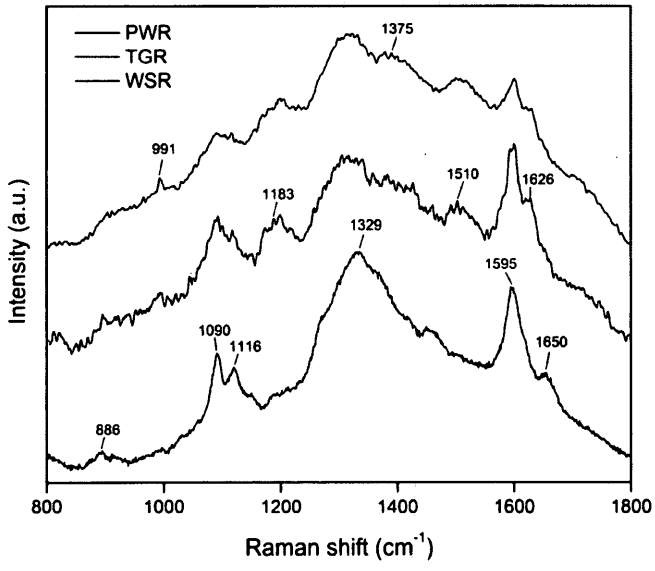

Fig. 7.7 Raman spectroscopy of hydrolysis residues

The Raman spectra of hydrolysis residues showed major vibrations in the region 1595-1650 cm^{-1} which were due to lignin (Fig. 7.7). Li et al. (2010) reported the presence of lignin in biomass as aromatic ring stretch at 1595 cm^{-1} and ring-conjugated C=C bond at 1626 cm^{-1}. In the same study, aromatic skeletal lignin at 1510 cm^{-1} and syringyl and guaiacyl condensed lignin at 1329 cm^{-1} were found in switchgrass. The residual cellulosic and hemicellulosic components

showed their presence at 886-1183 cm^{-1}. The Raman peak at 886 and 1090 cm^{-1} was assigned to amorphous and crystalline cellulose, respectively. Moreover, the bands at 1375 cm^{-1} represented C–H groups in cellulose and hemicellulose.

While FT-IR spectroscopy uses absorption of infrared light to sense dipole vibrations and measure the functional groups, Raman spectroscopy involves emission of scattered laser light to sense polar vibrations in C=C and aromatics to measure the molecular structure, making them an essential tool for analyzing biochars (Kim et al., 2011). In contrast to FT-IR spectroscopy that showed removal of functionalities in biochars at higher pyrolysis temperature (Fig. 7.6B), Raman spectroscopy showed significant increase in two broad bands at 1325-1380 and 1580-1610 cm^{-1} in biochars (Fig. 7.8). The characteristic broad peaks in biochars at 1325-1380 and 1580-1610 cm^{-1} represented the graphite (I_G band) and defect (I_D band) structures, respectively (Kim et al., 2011). The Raman spectra of biochars in the range of 1100-1800 cm^{-1} was deconvoluted and curve-fitted using the WiRE software into four pseudo-bands, namely I_I, I_D, I_{G*} and I_G (Kim et al., 2011). The assignments for these Raman bands are given in Table 7.5.

Table 7.5 Assignments for different Raman bands in biochars

Raman shift (cm^{-1})	Band name	Assignment
1160-1220	I_I	C–H aromatic rings, C–C hydroaromatic rings
1325-1350	I_D	Highly ordered carbon, C–C aromatic rings, aromatics with 6 or more fused benzene rings but less than graphite
1510-1540	I_{G*}	Amorphous carbon structures, aromatics with 3-5 rings
1580-1605	I_G	Graphite crystalline structures, aromatic ring quadrant breathing, C=C alkenes

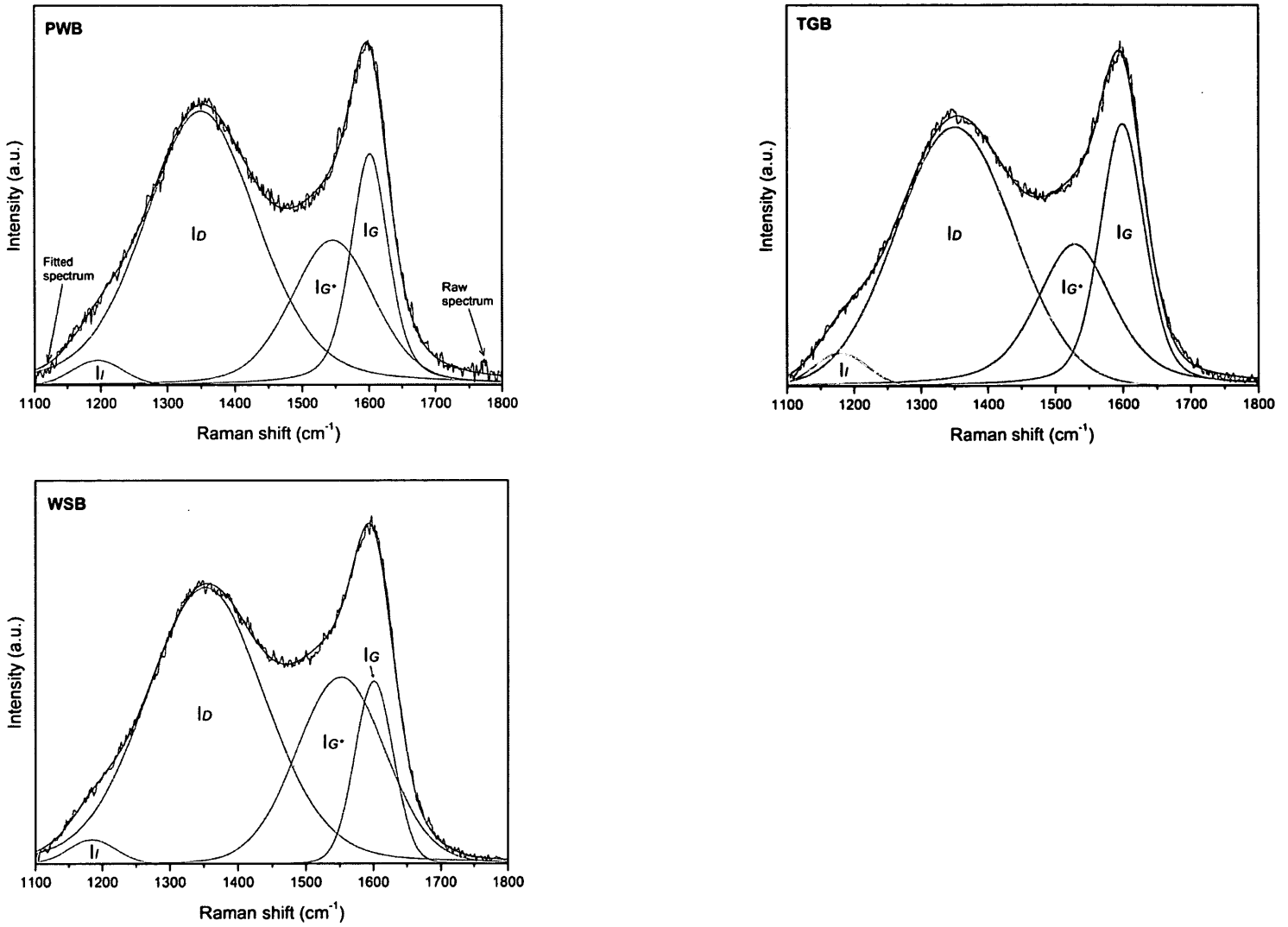

Fig. 7.8 Deconvolution of Raman bands from 1100-1800 cm^{-1} for biochars

The I_1 band (1160-1220 cm^{-1}) was assigned to C–H aromatic rings and C–C hydroaromatic rings in biochars, mostly $C_{aromatic}$–C_{alkyl} and aromatic (aliphatic) ethers. The I_D band (1325-1350 cm^{-1}) represented C–C aromatic rings. I_{G*} band (1510-1540 cm^{-1}) was assigned to amorphous carbon and aromatics with 3-5 rings, whereas I_G band (1580-1605 cm^{-1}) indicated crystalline graphite structures, aromatic rings with quadrant breathing and C=C alkenes.

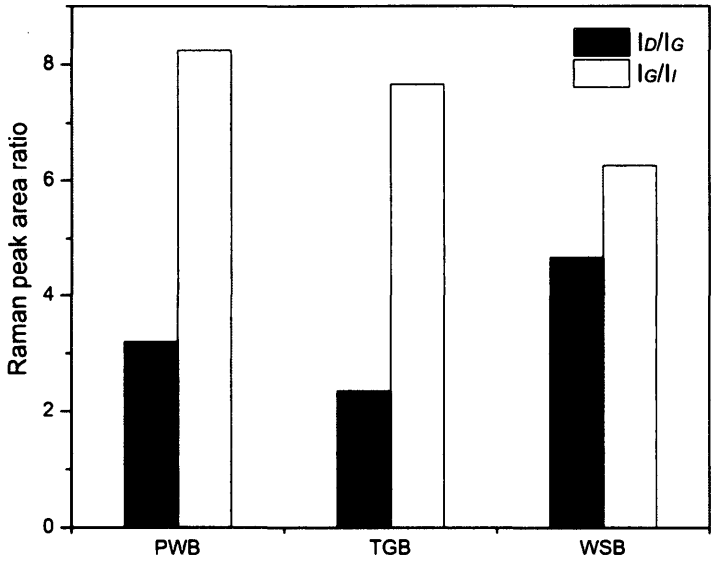

Fig. 7.9 Raman peak area ratio for biochars

The peak area ratio for I_D/I_G and I_G/I_1 for biochars is shown in Fig. 7.9. The I_D/I_G ratios describe the concentration of aromatic rings containing 6 or more fused benzene rings. The I_D/I_G ratios decreased in the order: WSB (4.7) > PWB (3.2) > TGB (2.3). The higher I_D/I_G ratio indicated increased evolution of aromatic rings due to the dehydrogenation of hydroaromatic compounds (Li et al., 2006). The increase in the aromatic rings is characteristic to biochars produced at higher temperatures which make them resistant to subsequent mineralization in soil (Kim et al., 2011). The I_D/I_G ratios in WSB showed higher values than those in PWB which implied a relatively lower thermal stability of WSB than PWB

because of structural differences and higher amount of catalytic alkali metals than PWB. This corresponds to the SEM (Fig. 7.3) and TGA analyses (Fig. 7.4).

Regardless of all, the aromatic nature of biochars offers a carbon negative benefit and helps them sequester carbon in soil for longer periods to mitigate climate change (Sohi et al., 2010; Spokas and Reicosky, 2009). Furthermore, the I_G/I_I ratio decreased in the sequence: PWB (8.2) > TGB (7.7) > WSB (6.3). The I_G/I_I ratio is the proportion of C=C graphitic structures to $C_{aromatic}$–C_{alkyl} structures. A higher I_G/I_I indicates loss of aromatic structures with progressive removal of O-containing functional groups and a stronger contribution of graphitic moieties with higher environmental stability (Keown et al., 2008). PWB with a greater I_G/I_I ratio demonstrated relatively low oxygen content (5.9 wt.%) and high thermal and structural stability as seen from TGA and SEM findings.

The I_I band is considered in the measurement of cross-linking density and substitution groups. The I_I band representing sp^2 and sp^3 structures are preferential sites of reaction with O_2. However, Keown et al. (2008) reported that Na and Ca act as catalysts in reacting with the biochar's aromatic sites efficiently than O_2. As a result of Na and Ca interaction with biochars, the aromatic sites are blocked for any cross-linking with O_2. In contrast, a less intensified I_I band indicates a loosened char structure and destabilized aromatic ring system resulting in increased access for O_2. The relative intensities of I_I band in the three biochars were lower compared to those of I_D, I_{G*} and I_G (Fig. 7.8), indicating high biochar porosity and increased access of O_2 for char oxidation. However, high levels of Na and Ca in the biochars (Table 7.3) could possibly prevent char oxidation by blocking the aromatic sites to O_2 and enhance its stability in soil.

7.3.5. NMR and chromatographic analysis

The liquid products obtained from the pyrolysis of PWR, TGR and WSR contained 33.2, 41.1 and 43.8 wt.% aqueous-rich phase (mostly water), respectively. The crude bio-oils were found to be polymerizing after a few days of

their production at room temperature due to high percentage of oxygen (23.8-34.0 wt.%) and water (33.2-43.8 wt.%) in them. Therefore, it could be suggested that the removal of water from the bio-oils is essential to improve their stability, storage and calorific value as liquid fuels. The H distribution through ^{1}H NMR analysis of bio-oils is given in Table 7.6.

The bio-oil fractions contained aromatics (2.1-9.6%), phenolic (OH) or olefinic proton (1.0-3.2%) and ring join methylene (11.2-21.3%). In addition, CH_3, CH_2 and CH_α to an aromatic ring (47.8-56.7%); CH_2 and CH_β to an aromatic ring (< 3%); β-CH_3, CH_2 and CH_γ or further from an aromatic ring (12.8-19.6%) and $CH_{3\gamma}$ or further from an aromatic ring (3.0-9.3%) were found in the NMR spectra of bio-oils. Based on the proton type, three different groups of chemicals can be quantified in bio-oil as aromatic, olefinic and aliphatic compounds.

Aliphatic protons included ring join methylene; CH_3, CH_2 and CH_α to an aromatic ring; CH_2 and CH_β to an aromatic ring; β-CH_3, CH_2 and CH_γ or further from an aromatic ring and $CH_{3\gamma}$ components. PWBL had larger amount of aromatic compounds. Overall, the H-compounds distribution in bio-oils varied in the range: aliphatics > aromatics > olefinics. However, among the aliphatics protons, α-C was the most abundant form followed by γ-C and β-C.

^{13}C NMR analysis of specific chemical shift regions in bio-oils fractions are shown in Table 7.6. The bio-oils contained carbonyls (11.1-26.1%), aromatics (30.3-35.8%), carbohydrates (< 7.5%), methoxy or hydroxy carbon (4.3-15.1%) and alkyl carbons including primary, secondary, tertiary or quaternary alkyls (27.4-38.4%). On an average, the C-groups in the integrated ^{13}C NMR spectra were distributed in the sequence: aromatics $\geq$ alkyl carbon > carbonyls > methoxy or hydroxyl carbon > carbohydrates. The carbohydrates showed the lowest amounts in bio-oils as most of the sugars were released in biomass hydrolysates for fermentation.

Table 7.6 ^{1}H and ^{13}C NMR analysis for bio-oils

Chemical shifts (ppm)	Components	PWBL	TGBL	WSBL
Type of hydrogen (% of total hydrogen)				
9.0-6.5	Aromatic	9.6	4.0	2.1
6.5-5.0	Phenolic (OH) or olefinic proton	3.2	3.0	1.0
4.5-3.4	Ring-join methylene (Ar-CH_2-Ar)	21.3	11.2	11.3
3.3-2.1	CH_3, CH_2 and CH_α to an aromatic ring	47.8	56.6	56.7
2.0-1.6	CH_2 and CH_β to an aromatic ring (naphthenic)	2.1	3.0	-
1.6-1.0	β-CH_3, CH_2 and CH_γ or further from an aromatic ring	12.8	19.2	19.6
1.0-0.5	$CH_{3\gamma}$ or further from an aromatic ring	3.2	3.0	9.3
Type of carbon (% of total carbon)				
215-163	Carbonyl	14.2	26.1	11.1
163-110	Aromatic	35.8	34.8	30.3
110-84	Carbohydrate	7.5	-	6.1
84-54	Methoxy or hydroxy	15.1	4.3	14.1
54-1	Alkyl carbons	27.4	34.8	38.4

The aromatic carbon (163-110 ppm region) in bio-oils was in the following order: PWBL (35.8%) > TGBL (34.8%) > WSBL (30.3%). This likely reflects the lignin levels in the native feedstocks as shown in Table 5.1: PW (20.4 wt.%) > TG (18.1 wt.%) > WS (16.3 wt.%). This trend was in accordance to the aromatic proton through ^{1}H NMR (9.0-6.5 ppm region) analysis as PWBL (9.6%) > TGBL (4.0%) > WSBL (2.1%). However, the acid/enzymatic pretreatments are effective in the removal of polysaccharides (cellulose and hemicellulose) while leaving behind most of the lignin associated with the biomass (Akin et al., 2007).

Most of the compounds in bio-oils identified through GC-MS included degradation products from lignin and residual polysaccharides in cellulose and monosaccharides occurring in hemicellulose. The chemical classes of the compounds identified are given in Table 7.7. The bio-oils contained numerous phenolic compounds derived from its lignin content. Phenyl rings with only one methoxy group i.e., 2-methoxy phenol predominated. The derivatives of lignin in the bio-oils comprised of 4-methylphenol; 4-methoxy phenol; 2,4-dimethylphenol; 2-methoxy-4-methylphenol; 1,2-benzenediol; 3,4-dimethoxytoluene; 4-ethyl-2-methoxyphenol; 2-methoxy-4-vinylphenol; 2,6-dimethoxy-phenol; eugenol; 1,2,4-trimethoxybenzene (Yong and Matsumura, 2012).

Table 7.7 GC-MS analysis of bio-oils

Components (wt.%)	PWBL	TGBL	WSBL
Phenols and alcohols	6.3	10.2	6.9
Ketones	5.0	6.7	4.2
Acids	8.3	10.7	3.6
Others	0.7	1.1	1.5
Total identified components	20.3	28.8	16.2

Note: All the data are average of replicate measurements

Phenol was the most abundant phenolic compound present in all bio-oils. The cellulose and hemicellulose derivatives found in the bio-oils consisted of 4-hydroxylbenzenesulfonic acid; 2-methoxyphenol; 1,2-methoxy-4-(1-propenyl)phenol; methyl-(2-hydroxy-3-ethoxy-benzyl)ether; 2,6-dimethoxy-4-(2-propenyl)phenol; 3,7,11,15-tetramethyl-2-hexadecane-1-ol (Pittman et al., 2012). The sum of the quantitated compounds through GC-MS represented an estimated 24.7, 28.8 and 13.2% by weight of PWBL, TGBL and WSBL, respectively.

Table 7.8 GC analysis of pyrolysis gases

Components (wt.%)	PWG	TGG	WSG
CH_4	0.9	0.9	0.04
H_2	17.8	11.8	3.3
CO_2	0.2	1.5	0.6
CO	2.1	6.5	4.3
C_2+	0.2	0.1	0.02

Note: All the data are average of replicate measurements

The GC studies of PW gases (PWG), TG gases (TGG) and WS gases (WSG) from pyrolysis at 600°C identified major amounts of H_2 and CO, and minor amounts of CH_4, CO_2, and C_2+ (ethane, ethylene and C_6+) components (Table 7.8). From the concentrations of H_2, CO, CH_4, ethane, ethylene and C_6+ compounds, the LHV of PWG, TGG and WSG were calculated as 26.3, 24.8 and 9.2 KJ/m^3, respectively. The concentration of H_2 was highest (17.8 wt.%) in the case of PWG, whereas CO was highest (6.5 wt.%) in TGG. The decreasing trend of H_2 levels in gases (PWG, 17.8 wt.% > TGG, 11.8 wt.% > WSG, 3.3 wt.%) could be related to the H levels in the residues which appeared in the similar manner as PWR (6.5 wt.%) > TGR (6.3 wt.%) > WSR (6.0 wt.%).

The H_2 rich nature of PWG suggests its use as a clean gaseous fuel. On the other hand, TGG and WSG could be used for the production of liquid biofuels by

using chemical catalysts through Fischer-Tropsch process or using microbial biocatalysts through syngas fermentation. However, the fermentation of syngas to ethanol by *Clostridium ljungdahlii* has been developed commercially that associates biomass gasification, syngas fermentation and distillation of ethanol from the reactor effluents (Henstra et al., 2007). Through syngas fermentation, the mesophilic microorganisms produce various short-chain fatty acids and alcohols from CO and H_2.

Based on the mass yields and heating values of the hydrolysis residues and their products, the energy recovery balance of the pyrolysis process was performed and mentioned in Table 7.9. The energy efficiency balance is essential in having a life cycle analysis of the biomass and its conversion products (Khoo et al., 2013).

Table 7.9 Energy recovery balance for residues and pyrolysis products

Material	Yield (wt.%)	Heating value (MJ/kg)	Energy recovery (%)	Total energy recovery (%)
PWR	-	18.5	-	99.5
PWB	41.7	31.1	70.1	
PWBL	22.3	23.9	28.8	
PWG	24.9	0.4	0.6	
TGR	-	15.8	-	85.4
TGB	39.6	20.1	50.4	
TGBL	18.6	29.3	34.5	
TGG	28.8	0.3	0.5	
WSR	-	14.2	-	97.0
WSB	38.9	22.2	60.8	
WSBL	19.8	25.9	36.1	
WSG	25.9	0.1	0.1	

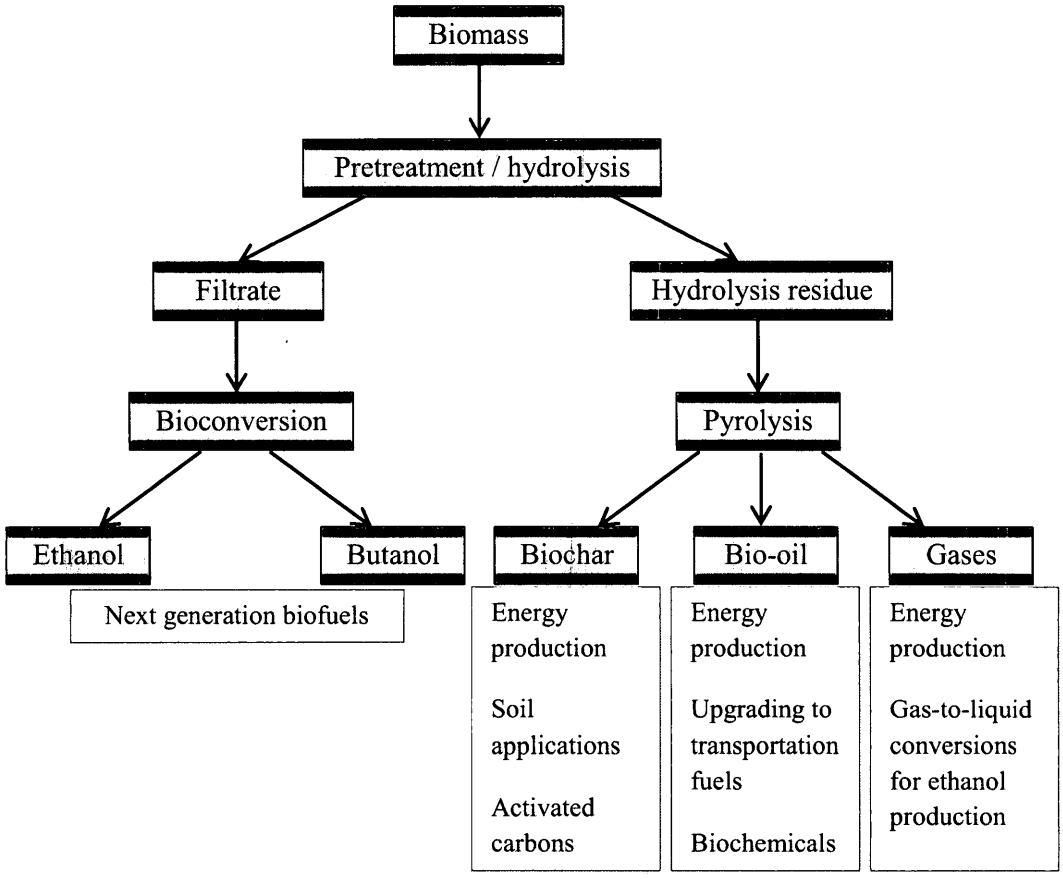

Fig. 7.10 Mechanistic model of hydrolysis waste valorization

The overall process of waste valorization in the current scenario can be illustrated in a mechanistic diagram as shown in Fig. 7.10. The pretreatment and hydrolysis of lignocellulosic feedstocks yields both hydrolysate (filtrate) and hydrolysis residues. Since the hydrolysate contains the fermentable sugars, it is used for bioconversion to fuel alcohols. The hydrolysis residues containing recalcitrant and non-hydrolysable carbohydrates can be pyrolyzed to produce biochars, bio-oils and gases. Along with the potentials to be used for soil amendment in enhancing the soil quality, biochars could also help sequester the carbon below-ground to mitigate the climate change. The industrial use of biochars could be in production of activated carbons for various commercial

applications such as air purification, water filtration, groundwater remediation etc. Bio-oils can be upgraded to transportation fuels and used for bio-chemical production. Pyro-gases could be used as a feed gas for syngas fermentation and Fischer-Tropsch catalysis to produce ethanol. Nevertheless, all the three pyrolysis products are capable in generating heat and power for the same biorefinery in which they are processed. This positively contributes in improving the economics of the refinery.

7.4. Conclusions

Hydrolysis residues from pinewood, timothy grass and wheat straw were pyrolyzed to produce biochars, bio-oils and gases at 600°C. The yield of biochar, bio-oil and gases from the residues ranged between 38.9-41.7, 18.6-22.3 and 24.9-28.8 wt.%, respectively. The high yield of biochar (41.7 wt.%) and bio-oil (22.3 wt.%) from PWR was because of its woody and fibrous nature. SEM analysis indicated the relatively firm and less fragmented structure of PWB compared to the porous and fragile structure of TGB and WSB. The XRD intensities confirmed PWR to contain relatively high crystalline residual cellulose than WSR and TGR. The presence of nitrate, phosphate and chloride peaks in biochars suggested their soil applications. Substantial amount of alkaline metals found in biochars could aid in reducing soil acidity, enhancing soil fertility and crop production.

FT-IR spectroscopy showed the removal of O- and H-containing functionalities in biochars, while Raman spectroscopy showed significant increase in two broad bands for defect (1325-1380 cm^{-1}) and graphite (1580-1610 cm^{-1}) carbon in biochars. The ^{1}H NMR of bio-oils showed the distribution of various H-components as: aliphatics > aromatics > olefinics. Similarly, C-components from ^{13}C NMR of bio-oils were distributed as: aromatics ≥ alkyl carbon > carbonyls > methoxy or hydroxyl carbon > carbohydrates. The gases obtained from pyrolysis of hydrolysis residues could potentially be used in various gas-to-liquid conversions such as Fischer-Tropsch process or syngas fermentation to generate liquid biofuels.

Chapter eight: Concluding remarks and recommendations

8.1. Concluding remarks

Lignocellulosic feedstocks have tremendous potentials to supplement the increasing demand for energy by providing a continuous supply of renewable fuels. This study was based on various aspects of lignocellulosic biomass characterization, pretreatment, conversion and waste valorization. These aspects could be considered as four major envisioning building blocks for any biorefinery. Lignocellulosic biomass represents a diverse group of waste feedstocks from different sources, origin and phenotypical make-up. More specifically, residues obtained from agricultural farms, forests, prairies and grasslands include lignocellulosic group of biomass. In addition, lignocelluloses also constitute the waste refuse that are generated from their industrial processing such as forest mill residues, saw mill refuse, sawdust etc. Considering these diverse sources of lignocelluloses, this dissertation involved pinewood as the forest residue, timothy grass as the energy crop (or perennial grass) and wheat straw as agricultural refuse.

As the composition of any biomass is critical in determining the type of conversion (e.g., biochemical or thermochemical) and any possible processing complexities, it is important to study their physico-chemical and biochemical characteristics. Despite the heterogenous sources of pinewood, timothy grass and wheat straw, in most cases timothy grass and wheat straw showed similar behaviour due to their herbaceous and fast-growing nature in contrast to pinewood's woody and slow-growing nature. The thermogravimetric analysis showed pinewood to be thermally stable due to its devolatilization at 380°C instead of 350°C as in the case of timothy grass and wheat straw. Timothy grass and wheat straw produced higher amount of ash (3.6 and 4.4 wt.%) compared to pinewood (2.3 wt.%), indicating higher amount of inorganic mineral ingredients. This led to the highly crystalline nature of ashes that demonstrated the mineral components to be carbonates, silicates, sulphates and chlorides. The X-ray diffractometry of feedstocks revealed Cellulose I, Cellulose II and hemicellulose at 15.5°, 21.7° and 34.5° 2-theta, respectively. All

these biomasses were found to contain 34.2-39.1 wt.% cellulose, 23.6-30.1 wt.% hemicellulose, 16.3-20.4 wt.% lignin and 15.7-19.2 wt.% total extractives. The high lignin content (20.4 wt.%) in pinewood was due to its woody and fibrous nature. FT-IR and Raman spectrometry revealed the presence of waxes, fatty acids, aldehydes, alcohols, ethers, carboxylic acids and esters with derivatives of cellulose, hemicellulose and lignin in biomasses. The physico-chemical resemblance of timothy grass with wheat straw suggested that perennial grasses could supplement the anticipated demand of agricultural residues in future as next generation biofuel feedstocks.

Pinewood, timothy grass and wheat straw were pyrolyzed at 450°C in two different scenarios, which are high heating rate or HHR (450°C/min) pyrolysis and slow heating rate or SHR (2°C/min) pyrolysis, to determine their bio-oil, biochar and gas yields. From the three feedstocks, SHR pyrolysis resulted in higher amount of biochar (41-44 wt.%), while HHR pyrolysis resulted in higher bio-oil (40-48 wt.%) productions. In contrast to HHR biochars, the biochars produced from SHR pyrolysis demonstrated higher ranges of heating value (20.3-29.2 MJ/kg) and elemental content (e.g., calcite, sulphite, phosphate and silicate). The richness of SHR biochars with alkaline metals (Na, Mg, K and Ca) along with greater levels of carbon, hydrogen and phosphorous indicated their soil applications. The application of SHR biochars to soils could not only reduce soil acidity but also improve its fertility and enhance crop production and soil microbial population. Furthermore, the long-term stability of SHR biochars in soil could also be justified by their relatively higher thermal degradation temperatures due to their stronger C–C and C–H bonds. On the other hand, bio-oils produced from HHR pyrolysis not only showed higher yields but also presented better fuel properties such as higher heating value (30.5-32 MJ/kg) and greater levels of carbon and hydrogen with lower levels of oxygen. These properties of HHR bio-oils suggested a better upgrading to synthetic fuels than SHR bio-oils.

Lignin is considered a barrier for the bioconversion of biomass to alcohols as it restricts the access of acids and enzymes to the polysaccharides for hydrolysis. Moreover, lignin is insoluble in acids and solvents except for some alkali, although their dispersion in biomass during acid or alkaline treatments is least understood. In this study, pinewood, timothy grass and wheat straw were hydrothermally treated and delignified using acidified sodium chlorite to study evolution of lignin and plant waxes during treatments. The delignified biomasses showed a significant decrease in lignin (0.7-1.2 wt.%) than the untreated feedstocks (20.1-24.2 wt.%). Moreover, the cellulose levels in delignified biomasses (77.4-82 wt.%) increased from the untreated feedstocks (46-51.9 wt.%) because of the gradual removal of lignin and hemicelluloses. With increase in cellulose content, the biomass crystallinity increased in delignified samples (~98.1%) and hydrothermally treated samples (~93.1%). As lignin contributes to the higher heating value of the biomass, the thermogravimetric analysis of delignified feedstocks demonstrated a decrease in their devolatilization temperature (240-250°C) due to lignin removal and modified cell wall structure. The hydrothermal pretreatment at 121°C caused the steam under pressure to penetrate plant cell wall, delocalizing lignin and re-depositing it on the biomass surface as spherical droplets. The absence of lignin peaks in FT-IR (1510 cm^{-1}) and Raman (1261, 1270 and 1510-1656 cm^{-1}) spectra in delignified samples confirmed their removal. The occurrence and distribution of lignin and plant waxes in the biomasses were studied through chemical maps generated using Raman mapping technique. The formation of vacuoles in the lignin matrix in hydrothermally treated feedstocks explained the modification of lignin arrangement due to penetration of steam under pressure into the plant cellular structure.

It is very important to pretreat the biomass prior to bioconversion to release the fermentable sugars as hydrolysates for ethanol and butanol productions. A dilute (0-2.5%) sulfuric acid pretreatment followed by enzymatic hydrolysis (cellulase, β-glucosidase and xylanase) of the three feedstocks was employed for the production of sugar monomers. A 2% H_2SO_4 treatment with enzymatic hydrolysis was efficient

in yielding highest levels of glucose (32.9 g/L) and xylose (35.6 g/L) from pinewood. In contrast, 1.5% H_2SO_4 pretreatment with enzymatic hydrolysis resulted in high yields of glucose (26.7 and 26 g/L) and xylose (30.7 and 37.6 g/L) from timothy grass and wheat straw, respectively. Pinewood demonstrated high ethanol yields (24.1 g/L), using *S. cerevisiae* ATCC 96581, followed by wheat straw (23.2 g/L) and timothy grass (22.6 g/L). Similarly, butanol production by *C. beijerinckii* B-592 was high in the case of pinewood (11.6 g/L) followed by wheat straw (11.2 g/L) and timothy grass (10.8 g/L). The culture toxicity caused by butanol resulted in lower final butanol yields compared to those of ethanol.

With the final objective of waste valorization, considerable amount of hydrolysis residues as obtained through biomass pretreatment and fermentation were pyrolysed at 600°C (heating rate: 5°C/min) to produce valuable bio-oils, biochars and gases. The pyrolysis of hydrolysis residues from pinewood, timothy grass and wheat straw resulted in 38.9-41.7 wt.% biochars, 18.6-22.3 wt.% bio-oils and 24.9-28.8 wt.% gases. Pinewood residue resulted in high yields of biochar (41.7 wt.%) and bio-oils (22.3 wt.%) because of its woody nature. Pinewood biochar indicated relatively rigid and less fragmented structure compared to the porous and fragile structure of timothy grass biochar and wheat straw biochar. Substantial amount of alkaline metals (Na, Mg, K and Ca) were found in the biochars suggesting their soil amendment applications for reducing soil acidity, enhancing soil fertility and crop production. The H-components in bio-oils occurred as: aliphatics > aromatics > olefinics, whereas C-components varied as: aromatics ≥ alkyl carbon > carbonyls > methoxy or hydroxyl carbon > carbohydrates. The high heating value (26.3 KJ/m^3) and H_2 rich (17.8 wt.%) nature of pinewood pyrolysis gas indicated its use for combined heat and power or in potential gas-to-liquid conversions to higher alcohols through Fischer-Tropsch process or syngas fermentation.

8.2. Recommendations

This study has shown the successful use of pinewood, timothy grass and wheat straw for fuel alcohols, bio-oils, biochars and gas productions through an array of biochemical and thermochemical pathways. As biomasses are biogenic wastes influenced by environmental factors, several developments and limitations were encountered during their investigations. These could be addressed by the following recommendations.

(i) Prior to pyrolysis, the feedstocks should be preferably oven-dried at 105°C for 2 h to remove moisture. This is recommended due to the fact that in a few experiments, moisture was found to adversely affect the pyrolysis process by creating restrictions in the heat transfer and compromising with the final product yields.

(ii) The inorganic components, especially Mg, K and Ca in the biomass ash are to be critically considered during pyrolysis due to their influence in ash melting and formation of slag. Higher levels of Mg and Ca in the ash have a tendency to increase its melting point, whereas K can decrease it. Hence, ash with higher levels of Mg and Ca should be separated from biochar through techniques such as electrostatic separation to prevent slag formation.

(iii) The biomass samples, after collection and prior to pulverizing, should be cleaned by dusting or brushing to remove any sediments and earthy components from their surface. The biomass with soiled surface may add mineral matters that are not indigenous to the biomass species. This may adversely affect the biomass characterization and pyrolysis reactions.

(iv) High lignin containing biomasses such as woody feedstocks are suitable for thermochemical conversions due to their requirement of additional delignification procedures and higher acid levels during hydrolysis. In addition, the higher heating value of lignin is also contributed towards the

biochars and bio-oils produced from its pyrolysis. It could be suggested that pyrolysis is the optimal conversion method for ligneous biomass.

(v) The lignin and extractives (plant waxes) content in biomass result in biomass fluorescence during Raman spectroscopy. This phenomenon of sample fluorescence was found to mask the Raman intensities from the spot of analysis. However, to overcome this issue, photo-bleaching of the sample spot was performed at a lower laser power but same wavelength for Raman spectral analysis.

(vi) During delignification, the treatment of biomass with acidified sodium chlorite results in an efficient dissolution of lignin in the aqueous solution. The solution could be harvested for the purification of lignin either for pyrolysis and/or other bio-chemical production.

(vii) As acetone-ethanol-butanol production is overruled by culture toxicity from butanol, a relatively low final butanol level is found after clostridial fermentation. Two substantial engineering approaches should be considered to overcome this problem. First, process engineering strategies should be employed to successfully separate butanol from the medium and allow the *Clostridium* to continue growth and butanol production. Second, genetic engineering of the *Clostridium* spp. to tolerate high butanol levels could also improve butanol yields.

(viii) Although biochars produced from slow pyrolysis exhibited beneficial properties for soil applications, several field experiments are recommended for studying their practical functions in soil. The biochar properties such as alkalinity, porosity, thermal stability as well as high carbon and hydrogen content could explain the water holding capacity, cation exchange capacity, soil microbial proliferation, plant-microbial interaction and improved plant growth in biochar amended soils. The carbon sequestration and bioremediation properties of biochars could also be investigated through soil application studies.

Chapter nine: Original contributions to knowledge

(i) Although lignocellulosic biomasses are attractive feedstocks for production of next generation biofuels, yet there is insufficient information about their physico-chemical and biochemical characterization. In order to accommodate a wide range of lignocelluloses, three different biomasses were selected in the study i.e., woody biomass (pinewood), energy crop (timothy grass) and agricultural residue (wheat straw). A series of data on their chemical properties (proximate and ultimate), composition (cellulose-hemicellulose-linin), structural chemistry (X-ray diffraction, FT-IR and Raman spectroscopy) and thermal behavior (thermogravimetric analysis) were obtained for the first time.

(ii) The comparative investigation on slow and fast pyrolysis of lignocellulosic biomass is rare in literature. As a practical contribution, the present study demonstrated the production of bio-oils, biochars and gases from woody (pinewood) and herbaceous feedstocks (timothy grass and wheat straw) through slow and fast pyrolysis. The findings of this study gives the user an option to select between the type of pyrolysis and feedstock considering the major product of interest i.e., bio-oil or biochar.

(iii) The arrangement and distribution of lignin in the plant's cell wall is least understood. In order to provide comprehensive information about biomass-lignin organisation, chemical maps of untreated, hydrothermally treated and delignified biomasses were generated. This novel approach helped to achieve a new understanding of the arrangement of lignin and plant waxes and their changes during the biomass pretreatments.

(iv) A series of data were obtained for the first time on the chemical and enzymatic pretreatment of pinewood, timothy grass and wheat straw along with the butanol and ethanol yields. The pretreatment method was optimized in terms of the acid dose for maximum sugar yields.

(v) Valorization and effective management of hydrolysis residues from biomass pretreatment was carried out through pyrolysis. This led to the production of

biochars with favorable agronomic properties, bio-oils with fuel and chemical-production characteristics and gases with potentials for production of heat and power and/or higher alcohols through gas-to-liquid technologies. A mechanistic model of biomass conversion and waste utilization was developed to manage and valorize the biogenic waste. This study showed the possibility of making the biofuel production process as carbon neutral by sequestering the extra carbon in the soil through biochars.

Bibliography

1. Agarwal U.P. (2006) Raman imaging to investigate ultrastructure and composition of plant cell walls: distribution of lignin and cellulose in black spruce wood (*Picea mariana*). *Planta* 224:1141–1153.
2. Agarwal U.P., Ralph S.A. (1997) FT-Raman spectroscopy of wood: identifying contributions of lignin and carbohydrate polymers in the spectrum of black spruce. *Applied Spectroscopy* 51:1648–1655.
3. Akin D.E. (2007) Grass lignocellulose: strategies to overcome recalcitrance. *Applied Biochemistry and Biotechnology* 137–140:3–15.
4. Anon J.A.R., Lopez F.F., Castineiras J.P., Ledo J.P., Regueira L.N. (1995) Calorific values and flammability for forest wastes during the seasons of the year. *Bioresource Technology* 52:269–274.
5. Antonopoulou G., Lyberatos G. (2012) Effect of pretreatment of sweet sorghum biomass on methane generation. *Waste Biomass Valorization.* DOI: 10.1007/s12649-012-9183-x
6. ASTM D1762-84 (2007) Standard test method for chemical analysis of wood charcoal. *ASTM International*, Pennsylvania.
7. ASTM D3175-11 (2011) Standard method for volatile matter in the analysis sample of coal and coke. *ASTM International*, Pennsylvania.
8. ASTM D3176-09 (2009) Standard practice for ultimate analysis of coal and coke. *ASTM International*, Pennsylvania.
9. ASTM D5373-08 (2008) Standard test methods for instrumental determination of carbon, hydrogen, and nitrogen in laboratory samples of coal. *ASTM International*, Pennsylvania.
10. ASTM E1755-01 (2007) Standard test method for ash in biomass. *ASTM International*, Pennsylvania.
11. ASTM E871-82 (2006) Standard test method for moisture analysis of particulate wood fuels. *ASTM International*, Pennsylvania.

12. Azargohar R., Dalai A.K. (2008) Steam and KOH activation of bio-char: experimental and modeling studies. *Microporous and Mesoporous Materials* 110:413–421.
13. Azargohar R., Nanda S., Rao B.V.S.K., Dalai A.K. (2013) Slow pyrolysis of deoiled Canola meal: product yields and characterization. *Energy and Fuels* 27: 5268–5279.
14. Azzam A.M. (1989) Pretreatment of cane bagasse with alkaline hydrogen peroxide for enzymatic hydrolysis of cellulose and ethanol fermentation. *Journal of Environmental Science and Health, Part B* 24:421–433.
15. Balat M. (2011) Production of bioethanol from lignocellulosic materials via the biochemical pathway: a review. *Energy Conversion and Management* 52:858–875.
16. Ballesteros M., Oliva J.M., Negro M.J., Manzanares P., Ballesteros I. (2004) Ethanol from lignocellulosic materials by a simultaneous saccharification and fermentation process (SFS) with *Kluyveromyces marxianus* CECT 10875. *Process Biochemistry* 39:1843–1848.
17. Biely P., Kremnicky L. (1998) Yeasts and their enzyme systems degrading cellulose, hemicelluloses and pectin. *Food Technology and Biotechnology* 36:305–312.
18. Bisaria V.S. (1991) Bioprocessing of agro-residue to glucose and chemicals. In: Martin A.M. (ed.) Bioconversion of waste materials to industrial products. Elsevier, London, pp. 187–223.
19. Biswas A.K., Umeki K., Yang W., Blasiak W. (2011) Change of pyrolysis characteristics and structure of woody biomass due to steam explosion pretreatment. *Fuel Processing Technology* 92:1849–1854.
20. Boominathan K., Reddy C.A. (1992) cAMP-mediated differential regulation of lignin peroxidase and manganese-dependent peroxidase production in the white-rot basidiomycete *Phanerochaete chrysosporium*. *Proceedings of the National Academy of Sciences* 89:5586–5590.

21. Boucher M.E., Chaala A., Roy C. (2000) Bio-oils obtained by vacuum pyrolysis of softwood bark as a liquid fuel for gas turbines. Part I: properties of bio-oil and its blends with methanol and a pyrolytic aqueous phase. *Biomass and Bioenergy* 19:337–350.
22. Bowles L.K., Ellefson W.L. (1985) Effects of butanol on *Clostridium acetobutylicum*. *Applied and Environmental Microbiology* 50:1165–1170.
23. Bridgwater A.V., Peacocke G.V.C. (2000) Fast pyrolysis processes for biomass. *Renewable and Sustainable Energy Reviews* 4:1–73.
24. Briens C., Piskorz J., Berruti F. (2008) Biomass valorization for fuel and chemicals production – a review. *International Journal of Chemical Reactor Engineering* 6:1–49.
25. Brown T.R., Wright M.M., Brown R.C. (2011) Estimating profitability of two biochar production scenarios: slow pyrolysis vs fast pyrolysis. *Biofuels, Bioproducts and Biorefining* 5:54–68.
26. Carrier M., Loppinet-Serani A., Denux D., Lasnier J.M., Ham-Pichavant F., Cansell F., Aymonier C. (2011) Thermogravimetric analysis as a new method to determine the lignocellulosic composition of biomass. *Biomass and Bioenergy* 35:298–307.
27. Chen B., Zhou D., Zhu L. (2008) Transitional adsorption and partition of nonpolar and polar aromatic contaminants by biochars of pine needles with different pyrolytic temperatures. *Environmental Science and Technology* 42:5137–5143.
28. Correa A.C., Teixeira E.D.M., Pessan L.A., Mattoso L.H.C. (2010) Cellulose nanofibers from curaua fibers. *Cellulose* 17:1183–1192.
29. Dabelstein W., Reglitzky A., Schutze A., Reders K. (2007) Automotive fuels. *Ullmann's Encyclopedia of Industrial Chemistry* 4:425–458.
30. Das K.C., Garcia-perez M., Bibens B., Melear N. (2008) Slow pyrolysis of poultry litter and pine woody biomass: impact of chars and bio-oils on microbial growth. *Journal of Environmental Science and Health, Part A* 43:714–724.

31. De La Torre Ugarte D.G., English B.C., Jensen K. (2007) Sixty billion gallons by 2030: economic and agricultural impacts of ethanol and biodiesel expansion. *American Journal of Agricultural Economics* 89:1290–1295.
32. Demain A.L. (2009) Biosolutions to the energy problem. *Journal of Industrial Microbiology and Biotechnology* 36:319–332.
33. Demirbas M.F. (2006) Current technologies for biomass conversion into chemicals and fuels. *Energy Source, Part A* 28:1181–1188.
34. Dien B.S., Cotta M.A., Jeffries T.W. (2003) Bacteria engineered for fuel ethanol production: current status. *Applied Microbiology and Biotechnology* 63:258–266.
35. Dry M.E. (2004) Present and future applications of the Fischer–Tropsch process. *Applied Catalysis A* 276:1–3.
36. Duff S.J.B., Murray W.D. (1996) Bioconversion of forest products industry waste cellulosics to fuel ethanol: a review. *Bioresource Technology* 55:1–33.
37. Duman G., Okutucu C., Ucar S., Stahl R., Yanik J. (2011) The slow and fast pyrolysis of cherry seed. *Bioresource Technology* 102:1869–1878.
38. Durre P. (2007) Biobutanol: an attractive biofuel. *Biotechnology Journal* 2:1525–1534.
39. Durre P. (2008) Fermentative butanol production bulk chemical and biofuel. *Annals of the New York Academy of Sciences* 1125:353–362.
40. Ehara K., Saka S. (2005) Decomposition behavior of cellulose in supercritical water, subcritical water, and their combined treatments. *Journal of Wood Science* 51:148–153.
41. Ezeji T.C., Qureshi N., Blaschek H.P. (2004) Acetone butanol ethanol (ABE) production from concentrated substrate: reduction in substrate inhibition by fed-batch technique and product inhibition by gas stripping. *Applied Microbiology and Biotechnology* 63:653–658.

42. Fisher T., Hajaligol M., Waymack B., Kellogg D. (2002) Pyrolysis behaviour and kinetics of biomass derived materials. *Journal of Analytical and Applied Pyrolysis* 62:331–349.
43. Fu P., Hua S., Xiang J., Sun L., Su S., Wang J. (2012) Evaluation of the porous structure development of chars from pyrolysis of rice straw: Effects of pyrolysis temperature and heating rate. *Journal of Analytical and Applied Pyrolysis* 98:177–183.
44. Fukuda H., Kondo A., Tamalampudi S. (2009) Bioenergy: sustainable fuels from biomass by yeast and fungal whole-cell biocatalysts. *Biochemical Engineering Journal* 44:2–12.
45. Garcia V., Pakkila J., Ojamo H., Muurinen E., Keiski R.L. (2011) Challenges in biobutanol production: how to improve the efficiency? *Renewable and Sustainable Energy Reviews* 15:964–980.
46. Garrote G., Dominguez H., Parajo J.C. (1999) Hydrothermal processing of lignocellulosic materials. *European Journal of Wood and Wood Products* 57:191–202.
47. Georgieva T.I., Skiadas I.V., Ahring B.K. (2007) Effect of temperature on ethanol tolerance of a thermophilic anaerobic ethanol producer *Thermoanaerobacter* A10: modeling and simulation. *Biotechnology and Bioengineering* 98:1161–1170.
48. Ghose T.K., Tyagi R.D. (1979) Rapid ethanol fermentation of cellulose hydrolysate. II. Product and substrate inhibition and optimization of fermentor design. *Biotechnology and Bioengineering* 21:1401–1420.
49. Girio F.M., Fonseca C., Carvalheiro F., Duarte L.C., Marques S., Bogel-Lukasik R. (2010) Hemicelluloses for fuel ethanol: a review. *Bioresource Technology* 101:4775–4800.
50. Gottwald M., Gottschalk G. (1985) The internal pH of *Clostridium acetobutylicum* and its effect on the shift from acid to solvent formation. *Archives of Microbiology* 143:42–46.

51. Govumoni S.P., Koti S., Kothagouni S.Y., Venkateshwar S., Linga V.R. (2013) Evaluation of pretreatment methods for enzymatic saccharification of wheat straw for bioethanol production. *Carbohydrate Polymer* 91:646–650.
52. Gray K.A., Zhao L., Emptage M. (2006) Bioethanol. *Current Opinion in Chemical Biology* 10:141–146.
53. Green Biologics (2013) http://www.greenbiologics.com/biobutanol-fuel.php. Accessed on July 20, 2013.
54. Gronowska M., Joshi S., MacLean H.L. (2009) A review of U.S. and Canadian biomass supply studies. *Bioresources* 4, 341–369.
55. Hallac B.B., Ragauskas A.J. (2011) Analyzing cellulose degree of polymerization and its relevancy to cellulosic ethanol. *Biofuels, Bioproducts and Biorefining* 5:215–225.
56. Heiskanen H., Virkajarvi I., Viikari L. (2007) The effects of syngas composition on the growth and product formation of *Butyribacterium methylotrophicum*. *Enzyme and Microbial Technology* 41:362–367.
57. Henstra A.M., Sipma J., Rinzema A., Stams A.J.M. (2007) Microbiology of synthesis gas fermentation for biofuel production. *Current Opinion in Biotechnology* 18:200–206.
58. Himmel M.E., Ding S.Y., Johnson D.K., Adney W.S., Nimlos M.R., Brady J.Y., Foust T.D. (2007) Biomass recalcitrance: engineering plants and enzymes for biofuels production. *Science* 315:804–807.
59. Himmelsbach D.S., Khalili S., Akin D.E. (2002) The use of FT-IR microspectroscopic mapping to study the effects of enzymatic retting of flax (*Linum usitatissimum* L) stems. *Journal of the Science of Food and Agriculture* 82:685–696.
60. Houghton T.P., Thompson D.N., Hess J.R., Lacey J.A., Wolcot M.P., Schirp A., Englund K., Dostal D., Loge F. (2004) Fungal upgrading of wheat straw for straw-thermoplastics production. *Applied Biochemistry and Biotechnology* 113:71–93.

61. Huang L., Gibbins L.N., Forsberg C.W. (1985) Transmembrane pH gradient and membrane potential in *Clostridium acetobutylicum* during growth under acetogenic and solventogenic conditions. *Applied and Environmental Microbiology* 50:1043–1047.
62. Huang Y., Wei Z., Yin X., Wu C. (2012) Pyrolytic characteristics of biomass acid hydrolysis residue rich in lignin. *Bioresource Technology* 103:470–476.
63. Hu F., Ragauskas A. (2012) Pretreatment and lignocellulosic chemistry. *Bioenergy Research* 5:1043–1066.
64. Huber G.W., Iborra S., Corma A. (2006) Synthesis of transportation fuels from biomass: chemistry, catalysts, and engineering. *Chemical Reviews* 106:4044–4098.
65. IEO, International Energy Outlook (2011) U.S. Energy Information Administration, Washington, DC. www.eia.gov/ieo/pdf/0484(2011).pdf. Accessed on 01 March 2011.
66. Jeguirim M., Trouve G. (2009) Pyrolysis characteristics and kinetics of *Arundo donax* using thermogravimetric analysis. *Bioresource Technology* 100:4026–4031.
67. Jensen P.A., Frandsen F.J., Dam-Johansen K., Sander B. (2000) Experimental investigation of the transformation and release to gas phase of potassium and chlorine during straw pyrolysis. *Energy and Fuels* 14:1280–1285.
68. Jones A., O'Hare M., Farrell A. (2007) Biofuel boundries: estimating the medium-term supply potential of domestic biofuels. Research report UCB-ITS-TSRC-RR-2007-4. University of California, Berkeley.
69. Jones D.T., Woods D.R. (1986) Acetone-butanol fermentation revisited. *Microbiological Reviews* 50:484–524.
70. Joshi J., Lawal A. (2012) Hydrodeoxygenation of pyrolysis oil in a microreactor. *Chemical Engineering Science* 74:1–8.

71. Keown D.M., Li X., Hayashi J.I., Li C.Z. (2008) Evolution of biomass char structure during oxidation in O_2 as revealed with FT-Raman spectroscopy. *Fuel Processing Technology* 89:1429–1435.
72. Kern S., Halwachs M., Kampichler G., Pfeifer C., Proll T., Hofbauer H. (2012) Rotary kiln pyrolysis of straw and fermentation residues in a 3 MW pilot plant – influence of pyrolysis temperature on pyrolysis product performance. *Journal of Analytical and Applied Pyrolysis* 97:1–10.
73. Khoo HH, Koh CY, Shaik MS, Sharratt PN. (2013) Bioenergy co-products derived from microalgae biomass via thermochemical conversion – Life cycle energy balances and CO_2 emissions. *Bioresource Technology* 143:298–307.
74. Kim P., Johnson A., Edmunds C.W., Radosevich M., Vogt F., Rials T.G., Labbe N. (2011) Surface functionality and carbon structures in lignocellulosic-derived biochars produced by fast pyrolysis. *Energy and Fuels* 25:4693–4703.
75. Kim S., Dale B.E. (2004) Global potential bioethanol production from wasted crops and crop residues. *Biomass and Bioenergy* 26:361–375.
76. Kim T.H., Kim J.S., Sunwoo C., Lee Y.Y. (2003) Pretreatment of corn stover by aqueous ammonia. *Bioresource Technology* 90:39–47.
77. Kristensen J.B., Thygesen L.G., Felby C., Jorgensen H., Elder T. (2008) Cell-wall structural changes in wheat straw pretreated for bioethanol production. *Biotechnology for Biofuels* 1:5.
78. Kumar P., Barrett D.M., Delwiche M.J., Stroeve P. (2009) Methods for pretreatment of lignocellulosic biomass for efficient hydrolysis and biofuel production. *Industrial and Engineering Chemistry Research* 48:3713–3729.
79. Lee S.Y., Park J.H., Jang S.H., Nielsen L.K., Kim J., Jung K.S. (2008) Fermentative butanol production by Clostridia. *Biotechnology and Bioengineering* 101, 209–228.
80. Lehmann J., da Silva Jr. J.P., Steiner C., Nehls T., Zech W., Glaser B. (2003) Nutrient availability and leaching in an archaeological Anthrosol and a Ferralsol

of the Central Amazon basin: fertilizer, manure and charcoal amendments. *Plant and Soil* 249:343–357.

81. Lehmann J., Rillig M.C., Thies J., Masiello C.A., Hockaday W.C., Crowley D. (2011) Biochar effects on soil biota – a review. *Soil Biology and Biochemistry* 43:1812–1836.
82. Lenihan P., Orozco A., O'Neill E., Ahmad M.N.M., Rooney D.W., Walker G.M. (2010) Dilute acid hydrolysis of lignocellulosic biomass. *Chemical Engineering Journal* 156:395–403.
83. Li C., Knierim B., Manisseri C., Arora R., Scheller H.V., Auer M., Vogel K.P., Simmons B.A., Singh S. (2010) Comparison of dilute acid and ionic liquid pretreatment of switchgrass: biomass recalcitrance, delignification and enzymatic saccharification. *Bioresource Technology* 101:4900–4906.
84. Li X.J., Hayashi J., Li C.Z. (2006) FT-Raman spectroscopic study of the evolution of char structure during the pyrolysis of a Victorian brown coal. *Fuel* 85:1700–1707.
85. Liang B., Lehmann J., Solomon D., Kinyangi J., Grossman J., O'Neill B., Skjemstad J.O., Thies J., Luizao F.J., Petersen J., Neves E.G. (2006) Black carbon increases cation exchange capacity in soils. *Soil Science Society of America Journal* 70:1719–1730.
86. Lin L., Yan R., Liu Y., Jiang W. (2010) In-depth investigation of enzymatic hydrolysis of biomass wastes based on three major components: cellulose, hemicellulose and lignin. *Bioresource Technology* 101:8217–8223.
87. Lin Y.L., Blaschek H.P. (1983) Butanol production by a butanol-tolerant strain of *Clostridium acetobutylicum* in extruded corn broth. *Applied and Environmental Microbiology* 45:966–973.
88. Liu S., Qureshi N. (2009) How microbes tolerate ethanol and butanol. *New Biotechnology* 26:117–121.

89. Lopez-Buendia A.M., Whateley M.K.G., Bastida J., Urquiola M.M. (2007) Origins of mineral matter in peat marsh and peat bog deposits, Spain. *International Journal of Coal Geology* 71:246–262.
90. Lv P.M., Xiong Z.H., Chang J., Wu C.Z., Chen Y., Zhu Z.X. (2004) An experimental study on biomass air–steam gasification in a fluidized bed. *Bioresource Technology* 95:95–101.
91. Mabee W.E., Saddler J.N. (2010) Bioethanol from lignocellulosics: status and perspectives in Canada. *Bioresource Technology* 101:4806–4813.
92. Malherbe S., Cloete T.E. (2002) Lignocellulose biodegradation: fundamentals and applications. *Reviews in Environmental Science and Biotechnology* 1:105–114.
93. Mattson Jr. W.J. (1980) Herbivory in relation to plant nitrogen content. *Annual Review of Ecology, Evolution, and Systematics* 11:119–161.
94. Mayak S., Tirosh T., Glick B.R. (2004) Plant growth-promoting bacteria confer resistance in tomato plants to salt stress. *Plant Physiology and Biochemistry* 42:565–572.
95. McKendry P. (2002) Energy production from biomass (part 1): overview of biomass. *Bioresource Technology* 83:37–46.
96. McMillan J.D. (1994) Pretreatment of lignocelluloses biomass. In: Himmel M.E., Baker J.O., Overend R.P. (eds.) Conversion of hemicellulose hydrolyzates to ethanol. American Chemical Society Symposium, Washington, pp. 292–324.
97. Mohanty P., Nanda S., Pant K.K., Naik S., Kozinski J.A., Dalai A.K. (2013) Evaluation of the physiochemical development of biochars obtained from pyrolysis of wheat straw, timothy grass and pinewood: effects of heating rate. *Journal of Analytical and Applied Pyrolysis* 104:485–493.
98. Mohammadi M., Najafpour G.D., Younesi H., Lahijani P., Uzir M.H., Mohamed A.R. (2011) Bioconversion of synthesis gas to second generation biofuels: a review. *Renewable and Sustainable Energy Reviews* 15:4255–4273.

99. Moore A.K., Owen N.L. (2002) Infrared spectroscopic studies of solid wood. *Applied Spectroscopy Reviews* 36:65–86.

100. Mosier N.S., Wyman C., Dale B., Elander R., Lee Y.Y., Holtzapple M., Ladisch R. (2005) Features of promising technologies for pretreatment of lignocellulosic biomass. *Bioresource Technology* 96:673–686.

101. Moreira A.R., Ulmer D.C., Linden J.C. (1981) Butanol toxicity in the butylic fermentation. *Biotechnology and Bioengineering Symposium* 11:567–579.

102. Naik S., Goud V.V., Rout P.K., Jacobson K., Dalai A.K. (2010) Characterization of Canadian biomass for alternative renewable biofuel. *Renewable Energy* 35:1624–1631.

103. Nanda S., Azargohar R., Kozinski J.A., Dalai A.K. (2013a) Characteristic studies on the pyrolysis products from hydrolyzed Canadian lignocellulosic feedstocks. *Bioenergy Research*. DOI: 10.1007/s12155-013-9359-7

104. Nanda S., Dalai A.K., Kozinski J.A. (2012) Characterization of Canadian lignocellulosic biomass for next generation biofuels- Butanol. 20th European Biomass Conference and Exhibition Proceedings, Milan, 1216–1221.

105. Nanda S., Kozinski J.A., Dalai A.K. (2013b) Biomass – An overview on classification, composition and characterization. In: Zhang B., Wang Y. (eds.) Biomass Processing, Conversion and Biorefinery. Nova Science Publishers Inc., USA, pp. 3–36.

106. Nanda S., Mohanty P., Pant K.K., Naik S., Kozinski J.A., Dalai A.K. (2013c) Characterization of North American lignocellulosic biomass and biochars in terms of their candidacy for alternate renewable fuels. *Bioenergy Research* 6:663–677.

107. Novaes E., Kirst M., Chiang V., Winter-Sederoff H., Sederoff R. (2010) Lignin and biomass: a negative correlation for wood formation and lignin content in trees. *Plant Physiology* 154:555–561.

108. Obernberger I., Brunner T., Barnthaler G. (2006) Chemical properties of solid biofuels–significance and impact. *Biomass and Bioenergy* 30:973–982.

109. Oh S.Y., Yoo D.I., Shin Y., Kim H.C., Kim H.Y., Chung Y.S., Park W.H., Youk J.H. (2005) Crystalline structure analysis of cellulose treated with sodium hydroxide and carbon dioxide by means of X-ray diffraction and FTIR spectroscopy. *Carbohydrate Research* 340:2376–2391.

110. Oosterveer P., Mol A.P.J. (2010) Biofuels, trade and sustainability: A review of perspectives for developing countries. *Biofuels, Bioproducts and Biorefining* 4:66–76.

111. Ozcimen D., Ersoy-Mericboyu A. (2010) Characterization of biochar and bio-oil samples obtained from carbonization of various biomass materials. *Renewable Energy* 35:1319–1324.

112. Pan X.J., Gilkes N., Kadla J., Pye K., Saka S., Gregg D., Ehara K., Xie D., Lam D., Saddler J. (2006) Bioconversion of hybrid poplar to ethanol and co-products using an organosolv fractionation process: optimization of process yields. *Biotechnology and Bioengineering* 94:851–861.

113. Pauly M., Keegstra K. (2008) Cell-wall carbohydrates and their modification as a resource for biofuels. *Plant Journal* 54:559–568.

114. Perez J., Munoz-Dorado J., de la Rubia T., Martinez J. (2002) Biodegradation and biological treatments of cellulose, hemicellulose and lignin: an overview. *International Microbiology* 5:53–63.

115. Pittman Jr. C.U., Mohan D., Eseyin A., Li Q., Ingram L., Hassan E.B.M., Mitchell B., Guo H., Steele P.H. (2012) Characterization of bio-oils produced from fast pyrolysis of corn stalks in an auger reactor. *Energy and Fuels* 26:3816–3825.

116. Prasad S., Singh A., Joshi H.C. (2007) Ethanol as an alternative fuel from agricultural, industrial and urban residues. *Resources, Conservation and Recycling* 50:1–39.

117. Putun E. (2010) Catalytic pyrolysis of biomass: Effects of pyrolysis temperature, sweeping gas flow rate and MgO catalyst, *Energy* 35:2761–2766.

118. Rhoades J.D., Chanduvi F., Lesch S. (1999) Soil salinity assessment: methods and interpretation of electrical conductivity measurements. FAO Irrigation and Drainage Paper 57, Rome, Italy.

119. Qureshi N., Blaschek H.P. (2001) ABE production from corn: a recent economic evaluation. *Journal of Industrial Microbiology and Biotechnology* 27:292–297.

120. Qureshi N., Ezeji T.C. (2008) Butanol, 'a superior biofuel' production from agricultural residues (renewable biomass): recent progress in technology. *Biofuels, Bioproducts and Biorefining* 2:319–330.

121. Qureshi N., Saha B.C., Cotta M.A. (2007) Butanol production from wheat straw hydrolysate using *Clostridium beijerinckii*. *Bioprocess and Biosystems Engineering* 30:419–427.

122. Qureshi N., Saha B.C., Dien B., Hector R.E., Cotta M.A. (2010) Production of butanol (a biofuel) from agricultural residues: Part I – use of barley straw hydrolysate. *Biomass and Bioenergy* 34:559–565.

123. Raveendran K., Ganesh A., Khilar K.C. (1995) Influence of mineral matter on biomass pyrolysis characteristics. *Fuel* 74:1812–1822.

124. Saarela K.E., Harjua L., Rajander J., Lill J.O., Heselius S.J., Lindroos A., Mattsson K. (2005) Elemental analyses of pine bark and wood in an environmental study. *Science of the Total Environment* 343:231–241.

125. Sanchez C. (2009) Lignocellulosic residues: biodegradation and bioconversion by fungi. *Biotechnology Advances* 27:185–194.

126. Segal L., Creely J.J., Martin Jr. A.E., Conrad C.M. (1959) An empirical method for estimating the degree of crystallinity of native cellulose using the X-ray diffractometer. *Textile Research Journal* 29:786–794.

127. Sarkar S., Adhikari B. (2001) Synthesis and characterization of lignin–HTPB copolyurethane. *European Polymer Journal* 37:1391–1401.

128. Shallom D., Shoham Y. (2003) Microbial hemicellulases. *Current Opinion in Microbiology* 6:219–228.

129. Shi J., Sharma-Shivappa R.R., Chinn M., Howell N. (2009) Effect of microbial pretreatment on enzymatic hydrolysis and fermentation of cotton stalks for ethanol production. *Biomass and Bioenergy* 33:88–96.

130. Siengchum T., Isenberg M., Chuang S.S.C. (2013) Fast pyrolysis of coconut biomass – an FTIR study. *Fuel* 105:559–565.

131. Silverstein R.M., Webster F.X. (1998) Spectrometric identification of organic compounds, 6th edn. Wiley, New York.

132. Sjostrom E. (1993) Wood chemistry fundamentals and applications, 2nd edn. Academic Press, San Diego.

133. Sluiter A., Hames B., Ruiz R., Scarlata C., Sluiter J., Templeton D. (2008a) Determination of sugars, byproducts, and degradation products in liquid fraction process samples. Technical report NREL/TP-510-42623. National Renewable Energy Laboratory (NREL), Colorado.

134. Sluiter A., Ruiz R., Scarlata C., Sluiter J., Templeton D. (2008b) Determination of extractives in biomass. Technical report NREL/TP-510-42619. National Renewable Energy Laboratory (NREL), Colorado.

135. Soccol C.R., de Souza Vandenberghe L.P., Medeiros A.B.P., Karp S.G., Buckeridge M., Ramos L.P., Pitarelo A.P., Ferreira-Leitao V., Gottschalk L.M.F., Ferrara M.A., da Silva Bon E.P., de Moraes L.M.P., de Amorim Araujo J., Torres F.A.G. (2010) Bioethanol from lignocelluloses: status and perspectives in Brazil. *Bioresource Technology* 101, 4820–4825.

136. Sohi S.P., Krull E., Lopez-Capel E., Bol R. (2010) A review of biochar and its use and function in soil. *Advances in Agronomy* 105:47–82.

137. Song W., Guo M. (2012) Quality variations of poultry litter biochar generated at different pyrolysis temperatures. *Journal of Analytical and Applied Pyrolysis* 94:138–145.

138. Spokas K.A., Reicosky D.C. (2009) Impacts of sixteen different biochars on soil greenhouse gas production. *Annals of Environmental Science* 3:179–193.

139. Sukumaran R.K., Surender V.J., Sindhu R., Binod P., Janu K.U., Sajna J.V., Rajasree K.P., Pandey A. (2010) Lignocellulosic ethanol in India: prospects, challenges and feedstock availability. *Bioresource Technology* 101:4826–4833.

140. Taherzadeh M.J., Karimi K. (2007a) Acid-based hydrolysis processes for ethanol from lignocellulosic materials: a review. *Bioresources* 2:472–499.

141. Taherzadeh M.J., Karimi K. (2007b) Enzyme-based hydrolysis processes for ethanol from lignocellulosic materials: a review. *Bioresources* 2:707–738.

142. Tamaki Y., Mazza G. (2010) Measurement of structural carbohydrates, lignins, and micro-components of straw and shives: effects of extractives, particle size and crop species. *Industrial Crops and Products* 31:534–541.

143. Theegala C.S., Midgett J.S. (2012) Hydrothermal liquefaction of separated dairy manure for production of bio-oils with simultaneous waste treatment. *Bioresource Technology* 107:456–463.

144. Tomas-Pejo E., Olive J.M., Ballesteros M. (2008) Realistic approach for full-scale bioethanol production from lignocellulose: a review. *Journal of Scientific and Industrial Research* 67:874–884.

145. Tsai W.T., Lee M.K., Chang Y.M. (2007) Fast pyrolysis of rice husk: Product yields and compositions. *Bioresource Technology* 98:22–28.

146. USEIA, U.S. Energy Information Administration (2013) U.S. Department of Energy, Washington. http://www.eia.gov. Accessed on 14 April 2013.

147. Vassilev S.V., Baxter D., Andersen L.K., Vassileva C.G. (2010) An overview of the chemical composition of biomass. *Fuel* 89:913–933.

148. Vassilev S.V., Baxter D., Andersen L.K., Vassileva C.G., Morgan T.J. (2012) An overview of the organic and inorganic phase composition of biomass. *Fuel* 94:1–33.

149. Vassilev S.V., Braekman-Danheux C., Laurent P. (1999) Characterization of refuse-derived char from municipal solid waste. 1. Phase-mineral and chemical composition. *Fuel Processing Technology* 59:95–134.

150. Wang Z., Lin W., Song W., Wu X. (2012) Pyrolysis of the lignocellulose fermentation residue by fixed-bed micro reactor. *Energy* 43:301–305.

151. Werkelin J., Skrifvars B.J., Hupa M. (2005) Ash-forming elements in four Scandinavian wood species. Part. 1. Summer harvest. *Biomass and Bioenergy* 29:451–466.

152. Westhuizen A.V.D., Jones D.T., Woods D.R. (1982) Autolytic activity and butanol tolerance of *Clostridium acetobutylicum*. *Applied and Environmental Microbiology* 44:1277–1281.

153. Wyman C.E., Dale B.E., Elander R.T., Holtzapple M., Ladisch M.R., Lee Y.Y. (2005) Coordinated development of leading biomass pretreatment technologies. *Bioresource Technology* 96:1959–1966.

154. Xu R., Ferrante L., Briens C., Berruti F. (2011a) Bio-oil production by flash pyrolysis of sugarcane residues and post treatments of the aqueous phase. *Journal of Analytical and Applied Pyrolysis* 91:263–272.

155. Xu R., Ferrante L., Hall K., Briens C., Berruti F. (2011b) Thermal self-sustainability of biochar production by pyrolysis. *Journal of Analytical and Applied Pyrolysis* 91:55–66.

156. Yaman S. (2004) Pyrolysis of biomass to produce fuels and chemical feedstocks. *Energy Conversion and Management* 45:651–671.

157. Yao Y., Gao B., Inyang M., Zimmerman A.R., Cao X., Pullammanappallil P., Yang L. (2011) Biochar derived from anaerobically digested sugar beet tailings: characterization and phosphate removal potential. *Bioresource Technology* 102:6273–6278.

158. Yemshanov D., McKenney D. (2008) Fast-growing poplar plantations as a bioenergy supply source for Canada. *Biomass and Bioenergy* 32:185–197.

159. Yong T.L.K., Matsumura Y. (2012) Reaction kinetics of the lignin conversion in supercritical water. *Industrial and Engineering Chemistry Research* 51:11975–11988.

160. Zaldivar J., Martinez A., Ingram L.O. (1999) Effect of selected aldehydes on the growth and fermentation of ethanologenic *Escherichia coli.* Biotechnology and Bioengineering 65:24–33.

161. Zaldivar J., Nielsen J., Olsson L. (2001) Fuel ethanol production from lignocellulose: a challenge for metabolic engineering and process integration. *Applied Microbiology and Biotechnology* 56:17–34.

162. Zhang Y.H. (2008) Reviving the carbohydrate economy via multi-product lignocellulosics biorefineries. *Journal of Industrial Microbiology and Biotechnology* 35:367–375.

163. Zhao X.B., Cheng K.K., Liu D.H. (2009) Organosolv pretreatment of lignocellulosic biomass for enzymatic hydrolysis. *Applied Microbiology and Biotechnology* 82:815–827.

164. Zheng Y.N., Li L.Z., Xian M., Ma Y.J., Yang J.M., Xu X., He D.Z. (2009) Problems with the microbial production of butanol. *Journal of Industrial Microbiology and Biotechnology* 36:1127–1138.

Contributors

- Dr. Ramin Azargohar
- Mr. Pravakar Mohanty
- Mr. Jason Maley
- Dr. Ramaswami Sammynaiken
- Dr. Jianzhong Fan

Dr. Ramin Azargohar is a research engineer in the Department of Chemical and Biological Engineering at University of Saskatchewan, Canada. His assistance in the pyrolysis of acid and enzyme hydrolyzed biomass is thankful.

Mr. Pravakar Mohanty is a PhD candidate at the Department of Chemical Engineering at Indian Institute of Technology Delhi, India. His contribution in generating biochars from the slow and fast pyrolysis of lignocellulosic biomass is acknowledged.

Mr. Jason Maley is a research officer in Saskatchewan Structural Sciences Centre at University of Saskatchewan, Canada. His involvement in structural analysis of biomass, especially chemical mapping of delignified and pretreated biomass is appreciated.

Dr. Ramaswami Sammynaiken is the manager of Saskatchewan Structural Sciences Centre (SSSC) at University of Saskatchewan, Canada. His discussions on various analytical equipment and facilities at SSSC are esteemed.

Dr. Jianzhong Fan is the manager of ICP-MS laboratory in Department of Geological Sciences at University of Saskatchewan, Canada. His assistance in ICP-MS analysis for the biomass, ash and biochar samples in this dissertation is recognized.

Equipment and facilities

Equipment or facility	Location
Agilent 4500 AFM microscope	Saskatchewan Structural Sciences Center, University of Saskatchewan
Agilent Series 1100 HPLC	Department of Chemical and Biological Engineering, University of Saskatchewan
Agilent 7890A GC	
Bruker Advance 500 MHz NMR spectrometer	Saskatchewan Structural Sciences Center, University of Saskatchewan
Bruker D8 Advance XRD	Department of Chemical and Biological Engineering, University of Saskatchewan
Elementar Vario EL III CHNS analyzer	
FEI Quanta 3D FEG DualBeam SEM microscope	Lassonde School of Engineering, York University
Micromeritics ASAP 2020 BET surface area analyzer	Department of Chemical and Biological Engineering, University of Saskatchewan
New Bruinswick Scientific Galaxy 170R CO_2 incubator	Lassonde School of Engineering, York University
Parr static oxygen bomb calorimeter	Department of Chemical and Biological Engineering, University of Saskatchewan
PerkinElmer FT-IR spectrum 100GX	
PerkinElmer NexION 300D ICP-MS	Department of Geological Sciences at University of Saskatchewan
PerkinElmer Pyris Diamond TG/DTA analyzer	Department of Chemical and Biological Engineering, University of Saskatchewan
Renishaw inVia Raman microscope	Saskatchewan Structural Sciences Center, University of Saskatchewan
Smiths Detection IluminatIR FT-IR spectrometer	
Varian CP-3800 GC	Department of Chemical and Biological Engineering, University of Saskatchewan
Varian Saturn 2000 GC-MS	